Bassoon mutation P3882A as a model to study proteinopathy in neuroinflammation and aging

Dissertation
zur Erlangung des akademischen Grades eines
Doktors der Medizin (Dr. med.)[1]
an der
Medizinischen Fakultät der Universität Hamburg

vorgelegt von
Julia Maria Gärtner
aus
Hagen

2024

[1] Doktorin der Medizin (Dr. med.)

Betreuer:in / Gutachter:in der Dissertation: Prof. Dr. Manuel A. Friese
Gutachter:in der Dissertation: Prof. Dr. Markus Glatzel

Vorsitz der Prüfungskommission: Prof. Dr. Markus Glatzel
Mitglied der Prüfungskommission: PD Dr. Alexander Volk
Mitglied der Prüfungskommission: Prof. Dr. Meliha Karsak

Datum der mündlichen Prüfung: 25.03.2025

Table of contents

List of figures

List of tables

1. Introduction

1.1 Multiple Sclerosis

1.1.1 Clinical overview

Epidemiology

Multiple Sclerosis (MS) is a chronic neuroinflammatory and neurodegenerative disease with complex and incompletely understood etiology and pathophysiology, affecting the central nervous system (CNS) (Attfield et al., 2022; McGinley et al., 2021). Throughout the course of the disease, patients experience both acute and chronic neurological symptoms, which vary in severity (Attfield et al., 2022; McGinley et al., 2021). MS is the most prevalent neurological disease among young adults (Attfield et al., 2022; Thompson et al., 2018), significantly impacting the quality of life of patients and their families. The disease typically manifests between the ages of 20 and 40, although, it can, in rare instances, present in childhood or later in life (Bermel et al., 2010; Krupp et al., 2013). Globally, approximately 50-300 individuals out of 100.000 are globally affected by MS (Browne et al., 2014). The prevalence of MS increases with latitude, with northern countries showing particularly high incidences (Browne et al., 2014). Additionally, disparities in disease severity are evident, with Black and Hispanic Americans experiencing more rapid disease progression (Browne et al., 2014).

Symptoms

The clinical presentation of MS encompasses a range of symptoms that manifest in distinct disease contexts which can be broadly categorized as relapse associated symptoms, chronically progressive symptoms, and paroxysmal symptoms. A relapse, by definition, lasts at least 24 hours, occurs at least 30 days after the onset of a preceding relapse and cannot be attributed to an infection or the Uhthoff phenomenon, which refers to the deterioration of symptoms as a result of an increase in body temperature (Compston & Coles, 2008; Thompson et al., 2018). Chronic and progressive symptoms, on the other hand, manifest independently of relapses (Oh et al., 2018; Thompson et al., 2018). The clinical onset of MS most commonly corresponds to the first or one of the first relapses, often presenting with a variety of subacute neurological deficits (Oh et al., 2018; Thompson et al., 2018). Among the initial symptoms, optic neuritis is frequently observed, with patients experiencing visual deterioration, visual field loss, loss of color vision or photopsia (Thompson et al., 2018). Initial presentations may also involve sensory and motor dysfunctions such as hypesthesia, paresthesia and paresis, and less frequently ophthalmoplegia (Oh et al., 2018; Thompson et al., 2018). Given that MS affects the entire CNS, a broad spectrum of neurological deficits might emerge during disease relapses or chronic progression, leading to

symptoms such as spasticity, sensory ataxia, cerebellar symptoms and vertigo (Compston & Coles, 2008; Oh et al., 2018; Thompson et al., 2018). In many patients, vegetative functions are also compromised during both relapses and chronic deterioration, resulting in symptoms such as miction disturbances, incontinence, and sexual dysfunction (Oh et al., 2018). Moreover, neuralgiform pain syndromes and neuropsychological symptoms, such as fatigue, depression and cognitive dysfunction, may significantly contribute to the overall disease burden (Compston & Coles, 2008; Oh et al., 2018; Thompson et al., 2018).

Clinical classification

MS encompasses various phenotypes that differ in their clinical disease course as well as in their inflammatory and neurodegenerative features. The clinically isolated syndrome (CIS) is defined as the first episode of neurological deficits that lasts at least 24 hours, without detectable dissemination of CNS lesions in time and space, which is necessary for a definitive diagnosis of MS (Miller et al., 2012). Symptoms in CIS might be monofocal which would be caused by an isolated focal lesion or multifocal (Miller et al., 2012). Not all cases of CIS develop into MS (Miller et al., 2012). If a spatiotemporal dissemination of inflammatory lesions is detected, or a spatial dissemination and oligoclonal bands (OCB), MS can be diagnosed (Dendrou et al., 2015; McGinley et al., 2021). Patients with relapsing remitting MS (RRMS) suffer from reoccurring symptom relapses from which they recover completely or partially (Dendrou et al. 2015, Oh et al. 2018). RRMS is the most common form of MS, affecting 85% of patients, with the majority transitioning to secondary progressive MS (SPMS) within 10-20 years (Dendrou et al., 2015). SPMS is characterized by a progressive accumulation of symptoms, though superimposed relapses might still occur (Dendrou et al., 2015). With advancing age, relapse activity diminishes, and chronic deficits become more prominent (Dendrou et al., 2015). Primary progressive MS (PPMS), occurring in approximately 10-15% of patients, is defined by a progressive accumulation of neurological deficits from disease onset, with or without superimposed relapses (Dendrou et al., 2015; McGinley et al., 2021). PPMS often presents with later onset (Dendrou et al., 2015; Oh et al., 2018). Whether these different MS phenotypes represent distinct disease entities or variations of a single disease remains an area of ongoing research (Attfield et al., 2022; Dendrou et al., 2015).

Diagnosis

Spatial and temporal dissemination of CNS lesions, necessitated for MS diagnosis, are assessed on magnet resonance imaging (MRI) in MS typical periventricular, juxtacortical, infratentorial or spinal localizations (Dendrou et al., 2015; McGinley et al., 2021; Oh et al., 2018). Older lesions, which may exhibit less or no contrast enhancement, aid in identifying

dissemination in time through MRI (Dendrou et al., 2015; McGinley et al., 2021; Oh et al., 2018). The detection of CNS restricted oligoclonal bands (OCB) in the cerebrospinal fluid (CSF), reflecting the intrathecal proliferation of immunoglobulin G and immunoglobulin M by clonally expanded B-cells, serves as evidence of a dissemination in time as well (Oh et al., 2018). Differential diagnoses must consider other CNS or systemic autoinflammatory conditions, metabolic disorders, and infections (Katz Sand, 2015). In particular, vitamin B12 deficiency, borreliosis, syphilis, infections with herpesviridae or human immunodeficiency virus, neuromyelitis optica spectrum diseases, myelin oligodendrocyte glycoprotein (MOG) antibody associated diseases, sarcoidosis and vasculitis should be considered (Oh et al., 2018).

Therapy

MS therapy comprises three primary branches: acute relapse therapy, disease modifying therapy (DMT) and symptomatic therapy (McGinley et al., 2021; Oh et al., 2018).

Acute relapse therapy involves intravenous, alternatively oral, glucocorticoids or plasmapheresis as an escalation, to rapidly suppress autoimmune activity and alleviate symptoms. However, acute relapse therapy does not provide long-term benefits with respect to disease progression (Attfield et al., 2022; McGinley et al., 2021; Thompson et al., 2018).

DMT aims to reduce the frequency and severity of relapses and is categorized into two regimens: intensive immunotherapy from the onset or escalating immunomodulation and immunosuppression based on disease activity (Attfield et al., 2022). No regimen has been proven superior to the other (Attfield et al., 2022). The “early intensive therapy” (Attfield et al., 2022) approach is frequently applied in PPMS and in patients with an early aggressive disease activity. The challenge lies in balancing disease control with the risk of side effects from immune suppression and drug toxicity (Attfield et al., 2022). DMTs can be divided into immunomodulatory therapies, like interferone beta or glatiramer acetate, which have milder, broader effects on the immune system, and immunosuppressive therapies, which offer more targeted and potent effects but come with an increased risk of severe side effects (Attfield et al., 2022; Reich et al., 2018; Thompson et al., 2018). There are multiple immunosuppressive therapies, including monoclonal antibodies and molecularly targeted therapies, specifically interfering with the metabolism, proliferation, migration or circulation of lymphocytes or monocytes. Treatment choices are individualized based on disease type, clinical and radiological disease activity, patient age and family planning (Attfield et al., 2022; McGinley et al., 2021; Thompson et al., 2018). Moreover, autologous hematopoietic stem cell therapy has become a therapeutic option for patients with a highly active disease course (Häußler et al., 2021). A holistic approach including a healthy lifestyle, diet and exercise, is also crucial for managing systemic inflammation and supporting neuronal plasticity

(Attfield et al., 2022; Belbasis et al., 2020; Dendrou et al., 2015). While current DMTs successfully reduce relapse rate and severity, they do not prevent eventual disease progression (Attfield et al., 2022; Friese et al., 2014; Scalfari et al., 2014).

The third therapeutic branch aims to achieve an alleviation of symptoms such as spasticity, fatigue, chronic pain and bladder dysfunction, using pharmaceutical therapy or physiotherapy. Psychological therapy and social support are equally important for disease management (McGinley et al., 2021; Thompson et al., 2018).

1.1.2 Etiology and immunopathology of MS

MS immunopathology unravels through a complex and multicellular interplay between the peripheral immune system, CNS resident immune cells, neurons and glia cells (Attfield et al., 2022; Dendrou et al., 2015). Regarding the disease inception, it remains unresolved whether the initiating key event takes place in the CNS or in the periphery (Dendrou et al., 2015).

Although the etiology of MS is not yet fully disentangled, it is assumed that MS is triggered by environmental factors in individuals that exhibit a genetical susceptibility to MS (Attfield et al., 2022; Dendrou et al., 2015). Crucial environmental factors include infection with herpes viruses, especially Epstein-Barr-Virus (EBV), vitamin D deficiency, obesity, smoking and a diet high in calories, fat and sugar (Attfield et al., 2022; Dendrou et al., 2015). Additionally, the microbiome is increasingly becoming appreciated in its potentially disease-promoting or protective role in MS (Attfield et al., 2022; Dendrou et al., 2015). Genetic factors for MS initiation have been studied in genome wide association analyses and a variety of gene loci associated with MS, such as variants in human leukocyte antigens (HLA) genes and single nucleotide polymorphisms in multiple immunological pathways, have been exposed (Dendrou et al., 2015). Environmental and genetic factors are potent in lowering the threshold of immune activation, but some factors need to be singled out as they are not only immunogenic but are also believed to incite an MS specific immune response, such as genetic variants in the HLA molecule and the EBV infection (Attfield et al., 2022; Dendrou et al., 2015). Epstein-Barr-Virus nuclear antigen 1 (EBNA-1) antibodies are detectable in 99,9% of MS patients, representing the seroconversion of an EBV infection (Bjornevik et al., 2022). Importantly, among other proposed pathophysiological pathways, EBV is believed to direct the immune response towards myelin produced by oligodendrocytes through molecular mimicry (Dendrou et al., 2015) and it has been shown that antibodies derived from MS patient exhibit high affinity towards EBNA1 and the glia cell protein GlialCAM (Lanz et al., 2022). This cross reaction suggests that, through molecular mimicry, an EBV infection might trigger the onset of MS in individuals with an environmental and genetic risk profile

(Lanz et al., 2022). The immunogenic B cell tropism of EBV might also play an important role in EBV related MS immunopathology (Attfield et al., 2022). Additionally, genomic interferences of EBV in MS risk associated gene loci have been shown which could also mediate MS specific immunogenicity of EBV (Attfield et al., 2022).

Autoimmunity in MS is perpetuated by acute and chronic inflammation, which can be perceived as two distinct but interlinked immune processes in the immunopathology of the disease (Attfield et al., 2022; Dendrou et al., 2015). Acute inflammation is driven by infiltrating peripheral immune cells which cause focal demyelinating lesions. Clinically, these acute and focal events translate into relapses (Attfield et al., 2022). In contrast, chronic inflammation is constantly and globally perpetuated by CNS resident cells, mostly innate immune cells, but also tissue resident lymphocytes (Attfield et al., 2022; Dendrou et al., 2015). Accordingly, chronic inflammation assumably plays a crucial role in disease progression independent of relapse activity and global brain atrophy (Attfield et al., 2022; Dendrou et al., 2015; Kappos et al., 2020).

Once MS is triggered, acute inflammatory infiltrates from the periphery, containing monocytes, autoreactive T cells, most prominently CD8+ cells, but also CD4+ TH1 and TH17 cells, breach the blood brain barrier (BBB) (Attfield et al., 2022; Dendrou et al., 2015). Innate lymphoid cells and unconventional T cells enter the CNS as well (Attfield et al., 2022). The proportion of infiltrating plasma cells and B cells increases with the disease course (Dendrou et al., 2015; Frischer et al., 2009). Chemotaxis due to a high level of cytokines and the education of peripheral immune cells within peripheral lymph nodes jointly enable the entry of blood immune cells into the inflamed CNS (Attfield et al., 2022). In contrast, the healthy CNS represents an immune privileged site (Attfield et al., 2022). As soon as the infiltrating immune cells are reactivated by antigen presenting cells (APCs) in the CNS, damaging demyelination is initiated in the form of acute lesions and inflammatory neuroaxonal damage occurs (Attfield et al., 2022; Dendrou et al., 2015). Eventually, the acute and focal inflammatory attack might resolve due to autoregulative mechanisms, for instance through regulatory T cells and immunosuppressive cytokines such as interleukine (IL)-10 (Attfield et al., 2022; Dendrou et al., 2015). But also, chronic active lesions exist and their frequency increases in later disease (Attfield et al., 2022). As adaptive immunity is directed towards a specific target, there was great endeavor to identify an antigen that initially leads adaptive immune cells to demyelination (Hohlfeld et al., 2016; Ransohoff et al., 2003; Schirmer et al., 2014). Although an initial key target could not be defined with certainty, it is assumed that myelin basic protein (MBP), MOG and proteolipid protein specific CD4+ T cells play an important role in directing the immune response towards myelin in early disease (Attfield et al., 2022; Dendrou et al., 2015; Krogsgaard et al., 2000). Through a process called epitope spreading, the specific immune response eventually expands to further neuronal targets,

aggravating the inflammatory aggression (Dendrou et al., 2015). During neuronal damage, not only damage-associated molecular patterns (DAMPs) amplify inflammation, but also damaged neuronal structures are presented as antigens on major histocompatibility complex (MHC) class II, giving rise to novel neuronal targets for the adaptive immune system (Dendrou et al., 2015; McMahon et al., 2005). For instance, neurofascin was proposed to represent such an extended neuronal target (Mathey et al., 2007). Epitope spreading via the presentation of antigens on MHC class I further ignites CD8+ T cell activity (Ji et al., 2013). Furthermore, beta-synuclein specific T-cells increasingly appear in SPMS and show association to grey matter destruction (Attfield et al., 2022). In the disease course, a variety of immune cell subsets from the adaptive and innate immune system participate in disease immunopathology, exerting both specific and redundant functions (Attfield et al., 2022). Some of these functions can also involve a protective, immunoregulative role, exemplified by natural killer cell like innate lymphoid cells (Attfield et al., 2022). At early disease time points, immune cell infiltration from the periphery predominates, decreasing during later disease stages with some of the innate and adaptive immune cells becoming resident in the CNS (Attfield et al., 2022; Dendrou et al., 2015). Inflammatory demyelination preferentially occurs in the white matter, but the prevalence of grey matter lesions increases with disease duration (Attfield et al., 2022). Inflammatory lesions can be classified into active lesions, chronic active lesions and chronic inactive lesions, depending on the presence of myelin phagocytosis and immune cell infiltration surrounding the area of demyelination (Attfield et al., 2022).

While acute inflammation, predominantly upheld by adaptive immune cells from the periphery, drives focal lesions, chronic inflammation appears to be a globally smoldering process within the CNS and is presumably mostly maintained by innate immune cells and blood cells that become CNS resident (Attfield et al., 2022; Dendrou et al., 2015; Fischer et al., 2012). In MS, macrophages, dendritic cells and microglia are globally in a chronic state of activity and their abundancy is correlated with the extent of neuronal demise as well as the accumulation of disability (Dendrou et al., 2015; Fischer et al., 2012; Meinl et al., 2008). Accordingly, inflammation and neuronal demise are present even in normal-appearing white matter (NAWM) which is macroscopically as well as radiologically healthy and free from plaques (Hauser & Oksenberg, 2006). Microglia are activated in the CNS even before the first acute lesions are formed (Maggi et al., 2014), supporting the concept of an early generalized inflammatory process. Presumably, an exhaustion of adaptive immunity in the course of MS alleviates acute inflammation while global and chronic innate cell driven inflammation is ongoing (Wherry, 2011). However, clinical and pathological progression of disease are independent of relapse activity (Kappos et al., 2020), indicating a key role of chronic and innate cell driven inflammation. In SPMS there is not only a dominance of

chronic and scattered inflammation, but also inflammation likely becomes more organized (Dendrou et al., 2015; Fischer et al., 2012; Wherry, 2011). Tertiary lymph nodes are forming in the meninges and mild meningeal inflammation becomes more prevalent (Dendrou et al., 2015; Magliozzi et al., 2006), both correlating with cortical lesion accumulation (Dendrou et al., 2015; Fischer et al., 2012; Magliozzi et al., 2006). Moreover, it has been suggested that in progressive disease forms inflammation is compartmentalized within the CNS (Attfield et al., 2022; Dendrou et al., 2015; Meinl et al., 2008). While inflammatory cuffs surrounding blood vessels in progressive MS are detectable, endothelial permeability of the BBB decreases (Attfield et al., 2022; Dendrou et al., 2015; Meinl et al., 2008). It has also been shown that adaptive immune cells such as TH 17 cells become CNS resident and thereby participate in chronic organized inflammation (M. Kaufmann et al., 2021). In consequence, the access of immunosuppressive pharmaceutics to sites of compartmentalized inflammation might be impeded (Maggi et al., 2014). The fact that early intensive DMT, in contrast to "step wise escalation therapy" (Attfield et al., 2022), reduces the severity of disease progression suggests that organization and compartmentalization of chronic inflammation arise early within the course of disease and, once fully developed, become invulnerable to DMT (Attfield et al., 2022; Meinl et al., 2008).

Taken together, once triggered, acute inflammatory activity appears to first extend from myelin directed attacks to attacks against multiple neuronal targets, before shifting to chronic compartmentalized inflammation and neurodegeneration as the disease progresses (Attfield et al., 2022). Thus, acute and chronic inflammation jointly constitute a highly inflammatory environment within the CNS, but eventually chronic and global organized inflammation becomes dominant (Dendrou et al., 2015). Given that progression in later disease stages is independent of relapse activity (Kappos et al., 2020), chronic and scattered innate cell driven inflammation might drive disease progression (Wherry, 2011). While a lot of research suggests that this might be a plausible temporal sequence of inflammatory events, there is also evidence of early global inflammation and neurodegeneration (Dendrou et al., 2015), raising the question whether global inflammation or neurodegeneration play a primary role in MS pathophysiology.

1.1.3 Neurodegeneration in MS

MS is both an inflammatory as well as a neurodegenerative disease (Attfield et al., 2022; Dendrou et al., 2015; Friese et al., 2014). The term neurodegeneration refers to a process of structural and functional damage to the CNS accompanied by neuronal demise (Soto & Pritzkow, 2018). Toxic protein aggregation and the cell-to-cell propagation of aggregates

are hallmarks of classic neurodegenerative diseases (Jucker & Walker, 2013; Soto & Pritzkow, 2018). Axonal densities of MS patients are reduced remarkably by 20-30% compared to the healthy population (Van Waesberghe et al., 1999). Neurodegeneration in MS can be disentangled from the perspective of a single neuron, but it can also be approached on a systemic brain level. The latter focuses on the spatiotemporal pattern of inflammation and neurodegeneration, on the relation between inflammation and neurodegeneration as well as on the neuronal connectome. Understanding MS related neurodegeneration requires insight into both cellular neuronal mechanisms and disease patterns on the organ level.

The cellular perspective aims to elucidate how acute and chronic inflammation incite neuronal demise through cellular and molecular events (Friese et al., 2014). Multiple maladaptive events perpetuate neuronal damage upon inflammation. Inflammatory demyelination leads to a loss of trophic support from myelin which results in neuronal energy deficiency and thus impedes basic neuronal functions such as axonal transport, protein synthesis and ionic balance (Friese et al., 2014). Among other mechanisms of toxicity, innate and adaptive immune cells release high levels of reactive oxygen and reactive nitrogen species (ROS, NOS). ROS also result from energy deficits which lead to a decline in antioxidative systems (Friese et al., 2014). ROS and NOS are key drivers of neuronal damage as they also impede basic neuroaxonal functions through direct molecular interaction (Friese et al., 2014). Importantly, ROS and NOS incite mitochondrial damage resulting in severe energy deficiency within the neuron (Friese et al., 2014). Mitochondrial damage is assumed to play a central role in further downstream mechanisms of neuronal death as levels of ROS increase further and basic neuroaxonal functions are impeded (Trapp & Stys, 2009). Additionally, acute inflammatory MS lesions are enriched with glutamate which leads to glutamate-mediated excitotoxicity (Azevedo et al., 2014; Friese et al., 2014; Piani et al., 1991). Infiltrating immune cells, but also astrocytes influenced by the inflammatory environment might be releasing glutamate (Azevedo et al., 2014; Piani et al., 1991). Anion channels, cysteine/glutamine antiporter and connexin hemichannels are also involved in the increase of extracellular glutamate concentration (Hardingham & Bading, 2010). The excitotoxic effects are thought to be mainly mediated by extrasynaptic ionotropic glutamate receptors (iGluR) (Hardingham & Bading, 2010), the activation of which induces an influx of intracellular calcium ions. Subsequently pro-apoptotic, necroptotic and autophagic pathways are initiated via calcium dependent enzymes (Hardingham & Bading, 2010; Kostic et al., 2013; Stirling & Stys, 2010; Wang & Qin, 2010). There are controversial reports as to which extent the loss of inhibitory input contributes to glutamate excitotoxicity in MS (Freria et al., 2010). Moreover, glutamate mediated excitotoxicity is exacerbated by an ionic imbalance in the inflamed neuron (Friese et al., 2014). Low intracellular adenosine triphosphate (ATP) levels and high calcium levels

lead to the overactivation of ion channels, such as *TRPM4* and *ASIC1*, causing ionic imbalance which leads to oncotic cell swelling and exacerbates excitotoxicity (Friese et al., 2007, 2014; Schattling et al., 2012). Ionic imbalance is further aggravated by a redistribution of ion channels due to inflammation-mediated transcriptomic alterations (Friese et al., 2007). Furthermore, it has been found that brains of MS patients are globally enriched with iron (Williams et al., 2012). The accumulation of iron induces ferroptosis, a type of cell death that is initiated by oxidative stress pathways triggered by high cellular levels of iron (Rothammer et al., 2022; Williams et al., 2012). Through epigenetic changes and transcriptomic regulation, inflammatory cytokines, intracellular damage signals and ionic imbalance lead to alterations in various cellular pathways that can be either protective or toxic for the neuron (Friese et al., 2014).

Zooming out of the single neuron level, understanding how acute and chronic inflammation lead to different patterns of neurodegeneration is important. As described in Chapter 1.1.2, acute and chronic inflammation are probably distinct but interlinked immunopathological processes in MS (Attfield et al., 2022; Dendrou et al., 2015), triggering different spatiotemporal patterns of neurodegeneration. Acute inflammation most likely causes a focal lesion pattern, while chronic inflammation evolves as a scattered process thereby causing widespread neurodegeneration (Attfield et al., 2022; Dendrou et al., 2015). For instance, general brain atrophy occurs with disease onset (Collorone et al., 2021; Kuhle et al., 2011; Miller, 2002; Trapp & Stys, 2009) and appears to be independent from acute inflammatory demyelination (Bø et al., 2003; Lucchinetti et al., 2011). Remarkably, brain atrophy is present in MS patients even before the detection of lesions is possible (Barkhof et al., 2009; Lucchinetti et al., 2011), supporting the idea of an early chronic inflammation. Diffuse axonal loss within normal appearing white matter (NAWM) does not correlate with acute demyelinating lesions (DeLuca, 2006; Evangelou, 2004; Kutzelnigg et al., 2005; Lovas et al., 2000), while chronic inflammation is diffusely present in NAWM and in the meninges, especially during progressive disease (Dendrou et al., 2015). This is in line with clinical observations revealing that there is only a very weak correlation between the accumulation of gadolinium enhancing lesions and chronically progressive clinical deterioration (Daumer et al., 2009). Accordingly, disease progression likely occurs at least partially independent of relapse activity (Kappos et al., 2020). Furthermore, Jürgens et al. have demonstrated that synaptic loss occurs uncoupled from axonal loss in MS brains, suggesting that inflammation and neurodegeneration uncouple from demyelination (Jürgens et al., 2016). Studies also reveal that the extent of cortical atrophy and grey matter focal lesions do not correlate (Kutzelnigg et al., 2005; Kutzelnigg & Lassmann, 2005; Lucchinetti et al., 2011). Hence, it is likely that inflammation and neurodegeneration represent rather generalized as opposed to focal processes within the CNS which both eventually contribute to disease progression.

Moreover, the spatio-temporal evolution of atrophy in MS follows a reproducible pattern (Eshaghi et al., 2018). Inflammation results in neuronal loss if axonal repair and remyelination mechanisms are overwhelmed by the amount of neuronal damage. Neuroaxonal loss in acute lesions might extend to connected areas via retrograde axonal degeneration (Frischer et al., 2009), but retrograde axonal degeneration from acute lesions does not entirely account for NAWM atrophy (Evangelou, 2004), supporting the concept of global inflammation and neurodegeneration. Neurodegeneration in MS is pronounced in certain areas at different time points of disease. Early on, regions with high energy consumption and connectivity are affected with greater severity (Eshaghi et al., 2018; Haider et al., 2016). Other factors, such as region-specific microglia activity, may exert influence on selective neuronal vulnerability (Eshaghi et al., 2018). As cortical lesions are pronounced in vicinity of large sulci where the circulation of CSF is decelerated, it was suggested that additionally, a soluble factor from the CSF might contribute to cortical neurodegeneration in chronic inflammation (Kutzelnigg & Lassmann, 2005).

Together, these observations suggest that acute inflammation causing the relapses is not the key driver of disease progression, but that neurodegeneration is rather driven by chronic and smoldering inflammation which becomes increasingly organized and irresponsive to DMT (Attfield et al., 2022; DeLuca, 2006; Dendrou et al., 2015; Evangelou, 2004; Kutzelnigg & Lassmann, 2005; Lovas et al., 2000). However, it is still an open question whether the described pattern of neurodegeneration can be fully attributed to chronic inflammation or if neurodegenerative mechanisms also play a primary role in the disease. While inflammation and neurodegeneration inevitably potentiate each other, it remains enigmatic if inflammation initiates neurodegeneration, if neurodegeneration triggers the inflammation or if inflammation simply exposes a disease specific neuronal vulnerability to neurodegeneration (Dendrou et al., 2015; Friese et al., 2014). Moreover, it has been proposed that MS can be viewed as an acceleration of neuronal aging (Cole et al., 2020) given common cellular mechanisms of cellular decay in MS and aging, such as elevated ROS levels (Friese et al., 2014; Hipp et al., 2019; T. Kaufmann et al., 2019).

1.1.4 The experimental autoimmune encephalomyelitis in C57BL/6 mice

Experimental autoimmune encephalomyelitis (EAE) in C57BL/J6 mice is initiated by MOG-specific $CD4^+$ T cells following immunization with MOG/Complete Freud's Adjuvant (CFA) and pertussis toxin. MOG-reactive CD4+ T cells then travel to the CNS inciting demyelination and inflammation (Bittner et al., 2014; McCarthy et al., 2012). The establishment of an inflammatory milieu leads to a recruitment of monocytes, CD8+ T cells, B cells, plasma cells and to microglia activation (Bittner et al., 2014; KUERTEN et al., 2007; McCarthy et

al., 2012). This results in an exacerbation of inflammation and neuroaxonal damage. The disease course can be described as a progressive sequence of motor dysfunction (Bittner et al., 2014; KUERTEN et al., 2007). The symptoms typically occur on day 7-10 post immunization and begin with tail paralysis. The paralysis then gradually ascends to the hind limbs first and then to the front limbs. Typically, the peak of the symptoms occurs around day 15 post immunization representing the acute phase (Bittner et al., 2014). The peak is followed by a chronic phase marked by a subtotal alleviation of the symptoms (Figure 1). Usually, the EAE lasts for 30 days (Bittner et al., 2014).

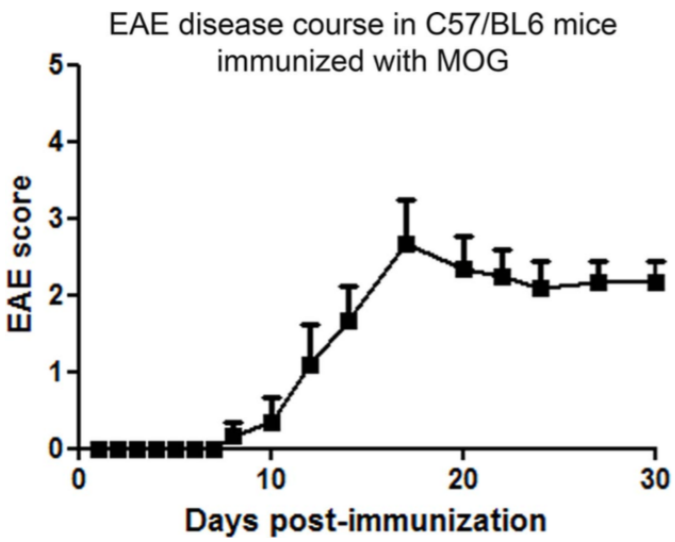

Figure 1: ***EAE disease course in C57/BL6 mice immunized with MOG*** (Quinn et al., 2011)

1.2 Proteostasis

1.2.1 Protein aggregation – definition and mechanism of toxicity

Aggregation of a protein occurs if the structural integrity of a protein or of proteostatic systems is perturbed, for instance, when the solubility of a susceptible protein decreases owing to misfolding (Hipp et al., 2019). The latter is promoted by high oxidative stress, energy deficiency and an impairment in the function of chaperones and protein degradation systems (Hipp et al., 2019). While oxidative stress and energy deficiency occur abundantly in MS (Friese et al., 2014), malfunction of stress defense or the chaperone system and a decline in ubiquitin proteasome system (UPS) and autophagy function are typical features of aging (Hipp et al., 2019). Thus, MS patients with increasing age are particularly prone to aggregation.

Aggregation can be defined as dense accumulations of heterogenous conformations of misfolded protein oligomers (Ross & Poirier, 2004). The misfolding and aggregation of a protein is a process of multiple stages composed of a gradual increase in density and decrease in solubility (Ross & Poirier, 2004). Therefore, it must be differentiated between oligomeric, globular intermediates and amyloid fibrils which are highly ordered, parallel and anti-parallel conformations of beta sheets (Lim & Yue, 2015; Ross & Poirier, 2004). Notably, misfolded protein monomers can assume heterogenous conformations while forming oligomerous aggregates (Klaips et al., 2018).

Proteinopathy does not only exist in the CNS, but also in systemic diseases such as amyloidosis that might occur as a consequence of an accumulation of acute phase proteins due to a strong inflammatory condition. Moreover, the accumulation of free antibody light chains might cause kidney and heart failure in multiple myeloma. While peripheral amyloidosis is marked by a high amyloid load, the mere presence of misfolded oligomers is sufficient to cause disease in the brain (Dobson et al., 2020).

The toxic mechanisms of aggregates include damage to cell membranes, endoplasmatic reticulum (ER) stress, mitochondrial damage and the formation of stress granules, which particularly impede protein biosynthesis by sequestering essential factors thereof (Peng et al., 2020). All these phenomena induce apoptotic and necroptotic pathways. By sequestering factors of the protein degradation system including molecular chaperones, aggregates may further weaken cellular defense systems (Hipp et al., 2019). Furthermore, the hypothesis of a prion like cell-to-cell transmission of toxic aggregates is becoming increasingly appreciated (Peng et al., 2020). It is based on the theory that toxic protein aggregates propagate from cell to cell and are capable of self-amplification by inducing the misfolding of healthy protein templates (Chung et al., 2018).

1.2.3 Proteostasis and its decline with age

Protein biosynthesis is prone to errors at all levels of the process (Saftig & Puertollano, 2021), demanding a complex quality control machinery that maintains proteome integrity in a concerted action. Given that a basic function of the CNS is plasticity and considering the complex communication through delicate compartmentalization, neuronal proteostasis is a particularly sophisticated challenge (Hetz et al., 2020; Sossin & Costa-Mattioli, 2019).

Proteostatic balance within the cell is based on protein stabilization, surveillance and degradation. Stabilization is primarily achieved by chaperone proteins located in the cytoplasm and the ER, but also in mitochondria (Jayaraj et al., 2020). The heat shock response (HSR) can be upregulated upon various environmental stressors (Li et al., 2017). During the folding

of proteins in the ER they are stabilized by chaperones until they assume a thermodynamically stable conformation where misfolding is less probable (Li et al., 2017). Chaperones shield vulnerable regions of a protein and counteract its intramolecular propensity to reach a state of energy minimum, which may be an insoluble conformation (Li et al., 2017). Moreover, chaperones are involved in surveillance and degradation (Li et al., 2017). The unfolded protein response (UPR) in the ER is activated by chaperones and membrane proteins sensing misfolding through surface exposed hydrophobic peptides (Hetz et al., 2020; Needham et al., 2019). Downstream, they slow down protein biosynthesis through the phosphorylation of eIF2alfa, but upregulate factors of the ER associated degradation (ERAD) (Travers et al., 2000). If activated continuously, the UPR leads to the upregulation of proapoptotic factors (Travers et al., 2000). Proteins recognized by the UPR are translocated to the cytoplasm by an ER membrane protein exhibiting E3 ligase function. After receiving a ubiquitin tag, the protein is degraded by the proteasome in the cytoplasm (Travers et al., 2000). The Ubiquitin-Proteoasome-System (UPS) coordinates the recognition, ubiquitin tagging and subsequently the degradation of misfolded proteins. Degradation is executed by the proteasome, a proteolytic enzyme complex consisting of an enzymatic core complex and a regulatory complex (Betegon & Brodsky, 2020). It is rather specialized in smaller proteins and peptides (Jayaraj et al., 2020). The autophagy system is mainly composed of macroautophagy, microautophagy and chaperone mediated autophagy (Schuck, 2020). Substrates destined to be degraded by the autophagy pathway are coated into autophagosomes, which then fuse with a lysosome giving rise to the autophagolysosome in which the substrate is degraded enzymatically (Saftig & Puertollano, 2021). Autophagy is, among metabolic factors (*AMPK, mTOR*), regulated by factors orchestrating the nucleation of phagophores such as autophagy related genes (Atg) (Saftig & Puertollano, 2021). Various environmental stressors enhance lysosomal biogenesis through *TFEB*, promoting autophagy (Saftig & Puertollano, 2021). Macroautophagy is assumed to play a key role in the clearance of aggregates as the proteasome is merely capable of coping with misfolded polypeptide chains (Kopito, 2000; Lamark & Johansen, 2012).

Cellular proteostasis is imperfect, leading to misfolded proteins not being recognized or proteins being degraded prematurely before they have the chance to assume their correct conformation (Labbadia & Morimoto, 2015). The capacity of protein surveillance and degradation can only accommodate for a limited extent of misfolding and aggregation. As elaborated above, age and inflammation among other factors promote proteostatic imbalance (Hipp et al., 2019). The latter is exacerbated by a vicious cycle resulting from the sequestration of chaperones and by protein aggregates (Hipp et al., 2019). While neurons incriminated by aggregation may benefit from boosting protein degradation, an overactivation of

protein degradation systems impairs learning and cognitive function and is also associated with disease (Hipp et al., 2019; Wojcikiewicz et al., 2009). Finally, cell division can reduce the aggregate load of a single cell through distribution, alleviating the imbalance between stressors and defense mechanisms (Hipp et al., 2019). Therefore, particularly in neurons, which are incapable of cell division protective mechanisms quickly become overwhelmed by accumulating toxic protein deposits.

1.3 Bassoon

1.3.1 Bassoon - a major cytomatrix active zone protein

The cytomatrix active zone (CAZ) is a presynaptic protein complex orchestrating vesicle exocytosis based on multiple direct and indirect protein interactions. Moreover, the CAZ is responsible for the accurate organization of ion channels and proteins at the presynaptic membrane to ensure an efficient neurotransmitter release, which requires a delicate regulation of proteostasis (Gundelfinger et al., 2016).

With 416 kDa, Bassoon is a protein of remarkable size with multiple zinc finger domains, coiled-coiled protein interaction sites and a large poly Q stretch (Gundelfinger et al., 2016). Interestingly, Bassoon consists of up to 90% of intrinsically disordered residues (IDR), which are defined as unstable amino acid sequences that do not have a defined tertiary structure (Schattling et al., 2019). Taken together, its size, the Poly Q stretch and the enrichment with IDRs render the protein prone to aggregation. Poly Q stretches have been shown to be toxic for the cell by inducing ER damage and by increasing the propensity of a protein to aggregate (Vidal & Hetz, 2012). Bassoon is one of at least five scaffold proteins of the CAZ, where it colocalizes particularly with calcium channels, implicating a role of Bassoon for the priming and positioning of voltage gated calcium channels (VGCC) (Gundelfinger et al., 2016). The interaction of Bassoon with RIM-binding protein (RBP), which is an important scaffold protein within the CAZ, is essential for the positional priming of voltage gated calcium channel 2.1, a presynaptic VGCC (Frank et al., 2010). The loss of Bassoon can, however, be compensated by voltage gated calcium channel 2.2 (Frank et al., 2010).

A role of bassoon in recruiting synaptic vesicles to destined release sites has been implicated repeatedly (Davydova et al., 2014; Frank et al., 2010; Hallermann et al., 2010; Jing et al., 2013). Bassoon was shown to indirectly participate in vesicle clustering and reloading (Mendoza Schulz et al., 2014), while it directly regulates presynaptic proteostasis: Bassoon seems to be an important regulator in compartment specific proteostasis in the presynapse (Mendoza Schulz et al., 2014; Montenegro-Venegas et al., 2021; Okerlund et al., 2017). In

that role, Bassoon controls ubiquitination and degradation in both autophagy and the UPS via inhibition of the autophagy associated protein *Atg 5* and the E3-ligase *Siah1* which is known to mediate the ubiquitination of many presynaptic proteins (Okerlund et al., 2017). Most recently, multiple binding sites in Bassoon specific for *PSMB4* have been identified (Montenegro-Venegas et al., 2021). By inhibiting *PSMB4,* Bassoon prevents the assembly of the proteasome and thereby negatively controls its activity in ubiquitination-dependent and independent pathways (Montenegro-Venegas et al., 2021). While Piccolo, another CAZ protein, shares many homologies and functions with Bassoon, the interaction with *PSMB4* is unique for Bassoon (Montenegro-Venegas et al., 2021). A knockout of the Bassoon gene *Bsn* ($Bsn^{-/-}$) leads to a significantly reduced abundance of presynaptic proteins (Okerlund et al., 2017). Its role in proteostasis regulation indicates that a dysfunction of Bassoon, for instance due to aggregation or translocation, could lead to increased presynaptic turnover, reduced synaptic vesicle release, and potentially even synapse malfunction and loss, while an overactivity would promote aggregation of presynaptic proteins (Okerlund et al., 2017).

Through binding of the transcription factor *CTBP1*, Bassoon participates in activity dependent regulation of gene expression (Gundelfinger et al., 2016). Bassoon is one of the first proteins at nascent synapses (Friedman et al., 2000; Waites et al., 2013; Zhai et al., 2000), implying a role of Bassoon in synapse formation and development. Bassoon is delivered to the synapse via precursor vesicles, which contain pre-assemblies of CAZ protein complexes (Shapira et al., 2003). Transport impairments, which occur in damaged neurons, could therefore hinder the transport of Bassoon to the presynapse, promoting accumulation in the soma.

1.3.2 Bassoon proteinopathy in MS

By using the translating ribosome affinity purification (TRAP) method to selectively study the transcriptome of motor neurons in the MS mouse model EAE, Bassoon has been identified as one of the upregulated candidate genes (Schattling et al., 2019). Moreover, immunohistochemical stainings of Bassoon have shown its accumulation in the soma of day 15 EAE motor neurons and in human postmortem spinal cord specimen of MS patients. Day 15 EAE spinal cords were stained with an aggregation detection dye (Proteostat), revealing a high aggresome load of EAE motor neurons. Remarkably, the abundancy of aggresomes in the EAE was almost completely abolished in $Bsn^{-/-}$ mice and significantly reduced in mice treated with IU1, a proteasome activator. Clinically, $Bsn^{-/-}$ mice showed an ameliorated EAE course and an alleviation of neuronal loss in spinal cord immunohistology, pointing to an *in vivo* toxicity of Bassoon. Accordingly, a toxicity of Bassoon overexpression has been demonstrated *in vitro (*Schattling et al., 2019).

Together, these findings shed light on a novel concept of MS pathophysiology that is based on proteinopathy mediated neurodegeneration by Bassoon. However, it is still unknown which mechanisms drive the transcriptional upregulation of Bassoon during EAE and which exact mechanisms results in the accumulation of the protein in the soma. Likewise, for MS it has not been investigated yet whether inflammation causes Bassoon upregulation and aggregation or if a primary pathology of Bassoon triggers inflammation. Possibly, also a low-level inflammation could cause an initial Bassoon pathology, subsequently igniting a more destructive inflammatory response.

1.3.3 The human missense Bassoon mutation P3866A

The autosomal-dominant missense mutation P3866A, replacing Prolin by Alanin, has been detected in a Japanese family with cases of an atypical Parkinson syndrome (Yabe et al., 2018). All four family members that expressed Bassoon P3866A showed symptoms of cognitive impairment, memory disturbances, supranuclear palsy as well as rigidity and severe postural instability among other symptoms of parkinsonism. The syndrome was classified as a progressive supranuclear palsy (PSP) like syndrome with aspects of frontotemporal dementia. The severity of symptoms differed between the family members.

Using histopathology, an increased aggregation of Tau was detected in affected individuals. The age of onset varied between 45 – 85 years, suggesting age as an important factor for disease development. Mutated Bassoon was associated with a decreased solubility in HEK293 cells implying an increased propensity for aggregation. A genome wide analysis revealed that the mutation was detected only in the four patients with the PSP like syndrome but not in healthy controls. Additionally, the mutation is located in an IDR, near the N-terminus subsequent to the poly-Q stretch (Winter et al., 1999).
The implication of mutated Bassoon (Bassoon MUT) in an age-associated neurodegenerative disease further strengthens the concept of an aggregation prone protein that drives neuronal demise in the state of proteostatic imbalance, oxidative stress and energy deficiency, which all together constitute features of inflammation and aging (Friese et al., 2014; Hipp et al., 2019). The human Bassoon mutation P3886A corresponds to the mouse Bassoon mutation P3882A.

1.4 Hypothesis

The presynaptic protein Bassoon has been shown to form toxic deposits during neuronal stress that might drive neurodegeneration in MS (Schattling et al., 2019). The role of Bassoon has not only been discussed in the context of MS. A dominant missense mutation of Bassoon (Bassoon P3866A) has been identified in a Japanese family with a hereditary atypical Parkinson syndrome (Yabe et al., 2018). Bassoon has also been implicated in other neurodegenerative diseases. For instance, it has been shown to participate in protein aggregates in Huntington's disease (Huang et al., 2020). This indicates a pathological potential of Bassoon in the context of neurodegeneration. The identification of a Bassoon mutation (Yabe et al., 2018) associated with a neurodegenerative disorder implies that the mutation demasks the toxic potential of Bassoon. It is conceivable that the presynaptic protein Bassoon exhibits a structural susceptibility to aggregation which is exacerbated by the Bassoon mutation (Yabe et al., 2018). Challenges such as neuroinflammation and age might be a trigger for Bassoon proteinopathy, which might be exacerbated by the Bassoon mutation identified by Yabe et al.

The main hypothesis of this work is that the Bassoon mutation P3866A (Bassoon MUT) increases the toxicity of Bassoon in cell culture as well as *in vivo* in the context of neuroinflammation. A verification of this hypothesis would facilitate the generation of a novel model to study Bassoon proteinopathy in the context of neuroinflammation. Secondly, it was hypothesized that the mechanism behind the increased toxicity in the Bassoon MUT protein is an increased propensity for aggregation and aggregation mediated toxicity.

With respect to its toxic potential, Bassoon aggregation and toxicity may also play a role in age-dependent neurodegeneration and other neurodegenerative disorders. Accordingly, the third hypothesis is that the Bassoon mutation demasks the role of Bassoon in age-dependent neurodegeneration and might therefore also serve as a model for Bassoon proteinopathy in the context of aging and other neurodegenerative diseases, as well.

1.5 Aims

Bassoon has been shown to play a pathophysiologically relevant role in inflammation-induced neurodegeneration (Schattling et al., 2019). Therefore, a model that facilitates a mechanistic investigation of Bassoon proteinopathy would be of great aid in investigations of the protein in the context of disease. By increasing the toxicity of Bassoon, the Bassoon mutation P3866A could provide such a model and assist in the identification of the exact mechanisms of Bassoon toxicity.

Investigation of toxic effects of the Bassoon mutation P3866A in cell culture
The toxicity of Bassoon MUT will be quantified *in vitro* in different cell culture models. First, the toxicity of the Bassoon mutation will be studied using an overexpression construct for the transfection of N2a cells. Secondly, the susceptibility of Bassoon MUT primary cortical neurons to glutamate excitotoxicity will be assessed. The third *in vitro* aim is to check for a subcellular translocation of Bassoon MUT in primary cortical neurons. Finally, as a fourth aim, the aggregation load of Bassoon MUT primary cortical neurons will be compared to Bassoon wildtype (WT) neurons.

Assessment of spontaneous neurodegeneration in Bassoon P3882A mutant mice
By quantifying neuronal loss in adult, 10-month-old mice, the aim is to exclude a developmental phenotype of the Bassoon mutation P3882A. Subsequently, 18-month-old mice will be analyzed with respect to neuronal loss and Bassoon accumulation in the soma of cortical neurons to assess a potential age dependent neurodegenerative effect of the Bassoon mutation.

Challenge of Bassoon P3882A mutant mice with in vivo inflammation
With respect to the *in vivo* analyses, the central aim is the phenotypic description of EAE in Bassoon MUT mice, focusing on the clinical severity as well as on histology and fluorescence activated cell sorting (FACS) based quantification of neuronal loss and Bassoon accumulation.

Deciphering neurodegenerative mechanisms in MS is crucial to facilitate drug development that halts neurodegenerative mechanisms and disease progression. Toxic protein aggregation in neurons has evolved into a contemporary paradigm of neurodegeneration (Hipp et al., 2019). In EAE and MS, Bassoon has emerged as a new candidate for proteinopathy-driven neurodegeneration (Schattling et al., 2019). This work aims to provide an initial overview of the Bassoon mutation P3866A (human) as a model for Bassoon toxicity in MS and EAE but also in the context of aging.

2. Materials and Methods

2.1 Materials

2.1.1 Reagents and chemicals

***Table 1**: Reagents and chemicals for animal experiments*

Reagent	**Company**
CO_2/O_2 gas mixture (80%/20%)	SOL
DietGel® Recovery	Clear H_2O
Freund's adjuvant, incomplete	Difco laboratories
Mouse $MOG_{35–55}$ peptide, MEVGWYRSPFSRVVHLYRNGK-NH_2	Schafer-N
Mycobacterium tuberculosis H37 Pertussis toxin, from Bordetella pertussis	Difco laboratories
from Bordetella pertussis	Calbiochem
Rompun® 2% (Xylazine)	Bayer
Ketanest® S 25mg/ml (Ketamine)	Pfizer Pharma

***Table 2**: Reagents and chemicals for genotyping*

Reagent	**Company**
dNTP Mix (10mM)	Thermo Scientific
DreamTaqTM Hot Start Green DNA Polymerase, 5 U/µl	Thermo Scientific
GeneRuler 1 kb DNA Ladder	Thermoscientific
Roti®-Safe GelStain	Carl Roth
UltraPureTM Agarose	In Vitrogen
Primer	Biomers
PSP5II restriction enzyme	Thermo FisherTM

Table 3: *Reagents and chemicals for immhunohistochemistry and immunocytochemistry*

Reagent	**Company**
High Precision Microscope Cover Glasses	Marienfeldt
Normal Donkey Serum	Merck
Triton-X® 100 reinst	Carl Roth
PAP pen 2 mm tip width (Liquid Blocker)	Sigma-Aldrich
ROTI®Mount FluorCare DAPI	Carl Roth
Superfrost PlusTM Adhesion Microscope Slides	Thermo FisherTM
4% PFA	
1x PBS	

Table 4*: Reagents and chemicals for nuclei isolation and FACS staining*

Reagent	**Company**
EZ Buffer	Sigma
NeuN-Alexa Fluor647	Abcam
30µm Pre-Seperation filters	Miltenyi
Hoechst 33342	Thermo Scientific

Table 5: *Reagents and chemicals for Plasmid purification*

Reagent	**Company**
Plasmid DNA Purification Extraction Kit Midi	Machery-Nagel

***Table 6**: Reagents and chemicals for N2a - cell experiments*

Reagent	Company
500 ml DMEM, high glucose, GlutaMAXTM Supplement	Gibco
Penicillin-Streptomycin	In Vitrogen
10% Fetal Calf Serum	Carl Roth
Tryp LE™	Gibco
Lipofectamine 2000	Thermo Scientific
Opti-MEM	Gibco
DPBS sterile filtered (1x)	Pan-Biotech
Cell Titer Glo Luminiscent Cell Viabiliy Assay	Promegea
EDTA (1M)	Gibco

***Table 7**: Reagents for PNCC*

Reagent	Company
DMEM-F12	Gibco
HBSS	Gibco
Poly-D-Lysine hydrobromide	Sigma-Aldrich
Hibernate medium	Gibco
PNGM	Gibco
Trypsin-EDTA (0.05%), phenol red	Gibco
L-glutamic acid	Sigma-Aldrich

***Table 8**: Reagents for Real Time Glo Glutamate stress assay*

Reagent	Company
Real Time Glo MT Cell Viablity Assay	Promega
L-glutamtic acid	Sigma Aldrich

***Table 9**: Primary antibodies for immunohistochemistry and immunocytochemistry*

Name	**Clone**	**Dilution**	**Company**
Mouse anti-Bassoon	Polyclonal	1:400	Enzo
Chicken anti-NeuN	Polyclonal	1:250	Millipore

***Table 10**: Secondary antibodies for immunohistochemistry and immunocytochemistry*

Name	**Clone**	**Dilution**	**Company**
Alexa Fluor® 647 donkey anti-mouse	Polyclonal	1:500	Jackson ImmunoResearch
Alexa Fluor® 488 Donkeyanti-chicken	Polyclonal	1:500	Jackson ImmunoResearch
Proteostat Aggresome dye	Polyclonal	1:2000	Jackson ImmunoResearch

2.1.2 Consumables

Table 11: *Consumables*

Name	**Company**
Cannulas	B. Braun
Cell culture dishes	Thermo Fisher Scientific
CELLSTAR Multiwell plates	Greiner Bio-One
ddH2O	ZMNH
Filter tips	Invitrogen
Pasteur pipette 230mm (glas)	Heinz Herenz Medizinbedarf
Round Bottom Polystyrene Tube, 5ml (FACS)	Sarstedt
SafeSeal Micro tubes	Sarstedt
Serological pipettes (sterile)	Sarstedt
StartGuard R Comfort gloves	Starlab
Syringes (1ml)	B.Braun
Eppendorf tubes	Sarstedt
Pipette tips	Sarstedt
Large scissor	FST
Iris Scissors – Delicate Pattern Sharp	FST
Blunt Forceps	FST
Scalpel	FST
Curved Vannas Spring Scissors 3mm blade	FST
Petri dish	FST

2.1.3 Equipment

Table 12: *Equipment and devices*

Name	Company
Bench Top Microcentrifuge	Eppendorf
Binocular Stereo Microscope	Leica
Biometra Thermocycler	Analytik Jena
Chemical fume hood	Kugel medical
Epifluorescence Microscope Eclipse	Nikon
Incubator (cell lines)	Memmert
Incubator (primary neurons)	Thermo Scientific
Intas Gel documentation	Intas Science Imaging Instruments
Light microscope	Olympus
LSM600 confocal microscope	Zeiss
Microme HM 560 Cryostat	Thermo Fisher Scientific
NanoDrop 1000 Spectrophotometer	Thermo Fisher Scientific
Neubauer cell count chamber	Marienfeldt
Perfusion system	Ismatec
Pipettes	Gilson, Satorius
Staining jars	Marienfeldt
Laminar flow hood	Thermo Fisher Scientific
Trypan blue Solution (0,4%)	Sigma- Aldrich
FACS Symphony A3	BD Biosciences
Tecan reader	

2.1.4 Software

Table 13*: Software*

Name	Company
FACSDiva	BD
FlowJo	FlowJo
Image J (Fiji)	https://imagej.nih.gov/ij/index.html
Prism 5	Graph Pad Software

2.2 Methods

In vitro methods

2.2.1 The neuroblastoma cell line Neuro-2A (N2a)

The N2a cell line was purchased from ATCC Manufacturing. Cells were cultured in Dulbeccos' Modified Eagle Medium (DMEM), high glucose, supplemented with GlutaMAX-medium and enriched with Penicillin-Streptomycin and 10% fetal calf serum (FCS). Cells were incubated at 37°C and 5% CO_2. The cell culture flask is permeable for CO_2 via the filter cap. At 80-85% confluency, cells were split. For this purpose, cells were washed with 1x Dulbeccos' phosphate-buffered-saline (DPBS) and incubated in 1-2 ml TrypLE express enzyme at 37 °C for 2 min to detach from the surface. Subsequently, cells were resuspended in 10 ml fresh medium and split 1:10 by transferring the cells into a new cell culture flask containing a pre-warmed medium. For the cell viability assays, cells were plated on µCLEAR R white 96-well plates that were coated with poly-D-lysine (PDL) in phosphate-buffered saline (PBS) (1:500) over night. The PDL was washed off 2 times with PBS and incubated with PBS for 10 min prior to the addition of 180 µl cell culture medium.

2.2.2 Transformation of bacteria and plasmid purification

Plasmids used for the transfection of N2a cells were purified from TOP10 competent bacteria. For amplification plasmids, were transformed into chemically competent bacteria, TOP10 bacteria. The plasmids contain a resistance against ampicillin, facilitating their selection. The rat Bassoon-WT (Bsn-WT) plasmids were obtained from the Dresbach laboratory. Bassoon-Mut (Bsn-MUT) plasmids were available in the lab. First, the bacteria were thawed on ice for 15 min. Next, 1 µl of the required plasmid was added to 50 µl bacteria and the mixture was incubated on ice for 15 minutes. To introduce a heat shock, the mixture was transferred to 42 °C for 45 s and subsequently put back on ice for 2 minutes. Superoptimal medium with catabolic repressor (SOC medium) was added to a total volume of 500 µl, and the bacteria were incubated at 37 °C, 350 rpm for one hour. The bacteria were then transferred into 100 ml LB-Ampicillin medium and were incubated over night at 37 °C while shaking with 250 rpm. The plasmids were purified using the Machery-Nagel Midi Kit. Briefly, the LB-Ampicillin medium containing the bacteria was centrifuged at 5000 g for 40 min at 4 °C and resuspended in 8 ml resuspension buffer. The cells were lysed with 8 ml lysis buffer and neutralized with 8 ml neutralization buffer. The falcons containing the lysed bacteria were transferred into column filters which were then washed with an equilibration buffer and eluted with 5 ml of an elution buffer into a new falcon and mixed with 3.5 ml isopropanol.

The suspension was centrifuged 30 min at 10000 g, 4 °C. The pellet was washed with 2 ml ethanol and dried at room temperature before it was resuspended in 50 µl VT1 water. The DNA concentration was measured with the NanoDrop.

2.2.3 Lipofectamine transfection of N2a cells

Prior to the transfection, the condition of the cells was observed under the light microscope. All cells were transfected at a confluency of 70%-80%. The N2a cells were transfected with an enhanced green fluorescent protein (EGFP) empty plasmid, a Basson MUT plasmid and a Bassoon WT plasmid. Three master mixes, one for each transfection condition, were prepared. For each condition two T75 flasks were inoculated with the transfection complex. First, the old medium was aspirated from the flasks and 10 ml new medium was added.

Transfection master mix preparation

Two 15 ml falcons were prepared

- 75 µl Lipocetamine 2000 TM in 1875 µl OptiMEM
- 38 µl DNA in 1875 µl OptiMEM

Three plasmid conditions

1. Enhanced green fluorescent protein (EGFP) - empty vector
2. EGFP - rBassoon wildtype
3. EGFP - rBassoon p3875A

The Lipofectamine 2000 solution was vortexed and added to the DNA solution. The mixture was vortex thoroughly and applied into the cell culture flask. After 5h the medium was changed.

2.2.4 Sorting and plating of transfected cells

Preparation

Forty-eight h after the transfection, the N2a cells were prepared for sorting. The T75 flasks were first washed with PBS before 3 ml TrypLE was added and incubated for 3 min at 37 °C. Cells were resuspended in 10 ml N2a cell medium, transferred into a falcon tube and centrifuged 5 min at 400 g at room temperature. The pellet was washed with PBS, centrifuged and resuspended in 3 ml PBS containing 1mM ethylenediaminetetraacetic acid (EDTA). The cell solution in the PBS/EDTA was then run through a 45 µm pre separation filter to remove cell clusters and transferred into a 15 ml falcon for the sorting on a BDAriaIII cell sorter (BD Bioscience).

Collection of EGFP+ and EGFP- cells

The cells were sorted by their GFP signal and GFP positive and negative cells from each condition were collected into cooled 15 ml falcons containing N2a cell medium.

After the cell sorting, the cells were centrifuged for 5 min at 400 g, room temperature. The pellet was resuspended in 500 µl medium. Using the Neubauer counting chamber the cells were counted in a 1:2 cell suspension/ trypan blue solution. The cells were plated at a density of 15K cells per well into a 96-well plate containing 180 µl pre-warmed N2a cell medium per well. The cell sorter was kindly operated by Dr. Nicola Rothammer.

Cell plating

The amount of cell solution *X* required to achieve the targeted density was calculated with the equation below:

X µl of cell suspension per well = (15000/ counted cell number ×10000) × 1000

The cells were seeded into a 96 well plate containing 180 µl N2a cell medium per well.

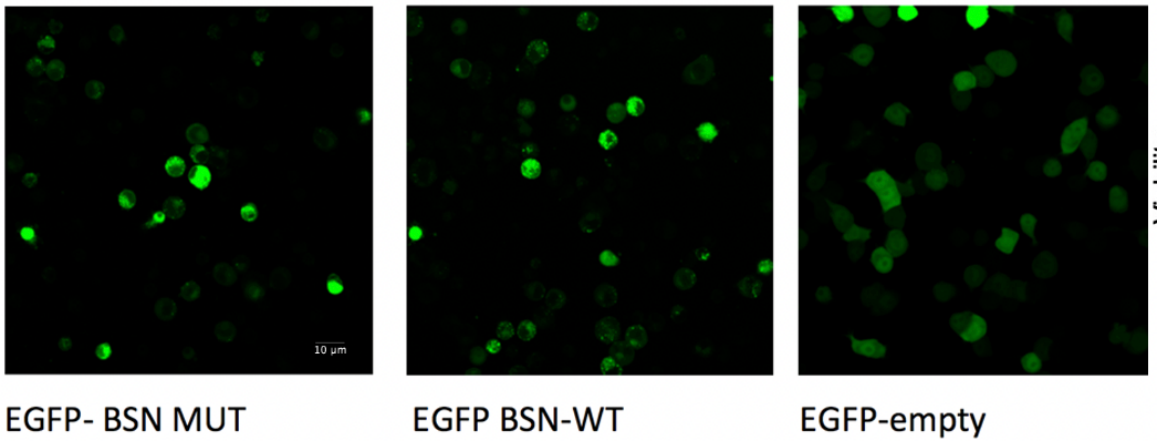

Figure 2: Transfected and sorted N2a cells *20x, scale bar is set to 10*µm

2.2.5 Cell viability assay of transfected N2a cells

After 48 h the cell viability was measured using the Cell Titer Glow R 2.0 reaction in the Tecan Spark^{TM} 10M Multimode microplate reader. The Cell Titer Glo indirectly measures the number of viable cells per well, as it is directly proportional to the ATP level released from lysed cells. The Ultra Glo TM Luciferase catalyzes a reaction between Luciferin, ATP and O_2 that produces light. The luminescence measured in each well represents the viability of cells in each well (Fig. 3). In other words, the amount of luminescence negatively correlates with the toxicity of the transfection constructs. 130 µl of cell medium was removed and 50 µl of the CTG solution containing the Ultra Glo Luciferase, Luciferin in a lysis buffer and Mg2+ were added to achieve a 1:1 ratio of cell medium and CTG solution. The Tecan was

programmed to shake for 120 s waiting for 10 min and afterwards, luminescence was measured. Background luminescence was obtained from wells containing only medium and was subtracted from the raw values. Corrected values were normalized to the GFP control. The mean values from the technical replicates were calculated for each condition.

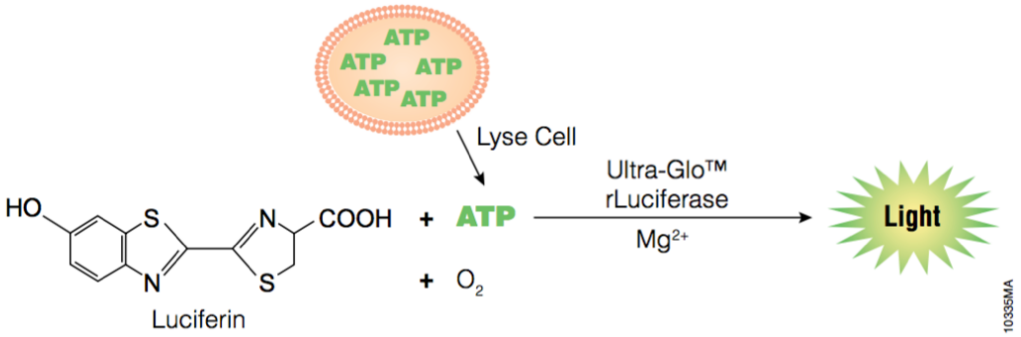

Figure 3: Cell Titer Glo reaction *The amount of light produced by the luciferase-based reaction is dependent on the intracellular ATP level which correlates with the presence of vital mitochondria and thus serves as an indicator of cell viability (Promega).*

2.2.6 Primary neuronal cell culture

Primary neuronal cell culture has been served to explore the effect of the Bassoon mutation during neuronal stress. For this purpose, neurons from cortices and hippocampi were prepared from Bassoon-MUT (MUT/MUT) C57BL/6J prenatal mice at gestational day 16.5. The preparation of embryos was performed using sterile instruments. All further steps were performed under a laminar flow hood.

Poly-D-Lysine coating

To facilitate optimal adherence of the cells, well plates have been incubated with PDL 1:500 in PBS over night at 37 °C. 100 µl were pipetted per well into a 96 well plate. For staining procedures, cover slips were transferred into a 24-well plate and covered with 500 µl PDL. Prior to the dissection, the PDL was removed, and the wells were washed 2x with PBS. The plates were incubated in DPBS for 10 min at 37 °C incubator. Afterwards, 180 µl or 1 ml PNGM was added to 96-well plates or 24-well plates per well, respectively.

Dissection

The pregnant mouse was anesthetized with a mixture of CO_2/O_2 and subsequently sacrificed with 100 % CO_2 before decapitation. The abdomen was soaked with 70% ethanol and the uterus was accessed through a midline incision in the abdomen and the peritoneum. By opening the uterus, embryos have been collected and transferred into a petri dish with 25 ml Hanks Balanced Salt Solution (HBSS) where they have been decapitated. A piece of the

medulla oblongata was removed for genotyping. Heads were collected in 2 ml tubes containing HBSS. The brain was taken out from the scull and conserved in 2ml Hibernate medium until the genotyping was completed. Cortices and hippocampi were prepared using a binocular with 4× magnification. The brains together with the Hibernate medium were poured into a 10 cm petri dish. The hippocampi and cortices from the same genotype were pooled in falcon tubes containing 10ml HBSS.

Dissociation

Subsequent to the dissection of the embryonal cortices and hippocampi, the following steps were performed under a laminar flow hood. After HBSS was aspirated, 1 ml pre-warmed Trypsin/EDTA (TE) was added, mixed by snipping and incubated in a 37 °C water bath for 6 minutes. Next, Trypsin/EDTA was removed by aspiration and 5 ml pre-warmed DMEM/F-12 + 10% FCS was added to the cortices and hippocampi. After they settled down, DMEM was aspirated and 1ml pre-warmed primary neuronal growth medium (PNGM) was added. The cortices and hippocampi were dissociated by pipetting up and down with a 1000 µl pipette followed by a narrowed pasteur pipette until homogenization. The cell suspension was diluted with 3ml PNGM.

Cell counting and plating

For cell counting, 10 µl trypan blue was mixed with 10 µl of the cell suspension and pipetted into the Neubauer Counting Chamber. Healthy cells were recognized by their transparent appearance under 10x optical zoom of the light microscope and counted in all the four outer quadrants of the Neubauer cell countig chamber. The volume of cell suspension *V* needed to achieve a seeding density of 50K was calculated according to the following equation:

V (cell suspension) = (50000 x cell number counted) / (number of squares x dilution)

2.2.7 Glutamate toxicity assay and Real Time Glo (RTG) of primary cortical neurons

Preparation

The glutamate stress viability assay was served to characterize the toxicity of the Bassoon mutation in primary neurons during glutamate excitotoxicity. The Real Time Glo was performed after 16 days in vitro (DIV). Neurons were plated to achieve a density of 50K cells per cm^2 in a white 96 well plate with glass bottom. The volume of the PNGM was adjusted to 150 µl. For background control, 150 µl of preconditioned media of WT and MUT cells were used.

Real Time Glo

5 ml fresh PNGM was mixed with the RTG NanoLuc Substrate and the NanoLuc luciferase. 50 µl of the solution were distributed to each well. Neuronal cultures were transferred into the Spark 10M multimode microplate reader (Tecan) that comprises an incubation chamber with settings at 37 °C and 5 % CO_2. Luminescence was acquired every 30 min over a total time period of 24 h.

Glutamate stimulation

After an equilibration period of the luminescence signal of 11 cycles, glutamate was added in different concentrations. A 100 µl solution was prepared for each condition as follows:

Table 14: *Preparation of glutamate dilutions*

Condition	Glutamate V	PNGM V	PBS V
100 µM	8 µl (50 µM stock)	92 µl	
2 mM	8 µl (1mM stock)	92 µl	
Control		92 µl	8 µl

Five µl of the corresponding solution were added per well to obtain the indicated concentration. 2 mM glutamate were used as a maximum death control to verify the reliability of the assay and PBS was used as a vehicle control. 5 technical replicates per condition were measured. According to figure 4 the amount of luminescence produced in each well was used as a marker for cell viability.

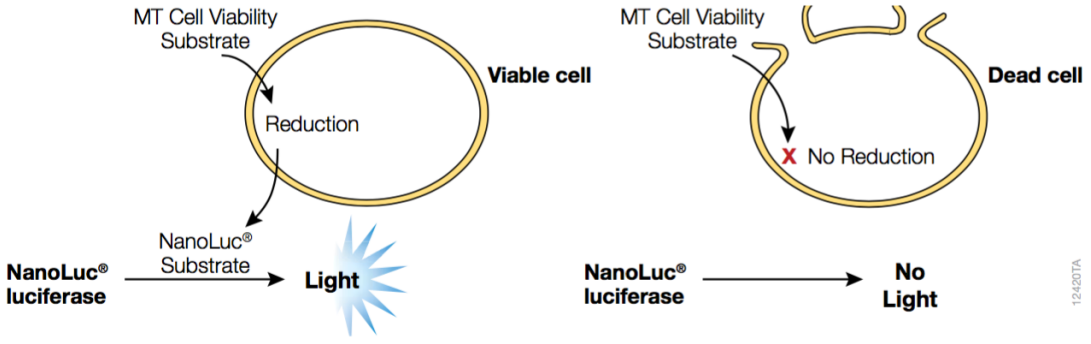

Figure 4: Real Time Glo reaction *The MT Cell Viability Substrate is reduced by viable cells. The NanoLuc luciferase reacts with the reduced Nano Luc Substrate to produce luminescence. The luminescence is proportional to cell viability and correlates negatively to neuronal toxicity (Promega).*

2.2.8 Immunocytochemistry of primary neurons and N2a cells

Immunocytochemistry was performed with embryonal primary cortical neurons after 14-18 days in vitro (DIV) or N2a cells 48 h post-transfection. For immunofluorescence, cells were cultured to a confluency of 50-60 % on PDL-coated coverslips in a 24-well plate. Cells were washed with cold PBS and incubated in 4% PFA for 10 minutes. Afterwards, PFA was removed and the fixed cells were washed with PBS. Next, the cells were permeabilized with 0.3 % Triton in PBS for 2.5 min. Then, 3 % normal donkey serum (NDS) in PBS was added to the cells for 30 min to block unspecific binding sides of the antibodies. The cover slips were incubated in the first antibodies for 1 hour in a wet chamber. After a PBS washing step, the secondary antibodies were incubated in 3% NDS in PBS for 1 h. The primary and secondary antibodies are listed in table 9 and table 10. Prior to mounting the coverslips with 4',6-diamidino-2-phenylindol (DAPI), a fluorescent DNA marker, containing mounting media cells were washed with 1x PBS and distilled water.

Confocal Image acquisition of primary cortical neurons

All images were acquired with the Zeiss LSM 700 Confocal microscope under 63x magnification (1440x1440 pixels, 8 bits bit depth). Digital gain was set to 1. Pinhole was adjusted to 1 airy units and the channels were set up as follows.

***Table 15**: Confocal settings for immunocytochemistry*

	Laser intensity %	Digital gain	Master gain
Bassoon 647	2	1	617
NeuN 488	2.4	1	660
Proteostat	3	1	630
DAPI	2.6	1	670

Z stacks were obtained for the quantification of Bassoon mean fluorescence intensity (MFI).

Soma/ axon ratio of Bassoon MFI in primary cortical neurons

CZI files were loaded into ImageJ. After maximal intensity projection, the soma and the axon were independently selected as a region of interest (ROI) in the NeuN channel, and the MFI was obtained in the Bassoon channel.

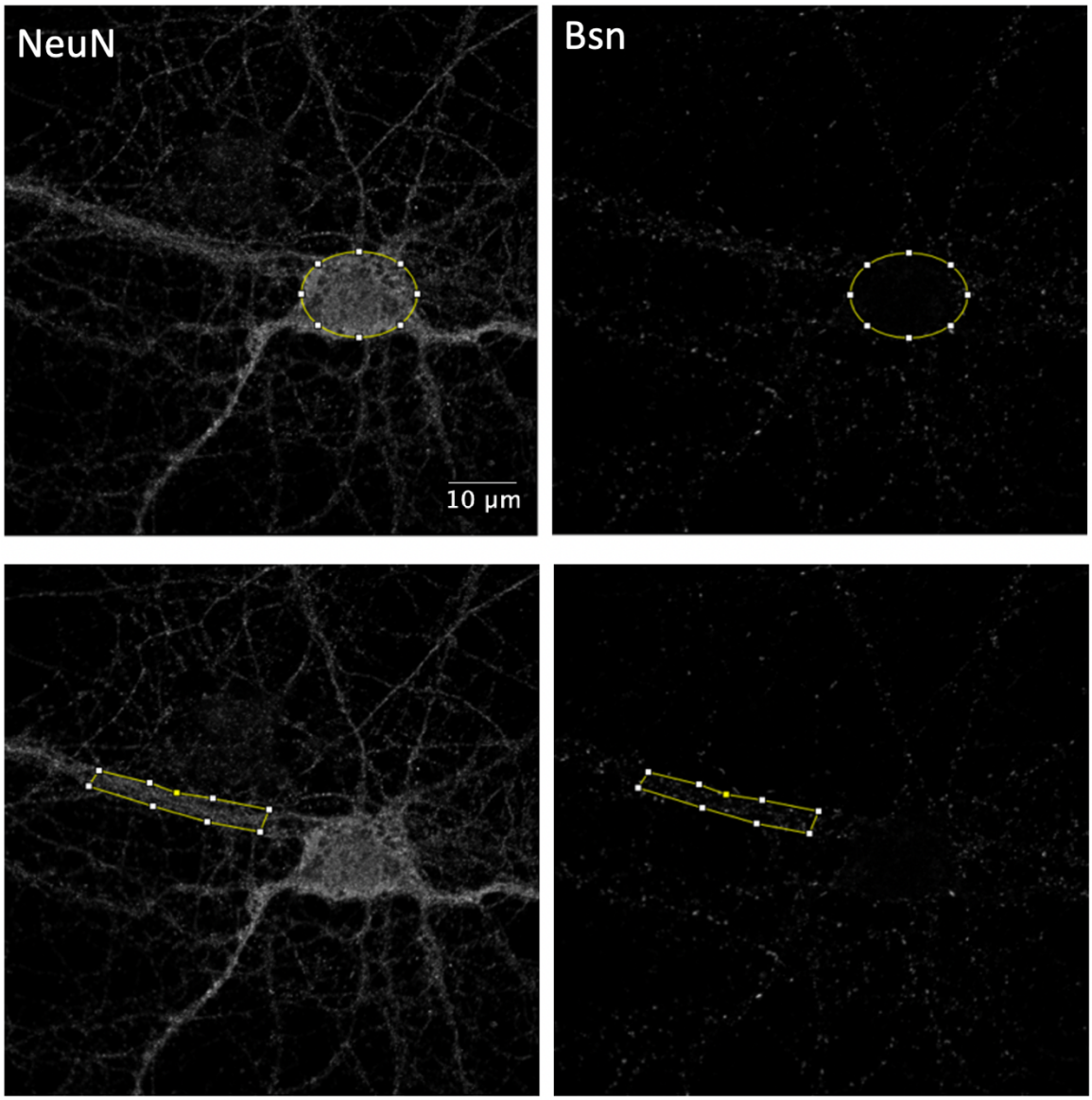

Figure 5: MFI measurements in primary neurons *Representative images for ROI selection in the somatic and the axonal compartment of the neuron, 63x,* scale bar is set to 10 µm

Aggresome count in primary cortical neurons

Aggresomes were identified by their punctually intense signal that can be distinguished from the Proteostat background signal. The number of aggregates per cell was counted manually.

In Vivo Methods

2.2.9 Laboratory animals

All mice were bred at the central animal facility at the University Medical Center Hamburg-Eppendorf. The animals were supplied with food and water ad libitum. The EAE mice were transferred into the institute two weeks before the start of the experiment for habituation. The Bassoon MUT mice, carrying the Bassoon mutation P3882A, were generated and bread at the central animal facility at the University Medical Center Hamburg-Eppendorf. The cages were individually ventilated, and the mice were housed under specific pathogen free conditions. The local ethic committee (Behörde für Soziales, Familie, Gesundheit und Verbraucherschutz in Hamburg) approved all the experiments conducted, TVA Nr. 122/17.

2.2.10 EAE induction

EAE was induced in C57BL/6 WT and Bassoon P3882 MUT mice. The mice were first anesthesized with 4 % isolflurane introduced with a 4 % flow that was reduced to 1,5 % for maintenance. The mice were then injected subcutaneously with 200 µg of $MOG_{35–55}$ peptide (Schafer-N) in complete Freund's adjuvant (CFA) (Difco, catalog no. DF0639-60-6) containing *Mycobacterium tuberculosis* (4 mg/ml) (Difco, catalog no. DF3114-33-8). They received 100 µl of 200 ng/100 µl pertussis toxin (PTX) i.p. The injection of PTX was repeated after two days. MOG – CFA injections were performed by Dr. Dr. Jan Broder Engler.

2.2.11 EAE scoring

The mice were weighed and scored daily, their appearance and body condition were documented. Mice that lost more than 25 % of their initial weight, as well as mice who received an EAE score of 4 or of 3.5 for more than seven days, were euthanized according to the regulations of the local animal welfare act. From the onset of motor symptoms, the mice received fleece mats and soft food to support their ability to process food and to move within the cage. The experiment was ended on day 30 post immunization.

According to the anticipated sequence of motor dysfunction in the B57BL/6 mice the following scoring system was established. The investigators were blind to the genotype. Animal scoring was independently performed by both Dr. Dr. Jan Broder Engler and myself.

Table 16: *Clinical criteria for the EAE score*

Score	Criteria
0	Tail of mice can be moved upwards, or mice pass the grid test and use the tail for climbing
1	Tail of mice cannot be upwards, and they do not use it for climbing
2	Walking on the grid, hind limbs fall from time to time or appear stiff
2.5	Hind limbs obviously fall down from the grid or slip, or mice start to toddle
3	Mice start to pull their legs behind them walking only with front paws
3.5	Mice are not able to move their hind limbs and are depressed
4	Mice are not able to use their hind and front limbs
5	Complete paralysis of the body or dead mouse

2.2.12 Histology

Perfusion

Perfusion was performed on day 30 of the EAE on 6 representative mice out of each cohort by Dr. Dr. Jan Broder Engler. For the histological analysis of Bassoon in aged mice 18- and 20-month-old Bsn-MUT and Bsn-WT mice were perfused. Kryosections were made from the tissue of the perfused mice and the aged mice cohort. The mice were deeply anaesthetized with a sublethal dose (over 10 µl/kg) of Ketamin/Xylazin (12 mg Ketamine, 1.6 mg Xylazin per 1 ml 0.9% NaCl). After establishment of deep anesthesia, the perfusion of the animals was performed by the biotechnical assistant. The thoracic space was accessed through the abdomen by cutting the diaphragma open and exposing the heart underneath

the rib cage. The heart was fixed with a forceps followed by the disruption of the right auriculum. The perfusion needle was inserted carefully into the apex of the left ventricle. PBS was infused for 90 s followed by an infusion of 4 % PFA for 4.5 minutes. The discoloration rate of the liver and the stiffness of the tail correlate to the perfusion efficiency. The brains and the spinal cords of the perfused animals were extracted and further kept in PFA for 30 min and then transferred into a 30 % saccharose solution until they were embedded in Tissue-Tek (Sakura Finetek USA, Torrance, CA).

Kryosections

The embedded brains and spinal cords were cut into 12 µm thick slices in a cryostat (L CM1850) and mounted on Super Frost Plus microscope slides (Fisher Scientific).

Immunohistochemistry

Immunohistochemistry was performed on the cryosections from the Bsn-Mut Bsn-WT EAE tissue and on the aged mice cohorts. The sections from the -80 °C storage were thawn for 30 min at room temperature. Slices were washed with aq. dest. before permabilization with 0.1 % Triton and blocking with 10 % normal donkey serum (NDS) for 30 min at room temperature followed by a washing step with PBS. The sections were incubated with primary antibodies overnight in 3 % NDS at 4 °C. After a PBS washing step, the secondary antibodies diluted in PBS with 3 % NDS were applied and incubated on the slices at room temperature for 3.5 h. The primary and secondary antibodies are listed in table 9 and table 10. Sections were subsequently washed with PBS and aq. dest. and mounted with 4',6-diamidin-2-phenylindole (DAPI) containing mounting media. Images were acquired with a Zeiss LSM 700 confocal microscope.

Confocal image acquisition

The slices were visualized using a Zeiss LSM 700 confocal microscope (1024x1024 pixels, bit depth: 8). Pinhole was set to 1 AU (Airy units). Channels were set up as follows:

Table 17: *Confocal settings for immunohistology*

	Laser intensity %	Master Gain	Digital gain
NeuN 488	2	523	1
Bassoon 647	2	589	1
DAPI	2	511	1

Confocal image acquisition for EAE

For neuronal count of the EAE tissue, tile scans picturing both ventral horns were made under 20x magnification. Tile scans showing all cortical layers of the margo cerebri superior were taken. Z-stacks of ventral horn were obtained under a 40x magnification with the oil immersion objective under the settings in table 17.

Confocal image acquisition for aged mice

Tile scans picturing all cortical layers from the margo cerebri superior were obtained from 4 independent slices of each animal for neuronal count and Bassoon MFI measurement under 20x magnification.

Picture analysis provided by the Image J software: MFI measurements of the Bassoon signal in EAE spinal cord neurons

All analyses were performed blinded with respect to the genotype. CZI files were loaded into Image J. The contrast of all images was enhanced equally by 0.3 % for the ROI selection. Multiple ROIs from both ventral horns were selected from the Z level with the highest intensity as portrayed in figure 6 and the fluorescence intensity, as well as the area were measured. Background intensity of all samples was measured and subtracted from the MFI values of all ROIs. A mean value for every animal was calculated.

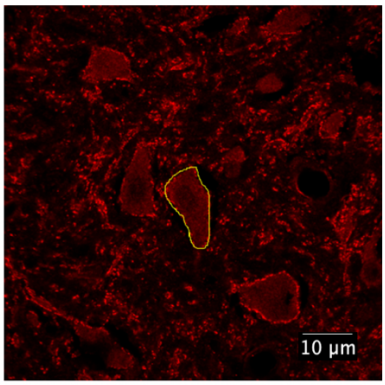

	Label	Area	Mean	Min	Max	IntDen	RawIntDen
1	299 sc bsn 647 z strack 1.czi:c:1/3 z:3/5 - 299 sc bsn 647 z strack 1 #1	572.747	18.458	2	62	10571.535	432775

Figure 6: **ROI selection of neurons in the ventral horn and MFI measurement in the Bassoon channel** *MFI measurement in the selected ROI, scale bar represents 10µm*

Picture analysis provided by the Image J software: Neuronal count in the ventral horn

Neuronal count in the ventral horn was performed on tile scans of the spinal cord. A line marking the ventral horn was drawn. Using the cell count plugin, the number of NeuN+

neurons in the ventral horn was recorded according to figures 6 and 7. Spinal cord neurons were identified by the NeuN staining (green).

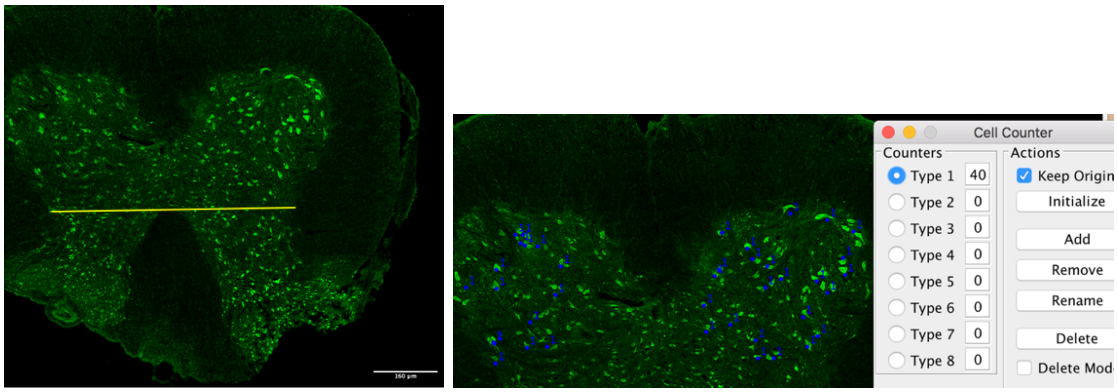

Figure 7: Marking of the ventral horn area for neuronal count *The scale bar represents 160* µm

Cortical neuron count in brains of EAE mice, adult and aged mice

Tile scans showing all cortical layers of the margo superior cerebri were loaded as CZI files into Image J. Up to 4 independent brain slices from each animal were analyzed. ROIs containing all cortical layers were selected and the area of the ROIs were measured. An intensity threshold of approximately 100-255 and a size threshold of 30-400 were set for particle analysis. The number of particles analyzed was then normalized to the area selected. Afterwards, a mean value was calculated for each animal.

Quantification of Bassoon MFI in the cortices of aged mice and EAE mice

An intensity and size threshold of the NeuN signal was used to define the coordinates of cortical neurons. For each defined coordinate the MFI was measured in the Bassoon channel after the channels were split and the NeuN channel was removed. A mean for each slice and then for each animal was calculated.

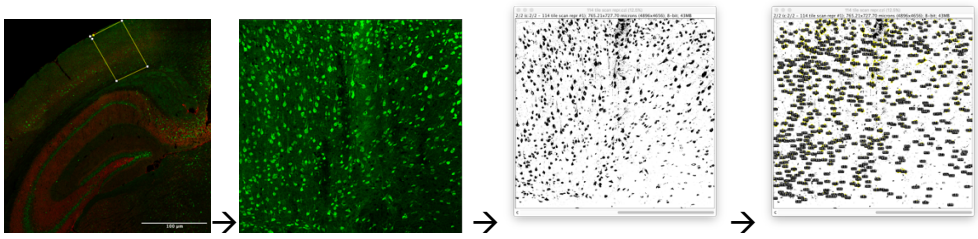

Figure 8: ROI selection and Threshold setting in the cortex for particle analysis

2.2.13 Bassoon P3882A genotyping

EAE mice or mouse embryos used for the preparation of primary neuronal cultures were genotyped. EAE animals were re-genotyped at the end of the experiment for quality control.

PCR reaction

Ear biopsies obtained from the EAE mice and the medulla oblongata from the mouse embryos were first lysed in 50 µl Quick Extract TM DNA Extraction Solution at 65 °C for 6 min at 500 rpm followed by a second heating step for 2 min at 98 °C at 350 rpm. A master mix including H_20, dNTPs, forward and reverse primers, Dream Green Buffer and the Dream Green Taq polymerase was prepared and distributed to the reaction wells. After the addition of the samples including positive and negative control and water the PCR reaction was started in the Thermo Cylcer as follows:

94 °C 2 min
94°C 30 s
66°C 30 s
72°C 30 s
72°C 5 min

Agarose gel preparation

A 1.5% agarose Gel was prepared in 1X tris-acetate-EDTA Buffer and boiled for approximately 2 min until the agarose was completely dissolved. Roti-Safe Gel Stain was added (1:500) and filled into the gel chambers. The Agarose solution was then kept in 4 °C for approximately 40 min allowing the agarose to polymerize.

Restriction enzyme reaction

Subsequent to the PCR reaction, the amplified Bassoon DNA was digested with the PspII restriction enzyme which was prepared in a master mix containing H_20 and the FastDigest Green Buffer (Thermo Scientific) for 45 min in 37 °C.

Gelelectrophoresis

After the restriction enzyme reaction was completed the gel pockets of the agarose gel were filled with 20 µl of the sample. The gel was run at 150-180 mV for approximately 20 minutes. The gel bands were recorded, documented and analyzed utilizing Adobe Photoshop CS6.

2.2.14 Nuclei isolation und flow cytometry frequency analysis

The isolation of nuclei and the measurement of NeuN frequency by flow cytometry was performed with the tissue of PFA perfused animals or Tissue Teq embedded spinal cords and brains from EAE and aged mice. To quantify the frequency of NeuN positive nuclei in the brains and spinal cords of EAE and aged mice, nuclei were isolated as follows:

Harvesting of the tissue and nuclei isolation

The nuclei incubation buffer was prepared using the ingredients from table 18. First, the Tissue Teq was thawn and the tissue was washed in PBS. The cortex was isolated from one hemisphere. The cortices or spinal cords were cut into 1x1 mm pieces and kept in 2 ml cold EZ Buffer on ice. Each sample was homogenized in 2 ml EZ Buffer using 25x strokes of a loose and a tight potter. The homogenate was transferred into a 15 ml falcon and mixed by inversion. This was followed by an incubation period of 5 min on ice. Next, the homogenate was centrifuged for 5 min with 500 g at 4 °C. Afterwards, the pellet was resuspended in 2 ml cold EZ buffer. Prior to the second centrifugation step, the suspension was incubated again for 5 min on ice. The pellet was resuspended in 2 ml cold Nuclei Incubation Buffer and then centrifuged. The suspension was transferred into a FACS tube using a 30 µm pre-separation filter.

Staining for Flow Cytometry

Prior to the antibody incubation the suspension was centrifuged, and the pellet was resuspended in 300 µl nuclei incubation buffer containing Hoechst and a NeuN Alexa Fluor647-labeled antibody (Abcam), both in a 1:1000 dilution. The incubation was maintained for 15 minutes, then the suspension was centrifuged and resuspended in 500 µl nuclei incubation buffer. Frequencies of NeuN-positive nuclei were acquired on a LSR II FACS analyzer (BD Biosciences) and analyzed using the FlowJo v10 software.

Flow Cytometer Gating

A Gating for single Nuclei (DAPI) and a NeuN positive population was set up as shown in figure 9.

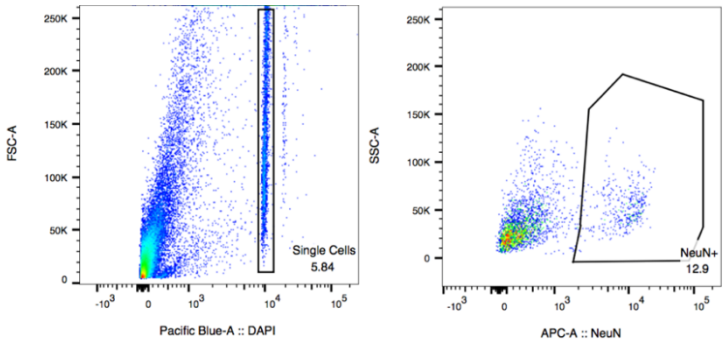

Figure 9: Gating strategy for single NeuN+ nuclei

Table 18: *Nuclei Incubation buffer*

	Final concentration	**Stock concentration**	**100 ml**	**150 ml**
Sucrose	340 mM	1 M	34.5 ml	51.6 ml
MgCl2	2 mM	500 mM	0.4 ml	0.6 ml
KCl	25 mM	1 M	2.5 ml	3.75 ml
Glycerophosphate	65 mM	1 M	6.5 ml	9.6 ml
Glycerol	5 %	100 %	5 ml	7.5 ml
EDTA	1 mM	0.5 M	200 µl	300 µl
BSA	1 %	100 %	1 g	1.5 g
H2O			100 ml	150 ml

2.2.15 Quantification of brain atrophy in 10-month-old mice

All mice were first anesthesized using mixture of 20 % O_2 and 80 % CO_2 and then killed with 100 % CO_2. Before dissection the body weight was obtained. Mice were perfused with 10 ml 1X PBS by Dr. Dr. Jan Broder Engler. Subsequently, the scull and the spine were opened, and the brain and the spinal cord were removed. Afterwards, the brain weight was taken.

2.3 Statistical analyses

All statistical analyses were conducted in GraphPad Prism 5.0. Tests were performed two-sided with a p-value <0.05 considered significant. Both paired and unpaired t-tests were used according to the experimental setup, taking into account dependencies within different runs of experiments. Mann-Whitney-U-tests were chosen when data were ordinally scaled. Fisher's exact tests were utilized to compare frequencies between groups.

3. Results

3.1 In vitro characterization of the Bassoon mutation P3882A

3.1.1 Effects of rat Bassoon P3875A overexpression on cell viability

The transfection of N2a cells with Bassoon WT has already shown toxic effects of the WT protein (Schattling et al., 2019). Increased molecular toxicity of Bassoon MUT compared to Bassoon WT was hypothesized.

To test for increased toxicity of Bassoon MUT compared to Bassoon WT, N2a cells were transfected with an EGFP-empty, a Bassoon WT and a Bassoon MUT construct. Afterwards, the cell viability was measured in a luciferase-based assay. N2a cells endogenously do not express Bassoon and therefore they cannot integrate the protein into their cellular function or into a destined cellular compartment (Rouillard et al., 2016). In the luciferase-based viability assay, luminescence produced via the Cell Titer Glo reaction is dependent on functional mitochondria that correlates with the cell viability, which was measured for EGFP only, EGFP-Bassoon WT and EGFP-Bassoon MUT transfected N2a cells (Fig. 10 a). Background luminescence was subtracted, and the raw values were normalized to EGFP-only transfected cells. The cell titer glow revealed a significant reduction of viability of EGFP-Bassoon MUT transfected cells compared to EGFP-Bassoon WT transfected cells using a paired t-test (p=0.0337) (Fig. 10 b). As follows, it can be assumed that the Bassoon mutation increases the molecular toxicity of the protein.

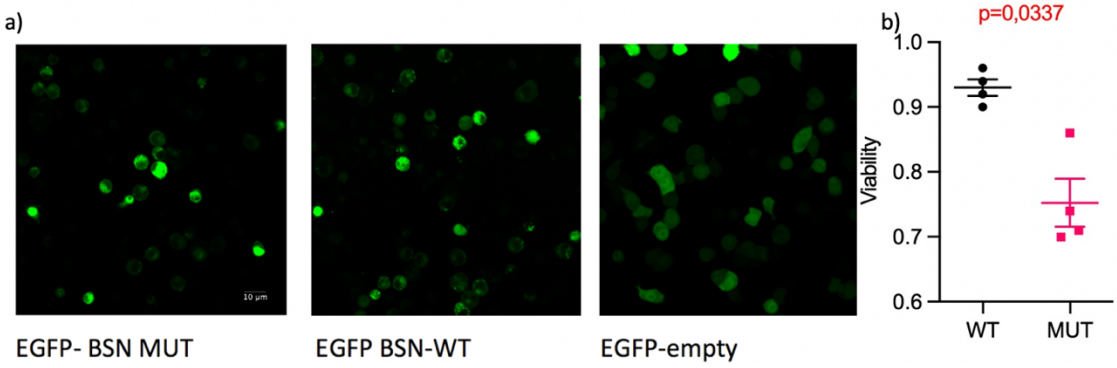

Figure 10*: *Viability of EGFP-Bsn WT, EGFP-MUT and EGFP-empty transfected and EGFP sorted cells *a) Representative image of EGFP Bassoon MUT, EGFP Bassoon WT and EGFP-empty vector transfected cells acquired with the confocal microscope, 20x, scale bar is set to 10* µm *b) Cell viability measured by the Tecan reader normalized to EGFP-only transfected cells, paired t-test, n=4*

3.1.2 Primary neuronal cell culture of Bassoon P3882A mutant mice

3.1.2.1 Glutamate excitotoxicity in Bassoon MUT primary cortical neurons

While an increase of Bassoon MUT toxicity has been shown in a transfection-based cell culture model, primary neuronal cell culture (PNCC) facilitated a characterization of cellular Bassoon MUT toxicity in a physiologically more adjacent environment. A glutamate stress assay was used to challenge Bassoon MUT neurons as glutamate toxicity might reinforce cellular Bassoon toxicity through multiple mechanisms: A glutamate enriched cellular environment causes an influx of calcium ions into neurons resulting in multiple downstream effects such as the activation of degrading enzymes, the downregulation of protective factors and a high level of ROS (Wang & Qin, 2010). Especially the latter might trigger or promote aggregation of a structurally unstable proteins by inducing misfolding (Dobson et al., 2020). Additionally, protective proteostatic systems such as chaperones, the UPS and the proteasome system might be overwhelmed (Hipp et al., 2019; Yabe et al., 2018). Assuming that Bassoon MUT primary neuronal cultures are more prone to aggregation, it is possible that the aggregation burden is greater in Bassoon MUT cultures compared to Bassoon WT cultures. As follows, this would lead to increased toxicity. The aim was to trigger a cellular Bassoon pathology in Bassoon MUT primary neurons with the underlying hypothesis that Bassoon MUT neurons are more prone to cell death upon excitotoxic stress due to the structural instability of Bassoon MUT (Gundelfinger et al., 2016; Schattling et al., 2019).

For this purpose, C57BL/6 mice were genetically modified to express the mouse Bassoon mutation P3882A that corresponds to the human Bassoon mutation P3866A**.** Embryonic neuronal cultures derived from homozygous Bassoon WT and Bassoon MUT embryos have been used for the glutamate excitotoxicity assays. Luciferase reaction was started right before the well plate was placed in the Tecan reader after adding the NanoLuc Enzyme and the NanoLuc Substrate to the cells. As the reduction of the NanoLuc Substrate by the NanoLuc Enzyme depends on the integrity of the mitochondrial electron transport chain, the amount of luminescence produced by the reaction in each well directly correlates with the proportion of viable cells. The luminescence was measured for 49 cycles in the Tecan reader and glutamate was added after 11 cycles, corresponding to 5 h. The reduction of cell viability in Bassoon WT and MUT primary neurons differed between the groups upon glutamate stimulation at all time points (Fig. 11 a). A significant difference in normalized cell viability could consistently be detected at time points 5 h ($p=0.0453$) (Fig. 11 b) and 10 h ($p=0.0342$) (Fig. 11 c) after glutamate stimulation, applying a t-test.

Hence, in this experiment, primary neurons of Bassoon MUT mice are more susceptible to glutamate induced excitotoxic stress, supporting the hypothesis that the Bassoon MUT leads to a structural destabilization of Bassoon and thereby to an increased aggregation propensity. To further investigate this mechanistic hypothesis, Bassoon dislocation or accumulation within the neuron could be evaluated.

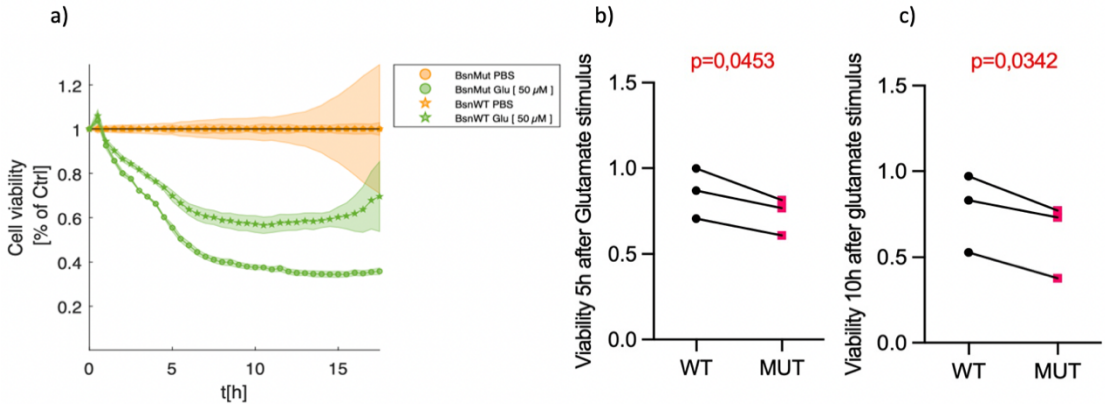

***Figure 11**: **Cell Viability of Bassoon WT and MUT primary cortical neurons E16.5 DIV 14-16 stressed with 100uM glutamate** a) Representative curve depicting cell viability over time after glutamate stimulation derived from one experimental replicate b) Cell viability 5h after glutamate stimulation, n=3, paired t-test. c) Cell viability 10h after glutamate stimulation, n=3, paired t-test*

3.1.2.2 Regional distribution of Bassoon in Bassoon mutant primary cortical neurons

Finding a mechanism behind increased toxicity in Bassoon MUT cell culture models would be an important step towards a better understanding of the role of the Bassoon mutation in the hereditary PSP-like syndrome and as well of Bassoon pathology in the context of EAE and MS. The hypothesis that the Bassoon mutation leads to a translocation of the protein from the presynapse to the soma could be a plausible explanation for Bassoon MUT toxicity upon glutamate excitotoxicity. It is conceivable that the mutation causes a structural destabilization of Bassoon impairing a transport to the presynapse via multiple mechanisms such as misfolding already occurring in the soma or an impeded CAZ preassembly (Friedman et al., 2000). This would not only result in aggregation mediated toxicity but also in a disturbance of the presynaptic homeostasis, due to the reduction of functional Bassoon in the presynapse (Hallermann et al., 2010).

To address the hypothesis of a translocation of Bassoon MUT from the presynapse to the soma of the neuron, primary cortical neurons were stained with a NeuN (Millipore) and a

Bassoon (Enzo) antibody after 14-16 DIV. The aim was to assess the cellular distribution of the immunofluorescent signal of Bassoon within neuronal compartments. For this purpose, a ratio between the Bassoon MFI in the soma and the MFI in the axon was calculated (Fig 12 a). A paired t-test did not reveal a significant difference in the distribution of the immunofluorescent signal (p=0.5778) (Fig. 12b). Consequently, there was no indication that a translocation of Bassoon MUT occurs in Bassoon P3882A primary neurons.

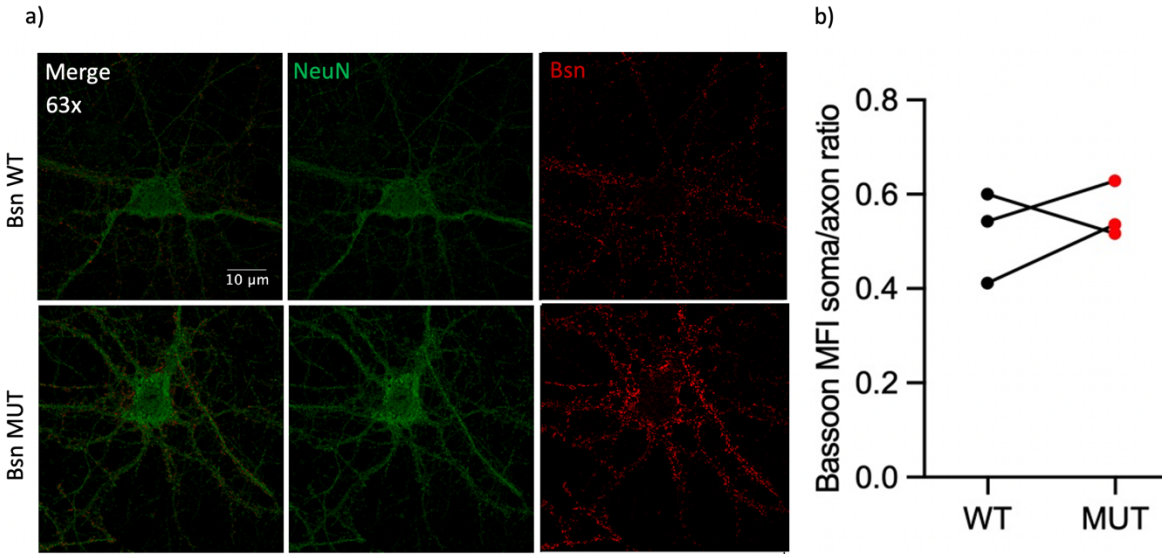

***Figure 12*: Subcellular localization of Bassoon in Bassoon WT and MUT cortical neurons E 16.5 DIV 14-16** a) *Representative images picturing immunocytochemical stainings of Bassoon and NeuN obtained under 63x magnification using Confocal microscopy, Bassoon in red, NeuN in green, scale bar is set to 10* µm *b) Bassoon MFI in the soma relative to Bassoon MFI in the axon, n=3, paired t-test*

3.1.2.3 Bassoon aggregation in Bassoon mutant primary cortical neurons

While there are strong indications for increased molecular toxicity of Bassoon MUT, a translocation within the neuron could not be detected in primary neuronal cell culture. As an increased propensity for aggregation in the Bassoon MUT neurons is, however, still a likely hypothesis (Schattling et al., 2019; Yabe et al., 2018) and aggregation might not necessarily be visible in a translocation assay, an aggregation detection dye was included to check for Bassoon aggregates in immunocytochemical stainings of Bassoon WT and MUT primary neurons.

Primary neuronal cell culture was derived from genetically modified mice that expressed Bassoon MUT. In this experiment, unstressed primary cortical neurons after 14-16 DIV were used to evaluate the aggregation propensity of the protein. For this purpose, neurons were

stained with the Proteostat aggregation detection dye which binds to insoluble and dense protein structures (Enzo) (Fig. 13 a). Within a strong background signal, aggregates were identified by their punctually intense signal.

Even in the absence of stressors, a significantly higher number of aggregates was detected in the soma of MUT cultures (p=0.0486) (Fig. 13 b), suggesting that the missense mutation has a notable impact on the tertiary structure of the protein. To correct for batch effects, a paired t-test was performed counteracting day to day variability in culture conditions that affected baseline neuronal aggregation load.

Thus, this experiment supports the hypothesis that the Bassoon mutation leads to a structural destabilization of Bassoon, increasing its susceptibility to aggregation. Subsequently, *in-vivo* experiments are needed to evaluate whether a clinical and pathological significance of the Bassoon mutation is existent.

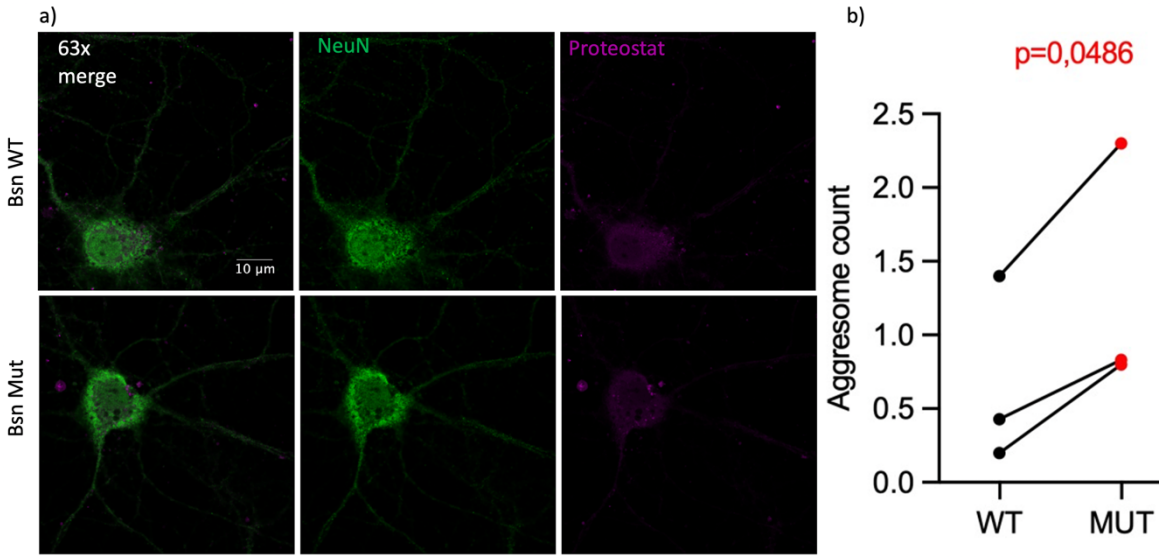

Figure 13: Aggresome count in Bassoon WT and MUT cortical neurons E16.5 DIV 14-16 *a) Representative images of immunocytochemical stainings of Bassoon, NeuN and the aggregation detection dye (Proteostat, Enzo), 63x, Bassoon in red, NeuN in green, Proteostat in magenta, scale bar is set to 10*µm *b) Aggresome count based on the aggregation detection dye, Bassoon WT vs MUT cortical neurons, n=3, paired t-test*

3.2 In vivo assessment of a developmental phenotype in adult Bassoon P3882A mutant mice

Given the implications to increased toxicity in Bassoon MUT cell cultures, *in-vivo* experiments are required to characterize the Bassoon mutation in a complex organism probing the clinical and histological significance.

3.2.1 Cortical neuronal density in adult 10-month-old Bassoon P3882A mutant mice

Before experimentally considering an age-dependent Bassoon MUT pathology, a developmental phenotype of the Bassoon mutation needs to be excluded. With this intention, a cohort of adult 10-month-old mice was examined with respect to neuronal abundancy using immunohistochemistry and flow cytometry of sorted neuronal nuclei as described for the aged mice cohort in 3.3.1 and 3.3.3. The cortices of the WT and the MUT group were analyzed as described above. Unpaired t-tests did not reveal significant differences in the neuronal density within the cortex and spinal cord, using immunohistochemistry in the cortex (p=0.3593), and flow cytometry for cortical (p=0.593) and spinal cord nuclei isolation (p=0.2334) (Fig. 14 a-c). As follows, there was no evidence for a developmental phenotype with respect to neuronal loss in adult Bassoon MUT mice.

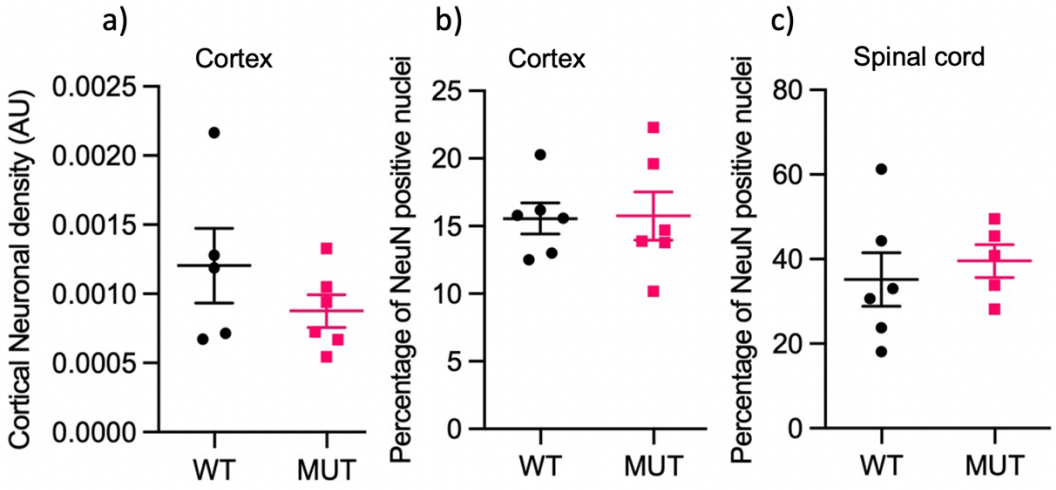

Figure 14: Quantification of neuronal loss in adult 10-month-old Bassoon WT and Bassoon MUT mice *a) Neuronal density in the cortex acquired via immunohistochemical count of NeuN positive cells per area in 10-month-old Bassoon WT (n=5) vs. Bassoon MUT mice (n=5), unpaired t-test, p= 0,3593 b) Percentage of NeuN positive nuclei isolated from the cortex of 10-month-old Bassoon WT (n=6) vs. Bassoon MUT (n=5) mice, unpaired t-test, c) Percentage of NeuN positive nuclei isolated from the spinal cord of 10-month-old Bassoon WT (n=4) vs. Bassoon MUT (n=5) mice, unpaired t-test*

3.2.2 Brain weight of adult 10-month-old Bassoon P3882A mutant mice

Since there was no early developmental loss of neuronal abundancy in adult Bassoon MUT mice in histology and flow cytometry, a quantification of brain atrophy was included subsequently. To assess whether general brain atrophy is already detectable in adult Bassoon MUT mice, the brain to body weight ratio in a 10-month-old Bassoon WT and Bassoon MUT mouse cohort was calculated comparatively. After the mice were first anesthetized with 20 % O_2 and 80 % CO_2, they were killed with 100 % CO_2 and the body weight was taken. The left ventricle of the heart was perfused with 10 % PBS before the CNS was extracted. Then, the brain was separated from the spinal cord directly caudal to the medulla oblongata and the brain weight was determined. Comparing the brain to body weight ratio between the Bassoon WT and Bassoon MUT cohort using a t-test, there was no significant difference (p=0.4478) (Fig. 15). As follows, there was also no macroscopic indication for a developmental phenotype in adult Bassoon MUT mice, allowing for the investigation of an age-induced pathology of Bassoon MUT.

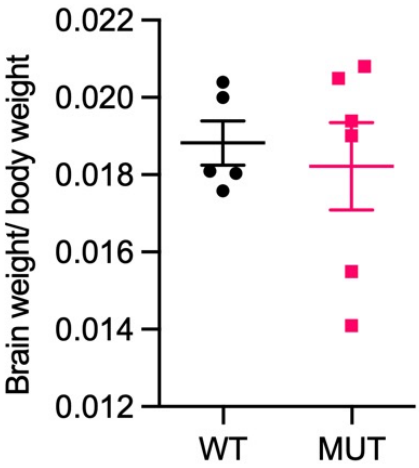

Figure 15: Brain weight to body weight ratio in Bassoon WT vs Bassoon MUT mice

Comparing the brain to body weight ratio in Bassoon WT (n=5) to Bassoon MUT (n=6) 10-month-old adult mice, there is no indication for a general brain atrophy induced by the Bassoon mutation in adult mice (unpaired t-test)

3.3 In vivo characterization of Bassoon P3882A in aged mice

3.3.1 Cortical neuronal density in aged 18-month-old Bassoon P3882A mutant mice

After the discovery of a Bassoon proteinopathy in MS (Schattling et al., 2019), the identification of the Bassoon mutation P3866A (human) in the context of an hereditary neurodegenerative disease (Yabe et al., 2018) further ignited the concept of Bassoon proteinopathy as a pathophysiological mechanism, accounting for neurodegeneration in MS and, potentially, also in aging. Given the age-dependent disease manifestation in the family members presented by Yabe et al (Yabe et al., 2018), it can be hypothesized that the mouse Bassoon mutation P3882A leads to a primary neurodegenerative pathology in aged mice,

potentially by accelerating physiological age-dependent Bassoon aggregation and neurodegeneration. A neurodegenerative effect of the mutation would facilitate the generation of an *in vivo* model to study Bassoon pathology in MS and aging.

The quantification of neuronal loss in aged mice in Bassoon WT and MUT cohorts served as a marker for neurodegeneration. To assess the neuronal abundancy in the cortices of both groups, NeuN count in immunohistochemical stainings was performed on coronary brain sections of 18-month-old mice. Animals were perfused with 4 % PFA, before brains were extracted for cryosections and stained with NeuN and Bassoon antibodies. Tile Scans in the NeuN channel served to select all layers of the cortex as a ROI to create a NeuN mask for particle measurement (Fig. 16 a). The cortical neuronal count was normalized to the area of the ROI. A significant difference in the density of cortical neurons could not be detected between the cohorts using a t-test (p=0.2338) (Fig. 16 b).

Thus, the results of the immunohistochemical quantification of neuronal loss did not reveal a neurodegenerative effect of the Bassoon mutation P3882A.

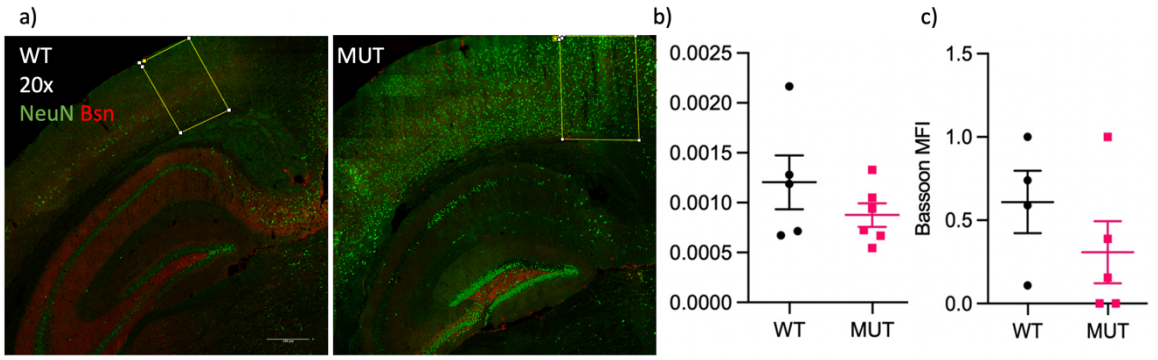

Figure 16:: Neuronal density and Bassoon MFI in the cortex of aged 18-month-old Bassoon WT and MUT mice *a) Representative images of a coronary section of the mouse brain picturing the ROI selection in Bassoon WT and MUT EAE animals, Bassoon signal in red, NeuN signal in green representing neurons, scale bar is set to 100* µm *b) Cortical density in Bassoon WT (n=5) vs Bassoon MUT (n=5) aged mice, unpaired t-test c) Bassoon MFI in NeuN puncta within the selected ROI in Bassoon WT (n=4) vs Bassoon MUT (n=5) mice, unpaired t-test*

3.3.2 Somatic Bassoon signal in cortical neurons in aged 18-month-old Bassoon P3882A mutant mice

Yabe et al have shown that the solubility of Bassoon MUT is decreased and Bassoon has been shown to form somatic deposits in EAE (Schattling et al., 2019; Yabe et al., 2018). Thus, it was hypothesized that age and a potential structural destabilization of the protein due to the point mutation trigger Bassoon accumulation in aged mice.

Testing for an increased Bassoon accumulation in Bassoon MUT mice, immunofluorescence served to quantify Bassoon enrichment in the soma of cortical neurons. The cryosections of brains from 18-month-old Bassoon WT and MUT C57BL/6 mice were stained with a Bassoon and NeuN antibody. Using the Image J software, a mask for NeuN+ events was created via fluorescence intensity and size and was then applied in the Bassoon channel to measure the MFI of Bassoon signal. For all NeuN coordinates within the ROI, the Bassoon MFI was measured. Comparing the MFI values between the WT and the MUT cohorts with a t-test, it cannot be concluded that the Bassoon mutation has influence on somatic Bassoon enrichment in 18 month old mice, as there was no significant difference ($p=0.8904$) (Fig. 16 c).

While physiological presynaptic Bassoon signal could be observed, signal resembling a somatic Bassoon deposition was not detected. A high heterogeneity in MFI values was observed. However, this experiment did not provide evidence for an age-dependent Bassoon accumulation in the cortices of Bassoon P3882A mice.

3.3.3 Frequency of NeuN+ nuclei in aged 18-month-old Bassoon P3882A mutant mice

An increase in age-dependent neuronal loss in Bassoon P3882A mice could not be shown using immunocytochemistry. To compensate for potential methodological limitations in immunohistochemistry a second experimental setting for the hypothesis, that neuronal loss is increased in aged Bassoon MUT mice, was included.

Flow cytometry of isolated nuclei was also included in the analysis of the aged mice cohort (Fig 17 a). A 1 mm^2 piece of the cortex from the margo cerebri anterior was used for the extraction of nuclei. The percentage of NeuN positive nuclei among the total number of extracted, DAPI marked nuclei in the cortex did not differ significantly between the cohorts using a t-test ($p=0.313$) (Fig. 17 b). The low mean percentages can be attributed to the reduction of immunoreactivity of NeuN with aging (PORTIANSKY et al., 2006).

One may conclude that using two experimental settings for the quantification of cortical neurons, there is no evidence for an increase in neuronal loss in 18-month-old Bassoon P3882A mice.

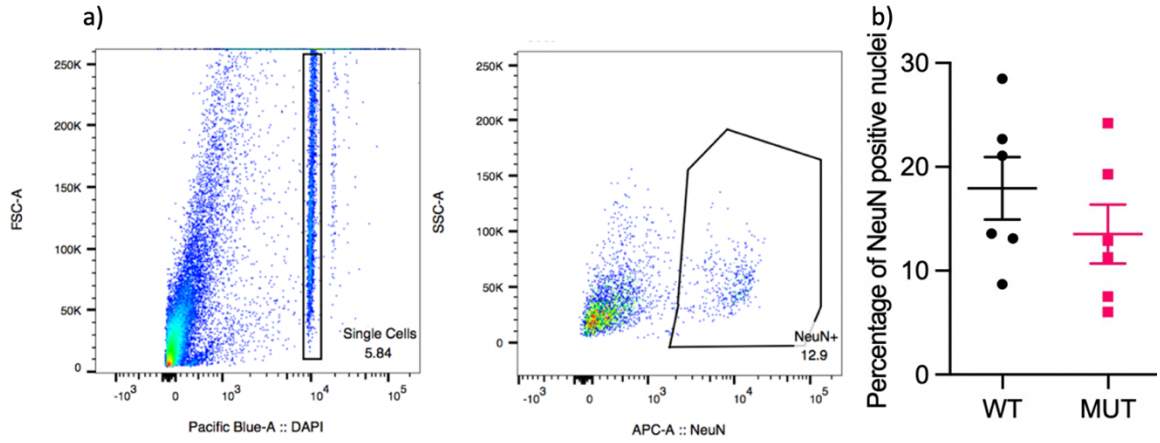

Figure 17: Frequency of NeuN+ nuclei by flow cytometry in the cortex of aged 18-month-old mice *a) FACS gating b) 18-month-old Bassoon WT (n=6) vs. Bassoon MUT (n=6) mice, unpaired t-test*

3.4 In vivo characterization of the Bassoon mutant mice in neuroinflammation

3.4.1 EAE phenotype of Bassoon mutant mice

Toxic somatic deposits of the presynaptic protein Bassoon have been detected in spinal cord motor neurons of EAE mice, and they have been shown to be more than an epiphenomenon in dying neurons, as they significantly contribute to disease severity (Schattling et al., 2019). As the toxic role of Bassoon WT accumulation for EAE has already been exposed, it was hypothesized that the severity of the EAE might be increased in Bassoon MUT mice. An impact of the Bassoon mutation on the EAE course would support the premise that the Bassoon proteinopathy is a key driver of neurodegeneration in neuroinflammation, since the mutation hypothetically further amplifies Bassoon pathology and exposes its structural instability.

Aiming to address this specific hypothesis, male and female C57BL/6 mice were immunized with MOG_{35-55} emulsified in CFA and the clinical disease course was monitored for 30 days on a daily basis. The acute phase of EAE in C57BL/6 mice is marked by a steady increase in disease burden until the symptoms peak on day 15. Following the acute phase, the animals enter a chronic phase in which symptoms are partially alleviated (Bittner et al., 2014).

In this MOG immunization based EAE model, mice expressing the Bassoon mutation P3882A did not exhibit an increased disease severity (Fig. 18 a, b). The cumulative EAE score represents the sum of EAE scores given to an individual animal over the course of 30 days. The cumulative scores of all WT and MUT animals were compared using a Mann-Whitney-U-test which revealed no significant difference (p=0.6833) (Fig. 18 b). The disease

courses of the WT and the MUT group are almost entirely overlapping except from day 15 which shows a small deviance from the MUT group towards a higher disease score. However, a Mann-Whitney-U-test did not reveal a significant difference in the disease scores of both groups on day 15 (Fig. 18 c; p=0.7956).

Thus, the clinical course of the MOG immunization based EAE in Bassoon P3882A did not indicate an increased severity in Bassoon MUT mice compared to Bassoon WT mice.

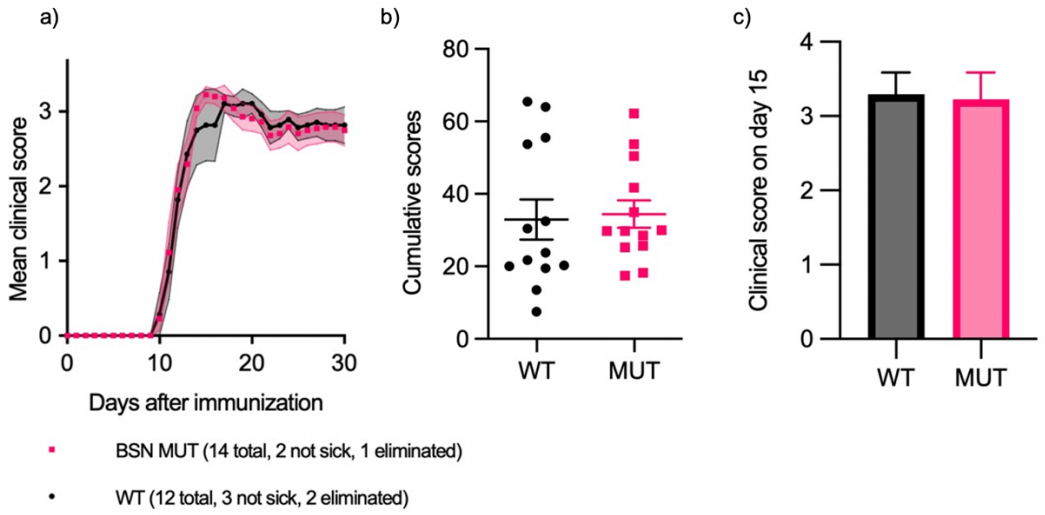

Figure 18: Clinical course of the EAE *a) visualization of clinical EAE course, b) Cumulative EAE scores Bassoon WT (n=13) vs Bassoon MUT (n=13) mice: Mann-Whitney-U-test c) Clinical score on day 15, Mann-Whitney-U-test*

3.4.2 Incidence and mortality in Bassoon mutant mice

Importantly, not all mice developed an encephalomyelitis following immunization. Moreover, there was a high interindividual variability in disease course and severity. Assuming that toxic protein aggregation plays a significant role in the disease, an increased propensity for aggregation of Bassoon MUT compared to Bassoon WT would render neurons more prone to neuronal damage in the state of inflammation. Hypothetically, this could affect both incidence and mortality in the EAE model. For this reason, mortality and incidence were compared between the WT and MUT cohort. Comparing both parameters between the cohorts with a Fisher's exact test, there was no significant difference in the mortality (p=0.44) and EAE incidence (p=0.88) (Fig. 19 a, b).

Thus, the mortality and incidence derived from this EAE did not provide support for the hypothesis that the Bassoon mutation increases the clinical disease severity or that it promotes the clinical onset of the disease.

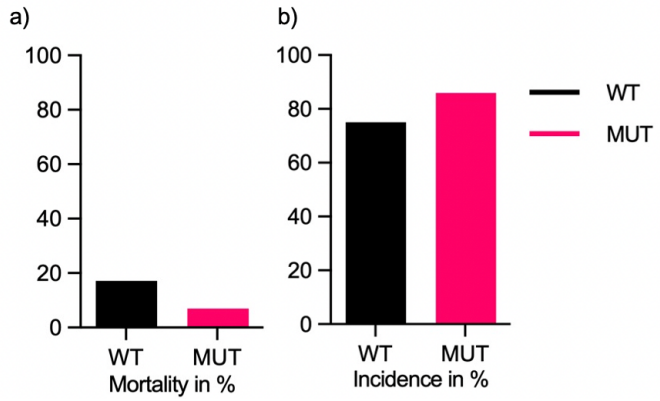

Figure 19: Mortality and incidence *a) EAE mortality in Bassoon WT (n=12) vs Bassoon MUT (n=14) mice, Fishers exact test b) EAE incidence in Bassoon WT (n=12) vs Bassoon MUT mice (n=14), Fisher's exact test*

3.4.3 Somatic Bassoon deposition in Bassoon mutant mice

Although a clinical difference between the WT and MUT cohort in EAE could not be identified, it is conceivable that there is a subclinical phenotype of the Bassoon mutation in immunohistology. WT EAE mice develop strong somatic Bassoon accumulation and aggregation that can be observed during the acute phase (day 15) and the chronic (day 30) phase of the disease (Schattling et al., 2019). The hypothesis was that the neuronal aggregation load might be further increased by the mutation. Such an effect could hypothetically be explained by a decrease of protein solubility in Bassoon MUT (Yabe et al., 2018).

Immunohistological analysis served to look for a subclinical phenotype of the Bassoon mutation. Spinal cords extracted on day 30 of the EAE from MOG immunized C57BL/6 mice served to compare the somatic Bassoon signal of ventral horn motor neurons between WT and MUT animals. Mice were perfused with 4 % PFA and cryosections were obtained for immunohistochemical stainings using a monoclonal Bassoon antibody and NeuN as a neuronal marker. For each animal, multiple independent MFI values were obtained from ventral horn neurons selecting the soma as the ROI. A significant difference in Bassoon MFI in ventral horn neurons could not be detected using a t-test (p=0.5404) (Fig. 20).

Consequently, the results of immunohistochemistry did not support the hypothesis that somatic Bassoon accumulation is increased in the spinal cord of Bassoon P3882A mice in EAE. However, it is still possible that neuronal loss in the spinal cord might be increased in the MUT cohort through distinct mechanisms.

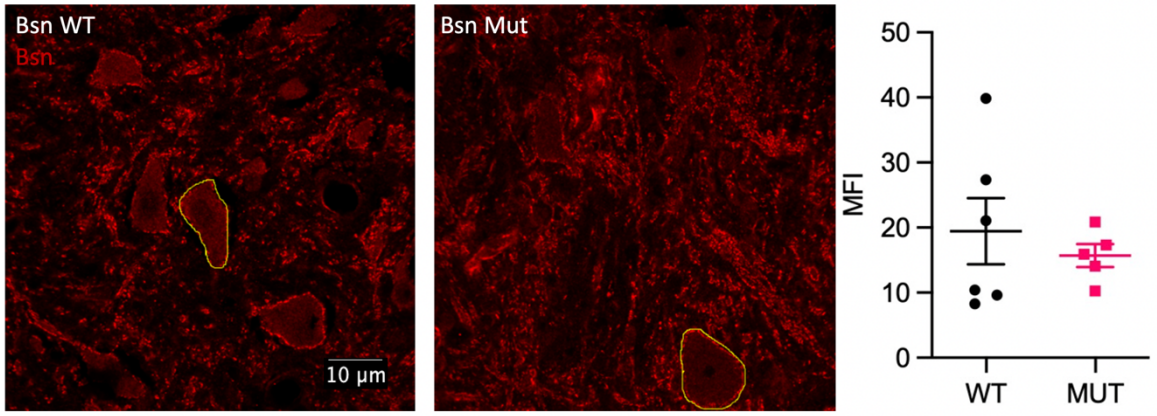

Figure 20: Representative images of neuronal Bassoon signal on day 30 of EAE *Bsn in red in 40x magnification; unpaired t-test, Bassoon WT (n=6) vs Bassoon MUT(n=5) mice*, scale bar is set to 10 µm

3.4.4 Neuronal loss in the ventral horn of Bassoon mutant EAE mice

Loss of motor neurons is a major histological signature in EAE (Bittner et al., 2014). Toxic bassoon accumulation is observed in motor neurons (Schattling et al., 2019), indicating that Bassoon deposition and aggregation could be a key driver in ventral horn neuronal loss during EAE. Hence, one could deduce that a mutation that might increase the toxicity of Bassoon might also lead to an enhanced neuronal decay.

Following this hypothesis, NeuN stained tile scans of day 30 EAE spinal cord cryosections were used to quantify the total neuronal count in the ventral horn using the cell counter tool in Image J (Fig. 21 a). There was no significant difference detectable between the cohorts using a t-test (p=0.0631) (Fig. 21 b). To increase the animal number for the detection of neuronal loss, tissue from an independent EAE that was performed under the same conditions by Dr. Dr. Jan Broder Engler was included for immunohistological analysis. The results were pooled for statistical analysis that revealed no differences between the groups using a t-test (p=0.3119) (Fig. 21 c).

In consequence, an increased neuronal loss located in the spinal cord of Bassoon P3882A mice during EAE was absent.

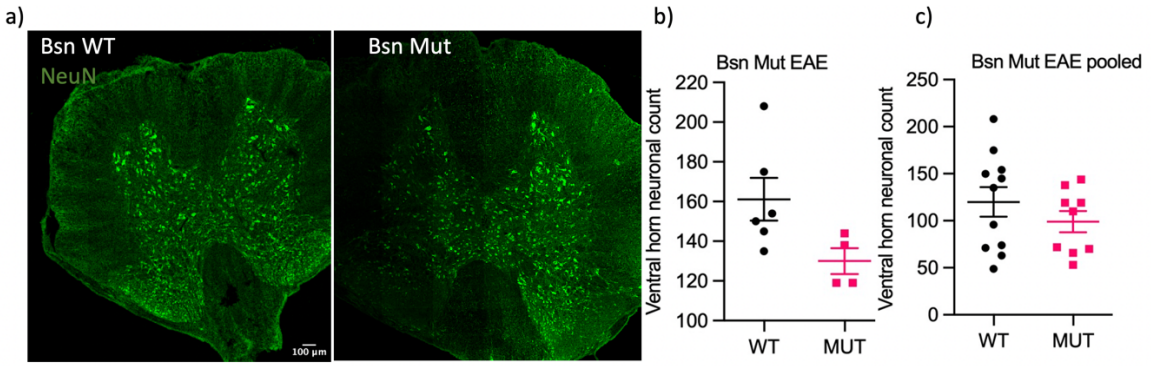

***Figure 21**: **Neuronal count in the ventral horn on day 30 of EAE** a) Representative images of spinal cord tile scans in 20x magnification, NeuN in green, scale bar is set to 100 µm b) Ventral horn neuronal count in Bassoon WT (n=6) vs Bassoon MUT (n=5) mice, unpaired t-test, c) Ventral horn neuronal count pooled with a previous EAE in Bassoon WT (n=10) vs Bassoon MUT (n=9) mice, unpaired t-test*

3.4.5 Cortical neuronal density in Bassoon mutant EAE mice

As the pathology of the reported PSP patients expressing mutated Bassoon was primarily located in the brain (Yabe et al., 2018), it is possible that the Bassoon mutation triggers an enhanced EAE pathology in the cortex.

With the intention to investigate this hypothesis, cortices of EAE mice were included for immunohistochemical analysis of neuronal loss. C57BL/6 MOG immunized mice develop histopathological lesions all over the CNS that seem to occur simultaneously in the acute phase (Bittner et al., 2014). Here, the aim was to investigate whether the Bassoon mutation triggers an increase in EAE induced neuronal loss and Bassoon accumulation in the brain. Coronary slices were obtained from d30 EAE tissue that was previously perfused with 4 % PFA. Tile scans of the parasagittal cortical zone were taken under 40x magnification. All cortical layers were analyzed within a selected ROI (Fig. 22 a). Using the Image J cell counter plug-in, the number of cells per area was calculated for each sample. There was no significant difference in the density of NeuN positive events found between Bassoon WT and MUT using an unpaired t-test (p=0.128) (Fig. 22 b).

Thus, a difference in neuronal loss located in the cortex of Bassoon WT and Bassoon MUT mice during EAE was not detectable using immunohistochemistry.

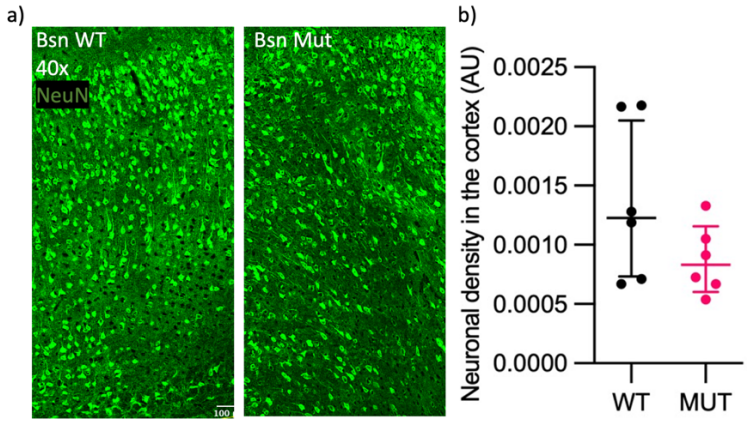

***Figure 22**: **Neuronal count in the cortex on day 30 of EAE** a) Representative picture of the cortical neuron count in 40x magnification, NeuN in green, scale bar is set to 100* µm *b) Neuronal density in the cortex in Bassoon WT (n=6) vs Bassoon MUT mice (n=6) on EAE day 30, unpaired t-test*

3.4.6 Frequency of NeuN+ nuclei in the cortex and ventral horn in Bassoon mutant EAE mice

To investigate the effect of the Bassoon mutation on neuronal loss in the EAE more robustly, neuronal abundancy in the spinal cord and cortex was quantified using flow cytometry of isolated neuronal nuclei. For this purpose, nuclei were isolated from cortices and spinal cords of d30 EAE tissue and stained with a NeuN antibody and DAPI as a nucleus dye. The percentage of NeuN positive nuclei among the total number of DAPI+ nuclei was assessed by flow cytometry for each animal (Figure 23 a, b). Applying an unpaired t-test, the analysis did not reveal a significant difference in neuronal loss between the cohorts in the spinal cord (p=0.2334) and in the cortex (p=0.3994) (Fig. 23 c, d).

Consequently, using two distinct experimental approaches, there was no detectable difference in neuronal loss in the spinal cord as well as in the cortex between Bassoon WT and Bassoon MUT mice during EAE.

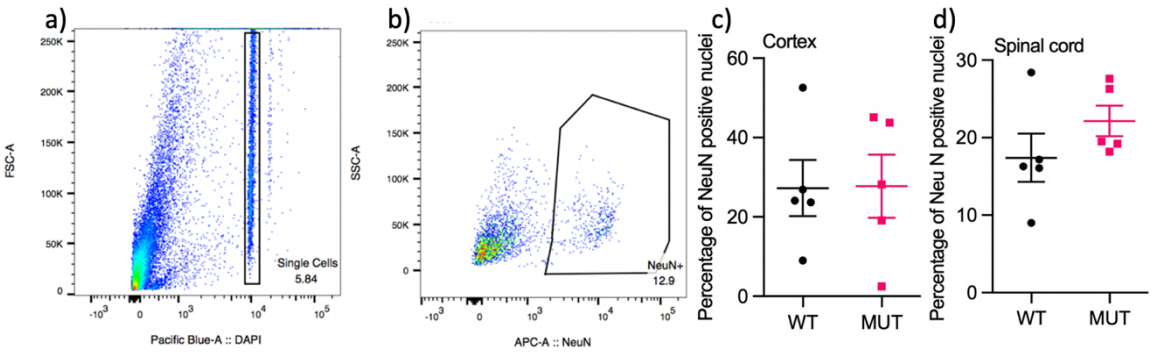

Figure 23: The abundancy on NeuN+ nuclei isolated from cortex and spinal cord tissue on day 30 of EAE *a) Representative image of FACS gating for DAPI signal representing all nuclei b) Representative image of FACS gating for NeuN signal representing neuronal nuclei c) percentage of NeuN+ nuclei in the cortex of EAE animals on day 30, Bassoon WT (n=5) vs MUT mice (n=5), unpaired t-test d) percentage of NeuN+ nuclei in the spinal cord of EAE animals on day 30, Bassoon WT vs MUT mice, unpaired t-test*

4. Discussion

4.1 The toxicity of the Bassoon mutation in transfected N2a cells

The first aim of this work was to investigate the toxicity of the Bassoon mutation in cell culture. The transfection of Bassoon WT has strong toxic effects on N2a cells (Schattling et al., 2019). By transfecting N2a cells with a Bassoon MUT construct, the intention was to assess, whether the toxicity of Bassoon is enhanced by the missense mutation. Using the Cell Titer Glo kit as a measurement of mitochondrial integrity, a significantly reduced viability of Bassoon MUT vs. Bassoon WT transfected cells was detected.

Due to its remarkable size (Gundelfinger et al., 2016) and the abundancy of IDRs (Schattling et al., 2019) it is plausible to hypothesize that the primary mechanism of Bassoon toxicity in transfected N2a cells is protein aggregation. As Bassoon is not endogenously expressed in N2a cells, it does not exert a specific function and it cannot be integrated into the cellular machinery of N2a cells (Rouillard et al., 2016). This fact alone, together with the size of Bassoon (Gundelfinger et al., 2016), makes Bassoon aggregation in transfected N2a cells very likely. However, it is likely that the Bassoon mutation exacerbates aggregation mediated toxicity, as a decreased solubility of Bassoon and Tau was proposed (Yabe et al., 2018). This is in line with a recent interpretation of mutations located in IDRs of proteins that have a propensity for insolubility (Tsang et al., 2020). Tsang et al. propose that a missense mutation in an IDR might be sufficient to further destabilize the tertiary structure of a susceptible protein and thus lower the threshold towards aggregation, resulting in either aggregation mediated toxicity or a loss of function of the protein. The reduced cell viability in Bassoon MUT transfected N2a cells supports this hypothesis, as it is likely that the mutation exacerbates the possible aggregation mediated toxicity of Bassoon WT.

It is, however, important to acknowledge that the transfection-based cell culture model used in this experiment is not ideal to study the toxicity of an exceptionally large protein such as Bassoon (Gundelfinger et al., 2016). It is conceivable that proteostatic systems in N2a cells are not prepared to cope with the enrichment of a large protein that does not have a specific function, localization, and regulation within the cell, as it is the case for Bassoon in N2a cells (Rouillard et al., 2016). Thus, proteostatic systems might be overwhelmed leading to high levels of cellular stress. The stress induced by the transfection of Bassoon WT might already approximate a maximum and hence it might be that the toxicity of Bassoon MUT is even higher than revealed by the experiment. On the other hand, posttranslational protein modifications might occur to a transfected protein that lead to a deviation from the physiological structure (Chong et al., 2021). Such posttranslational protein modifications might be

altered in Bassoon MUT. Consequently, the transfected protein might be further destabilized and gain toxic potential that exceeds its natural toxicity.

Despite possible experimental limitations and the inevitable toxicity of Bassoon transfection into N2a cells, the cell viability assay in N2a cells showed a significantly higher toxicity of Bassoon MUT compared to Bassoon WT pointing to an enhanced toxic effect of Bassoon MUT.

4.2 The Bassoon mutation in primary cortical neurons

Subsequent to detecting a significant increase in toxicity in Bassoon MUT versus Bassoon WT transfected N2a cells, experiments with primary neuronal cell culture derived from genetically modified Bassoon P3882A mice were conducted. Experiments with PNCC facilitated investigations into Bassoon MUT in a more physiological neuronal environment. Confounding effects, such as inevitable protein stress due to the transfection itself, were minimized in PNCC given the genetical insertion of the Bassoon mutation into the mouse line. The glutamate toxicity as measured via the Real Time Glo experiments revealed that Bassoon MUT primary neurons are significantly more susceptible to cell death upon glutamate stress compared to Bassoon WT primary neurons.

One plausible explanation for this observation is that the high level of ROS induced by the influx of calcium during glutamate excitotoxicity (Hardingham & Bading, 2010; Stirling & Stys, 2010; Wang & Qin, 2010) further destabilizes the tertiary structure of Bassoon and triggers more severe aggregation in Bassoon MUT neurons due to an increased instability of the tertiary structure in Bassoon MUT. This is in line with the hypothesis that the missense mutation, which is probably located in an IDR, lowers the threshold towards irreversible and toxic protein aggregation (Tsang et al., 2020). Additionally, Yabe et al have shown that the Bassoon mutation leads to a decreased solubility of Bassoon in Bassoon MUT transfected HEK293 cells, indicating that the Bassoon mutation might decrease the solubility of the protein, which further supports an increased aggregation mediated toxicity as a mechanistic explanation (Yabe et al., 2018).

A significant translocation of Bassoon to the soma was not detectable, but the increased aggregation load in Bassoon MUT neurons backs this mechanistic hypothesis. Using the Proteostat Aggregation Detection Dye (Enzo) a significantly higher number of aggresomes was observed in Bassoon MUT neurons compared to Bassoon WT neurons.

These findings support the hypothesis of a lower threshold towards aggregation in Bassoon MUT neurons. Notably, not only a lower solubility of Bassoon was observed in Bassoon MUT transfected HEK293 cells, but also of the Tau protein (Yabe et al., 2018), indicating that the Bassoon mutation might lead to proteostatic perturbations that affect other proteins as well. As Bassoon is an important regulator of compartment specific proteostasis (Montenegro-Venegas et al., 2021; Okerlund et al., 2017), a disruption of protein degradation within the neuron due to dysfunction of Bassoon MUT must be considered.

These findings are only a very first step in the evaluation of Bassoon MUT toxicity. A consolidation of the conclusions drawn could, for instance, be achieved by treating neurons with IU1, a proteasome activator (Schattling et al., 2019), prior to the addition of glutamate during the cell viability assay to verify that the toxic effect of the Bassoon mutation can be reversed upon proteasome activation. Furthermore, the solubility of Bassoon deposits in WT and MUT glutamate stressed and unstressed primary neurons could be tested by adding 1,6-Hexandiol to the cells (Hoffmann et al., 2021). The essay using 1,6-Hexandiol has been used by Hoffmann et al. to differentiate between dense, but still soluble protein condensates and insoluble aggregates (Hoffmann et al., 2021). In an attempt to understand the structural impact of the Bassoon mutation, this would help to further evaluate effects of the point mutation on the solubility of Bassoon MUT. Further experiments are required to characterize the pathophysiology of Bassoon P3882A aggregation. First, it needs to be differentiated between aggregation mediated toxicity and misfolding that leads to a loss of Bassoon function as a regulator of presynaptic protein homeostasis and CAZ organization (Montenegro-Venegas et al., 2021; Okerlund et al., 2017). Aggregation mediated toxicity involves membrane located, ER located and mitochondrial stress (Hipp et al., 2019). The formation of stress vesicles that may sequester factors of the proteostatic system and components of the protein biosynthesis machinery (Chung et al., 2018; Hipp et al., 2019) should be considered in the presence of aggregates. It is conceivable that Bassoon aggregates lead to the sequestration of Bassoon interacting proteins such as *SIAH1* and *ATG5*, resulting in an exacerbation of proteostatic dysregulation. Moreover, the composition of aggregates in Bassoon MUT neurons needs to be observed more closely, for instance by searching for other neuronal proteins within the aggregates and investigating their pathogenic contribution. At the same time, other possible mechanisms of toxicity should be experimentally evaluated in the future. The point mutation might also cause a loss of function of Bassoon by impairing complex protein interactions in the presynapse. Aside from proteostasis, this could also involve the organization of calcium channels within the CAZ, leading to ionic imbalance (Davydova et al., 2014) or synaptogenesis (Friedman et al., 2000).

This work indicates that Bassoon MUT neurons are more susceptible towards glutamate induced excitotoxicity and that Bassoon MUT is more prone to aggregation than Bassoon WT. However, further experiments are needed to consolidate the theory of an aggregation mediated toxicity of Bassoon MUT and to investigate other possible mechanisms of Bassoon MUT toxicity, taking the multiplicity of presynaptic functions of Bassoon into account.

4.3 The Bassoon mutation P3882A in adult and aged mice

As the missense mutation of Bassoon was originally identified in a hereditary age-dependent atypical Parkinson syndrome (Yabe et al., 2018), the aim was to perform a histological evaluation of neuronal loss and Bassoon accumulation in 18-month-old aged mice expressing the mutation. A cohort of 10-month-old mice was included into the analysis for the distinction between a developmental phenotype and an age dependent effect of the mutation. In both the 18-month and 10-month-old cohorts, neuronal abundancy in the cortex showed no significant difference between Bassoon WT and MUT mice, using immunohistological NeuN count and quantitative flow cytometry of NeuN-sorted nuclei. An increase in Bassoon MFI in the soma of cortical neurons, representing Bassoon accumulation, was also not observed in the aged mice cohort. Thus, the experiments provided do not indicate that the Bassoon mutation P3882A induces a neurodegenerative effect in 10-month and 18-month-old mice.

A potential biological explanation for these findings could be that the point mutation identified in the hereditary PSP-like syndrome presented by Yabe et al. was only associated with the phenotype presented by the patients and not causally linked to them. Besides, it is conceivable that the Bassoon mutation induces proteostatic imbalance that primarily affects other proteins such as the Tau protein. Accordingly, Yabe et al. have shown that the solubility of Tau is decreased in the presence of mutated Bassoon. With respect to the quantification of cortical neuronal loss in this work, it is conceivable that the analyses conducted did not include the brain regions affected by a potential Bassoon P3882A proteinopathy in mice. As the patients show symptoms of an atypical Parkinson syndrome and in particular symptoms of cognitive decline, it is possible that, at least in earlier stages of the disease, neurodegeneration occurs specifically in brain areas such as the brainstem, the basal ganglia or the hippocampus. Such a region-specific pattern of neurodegeneration would not be detectable by the cortical immunohistochemical analysis of this work. It could also be that the effect size in mice is smaller than in humans, necessitating a larger sample to reach statistical significance.

Importantly, methodological limitations of immunohistochemistry and flow cytometry of isolated nuclei must be considered. For instance, immunofluorescence signal can be subjected to heterogeneity (Johnson, 1999), making immunofluorescence-based quantifications prone to concealing effects. Additionally, the quantification of neuronal loss as a marker for neurodegeneration might not be sensitive enough for smaller effect sizes. Although the Bassoon antibody used for histology was already established, a malfunction of the aliquots used should be considered.

Taken together, the hypothesis that the missense mutation of Bassoon is associated with a primary neurodegenerative disorder in mice cannot be robustly falsified as of yet. This work does not provide evidence for an age-related Bassoon MUT proteinopathy in the mouse model, but further experiments in multiple brain regions, as elaborated further in section 4.5, are needed for a robust *in vivo* characterization of the mutation.

4.4 The Bassoon mutation P3882A in the EAE

One central aim of this project was to investigate the effect of the Bassoon missense mutation on the EAE. As the Bassoon proteinopathy has been proposed as an important driver of neurodegeneration in EAE and MS (Schattling et al., 2019), one could assume that the Bassoon mutation P3882A (Yabe et al., 2018) aggravates the severity of disease in both clinical course and histology. The hypothesized clinical and histological effects of the mutation on the EAE were not observed using a genetically modified mouse model. The clinical course, incidence and mortality of the EAE did not reveal a significant difference between MUT and WT animals. Accordingly, quantifications of neuronal loss in the ventral horn and cortex using immunohistochemistry and flow cytometry did not reveal a difference between the WT and MUT cohorts. Similarly, no increase in Bassoon MFI, indicating Bassoon accumulation, was detected in the soma of ventral horn neurons in the spinal cord or in cortical neurons. Thus, the hypothesis, that the Bassoon mutation increases the propensity of Bassoon to form toxic aggregates, resulting in a clinical and histopathological deterioration in EAE could not be verified in the underlying experiments.

One potential explanation for the absence of a clinical and histological phenotype of Bassoon P3882A in EAE could be that the hypothesized effect of the mutation is too small to be detected. Moreover, it must be taken into consideration that the human Bassoon mutation P3866A is only associated and not causally linked to the hereditary PSP-like syndrome.

At the same time, a potential saturation effect in the EAE must be considered. It is conceivable that Bassoon pathology in WT animals is already too severe to be increased further.

This would predominantly have affected animals with higher disease scores. Additionally, it is also not entirely clear which level of inflammation is required for the induction of Bassoon pathology and whether it is an inflammatory pathway that induces Bassoon pathology in the first place or rather a primary neurodegenerative cascade. A weaker immunization for the induction of the EAE could already be sufficient to trigger EAE onset and Bassoon pathology in the MUT cohort, while the Bassoon WT cohort might require a stronger immunization for the induction of EAE and Bassoon pathology. Possibly, such a low-dose immunization EAE could reveal a difference in incidence and mortality between Bassoon WT and MUT mice as well. One could investigate this assumption by performing a less immunogenic EAE induction regimen using a lower PTX dosage (Aharoni et al., 2021).

Besides a potential saturation effect, the limitations of immunohistochemistry that apply to the aged mice cohort, as described in section 4.3, must be considered for the EAE cohort, as well. Although all samples that were compared with each other were stained at the same time, a considerable variance in fluorescence intensity was observed in the EAE groups. This was only partially compensated by an increased number of samples and might have added to concealing smaller effects. Similarly, the FACS analysis of isolated nuclei showed a high variance that also might have contributed to a lack of power to detect significant differences. Additionally, NeuN positive nuclei were quantified relative to the total amount of DAPI stained nuclei. Given the abundancy of immune cells during EAE, it might be that a higher total cell count extracted from the tissue has led to a lower proportion of neuronal nuclei. This effect would have affected the WT and the MUT group. However, it is possible that such an effect is stronger in the MUT group owing to a potentially stronger inflammation.

Importantly, the EAE must be acknowledged as only a simplified model of MS, as it does not represent the entire complexity of inflammation and neurodegeneration in MS due to its very specific and immediate induction and onset (Dendrou et al., 2015). Although the EAE is a valuable mouse model for inflammation in MS, possible limitations regarding the representation of complex neurodegenerative mechanisms, that are specific to MS, must be considered. There are multiple different EAE models that represent distinct features of MS (Gold, 2006). Thus, an EAE model that models a chronic form of neuroinflammation might be more suitable as the MOG immunization based EAE model rather represents the acute phase (Bittner et al., 2014; Gold, 2006).

4.5 Bassoon mutation P3882A as a tool to study the Bassoon proteinopathy in MS and aging

A central aim of this work was to explore the potential of the Bassoon missense mutation P3882A as an *in vivo* model to study the Bassoon proteinopathy in the context of EAE and aging. As MS is not only a neuroinflammatory but also a neurodegenerative disease (Friese et al., 2014) the paradigm of toxic protein aggregation must be applied on MS as well. Identifying candidates for protein aggregation in MS is an important step towards a better understanding of dysregulated protein networks in inflamed neurons, which facilitates the emergence of new therapeutic targets. Subsequent to the identification of candidates, the exact pathogenesis of aggregation and the mechanisms of toxicity need to be investigated. For this purpose, endeavors to define the role of toxic Bassoon aggregation in MS with respect to its significance for disease progression and possibly disease onset are required.

Considering implications of Bassoon aggregation in other age-related neurodegenerative diseases, including Huntington's disease (Huang et al., 2020; Yabe et al., 2018), the relevance of toxic Bassoon aggregates for a broader spectrum of neurological disorders could be a research subject in the future. An animal model that represents Bassoon pathology would be of great use for such an agenda. Recently, it has been shown that Bassoon not only participates in tau aggregates in a mouse model for Tau proteinopathy, but also, enhances the toxicity and transmission of tau seeds *in vivo* (Martinez et al., 2022). This supports the theory that Bassoon has great pathogenic potential by fueling the aggregation of other neuronal proteins. Bassoon aggregation, sequestration and loss of function might be drivers of aggregation mediated neurodegeneration across different disease entities. Thus, a detailed pathomechanistic assessment of Bassoon is imperative not only for MS research but for other diseases mediated by protein aggregation, which further stresses the need for a research model for Bassoon proteinopathy. As emphasized before, the Bassoon mutation is not only associated with a primary neurodegenerative disorder, but it also decreases the solubility of Bassoon and Tau *in vitro*, likely resulting in a lowered threshold for aggregation (Yabe et al., 2018). It has already been proposed that a single missense mutation within the IDR of a structurally aggregation prone protein may further lead to a destabilization of the tertiary structure, promoting severe misfolding and aggregation (Tsang et al., 2020). The Bassoon mutation P3866A (human)/ P3882A (mouse) could have such a destabilizing effect on the protein structure. In other words, there are multiple indication that the mutation of Bassoon might potentiate the protein's pathogenic capacity which is rooted in its instable tertiary structure. By exposing the pathology of Bassoon, the Bassoon mutation might show utility as an *in vitro* and *in vivo* model for Bassoon proteinopathy.

This work does not provide evidence for the qualification of the Bassoon P3882A mouse model as an *in vivo* research tool for Bassoon proteinopathy in MS or aging. However, in order to robustly assess the potential utility of the mutation in *in vivo*, experiments using a broader spectrum of histological read outs as well as a PTX low dose EAE (Aharoni et al., 2021) to counteract a possible saturation effect could be conducted. Intending to assess the neurodegenerative impact of the Bassoon mutation more thoroughly in EAE and aging, further experiments that include a wider range of read-outs are needed. For immunohistochemistry, not only *phosphorylated neurofilament* and *amyloid precusor protein* stainings as neuronal damage markers could be used, but also mitochondrial, membrane and ER damage could be investigated specifically. Additionally, an aggregation detection dye might also be used in aged mice on larger cohorts to ensure that also smaller effect sizes are detected. Stainings for other neuronal proteins such as Tau, alpha-synuclein and Bassoon interacting presynaptic proteins could be performed on Bassoon P3882A brain and spinal cord tissue in EAE and aged mice to detect a translocation or accumulation of other proteins. Furthermore, different Bassoon antibodies for immunohistochemistry could be used or aggregates could be identified in histology using the Proteostat aggregation detection dye (Enzo). Importantly, a variety of brain regions should be selected for the analysis, screening for a region-specific pattern of neurodegeneration. In particular, brain stem regions and the hippocampus should be included in the histological analysis of the adult and aged mice cohort. As an alternative to immunohistochemistry, *in vivo* MRI could be helpful in quantifying global and regional atrophy patterns in Bassoon MUT mice in EAE. Accordingly, positron emission tomography could hypothetically be used in mice to reveal hypometabolic regions as a surrogate marker for neurodegeneration. Furthermore, the frequency of this and other Bassoon missense mutations within the MS population could be an interesting research subject in the future, as it is conceivable that a Bassoon mutation might be associated with an increased disease severity in MS patients.

Controversially, it must be considered that the human Bassoon mutation P3866A is only associated and not causally involved in the disease presented by Yabe et al. (Yabe et al., 2018). However, given the 100 % penetrance of the mutation within the affected family, it's in vitro effects on Bassoon and Tau solubility and the toxicity of Bassoon MUT *in vitro* shown by this work, this hypothesis seems less likely.

The *in vitro* experiments performed in this work indicate an enhanced toxicity in Bassoon MUT compared to Bassoon WT neuronal cell cultures. These findings make further *in vitro* investigations into the mechanisms of Bassoon P3882A toxicity important. The increased

aggregation load in unstressed Bassoon MUT PNCC points to an increased aggregation propensity of Bassoon P3882A. Using the mutation as an additional trigger for Bassoon aggregation might be helpful in identifying the exact nature of Bassoon aggregates with respect to the precise composition of aggregates and their functional consequences for the presynapse, including proteostasis, vesicle exocytosis and ionic balance.

Taken together, the Bassoon mutation might help disentangle the nature of protein aggregation in EAE and MS as well as in primary neurodegenerative diseases by exposing the pathogenic potential of Bassoon, which lies in its size, disordered structure, its involvement in presynaptic proteostasis and organization. Moreover, *in vitro* experiments with Bassoon P3882A primary neurons might be a helpful tool in the discovery of other mechanisms of Bassoon toxicity. Further, *in vivo* investigations using different forms of neuroinflammation, thorough quantitative and qualitative analysis of protein aggregation and a broader spectrum of neuronal damage markers in multiple brain regions are required to finally assess the potential of a Bassoon P3882A *in vivo* model.

4.6 The potential of the Bassoon mutation for studying Bassoon physiology

The Bassoon mutation might not only expose the pathological potential of Bassoon, but it might also shed light on novel aspects concerning the physiology of Bassoon. Possibly, investigating the effects of the mutation could pave the way for a better understanding of presynaptic organization.

Hoffmann et al. and Tsang et al. hypothesize that the formation of insoluble protein complexes via liquid-liquid phase separation from the cytoplasm is required for the formation of so-called condensates (Hoffmann et al., 2021; Tsang et al., 2020). The term condensate refers to a cell organelle like protein complex that phase separates from the cytoplasm and is functionally relevant for presynaptic function (Hoffmann et al., 2021). In their review Tsang et al. also propose that the susceptibility of proteins to aggregation appears to be the evolutionary trade-off of a functionally relevant tendency towards insolubility. It has been shown that alpha-synuclein, a neuronal protein with an unstable tertiary structure, participates in synapsin condensates (Hoffmann et al., 2021). The previously described enrichment of Bassoon with IDRs (Schattling et al., 2019) renders Bassoon a suitable candidate to participate in presynaptic condensates, as well. As a scaffold protein of the CAZ, Bassoon has many functions such as regulation of proteostasis (Montenegro-Venegas et al., 2021; Okerlund et al., 2017; Waites et al., 2013), positional priming of VGCCs (Davydova et al., 2014) and vesicle exocytosis (Hallermann et al., 2010). For each of these functions, it is conceiv-

able that a condensate-like protein complex is the form of spatial organization that is required for compartmentalized protein interactions. Perceiving protein complexes as condensates that represent dynamic and functional organelles within the cell as they phase separate from the cytoplasm would add a new layer of complexity to the understanding of presynaptic organization.

Thus, the concept of presynaptic condensate formation and its role for synaptic vesicle release and protein homeostasis must also be applied on Bassoon and other CAZ members. In this physiologic process lies a pathogenic potential, as protein excess (Hoffmann et al., 2021) or misfolding in the state of inflammation and aging (Hipp et al., 2019) may lead to irreversible aggregation. Understanding the physiology is the foundation for a profound comprehension of pathology and for the development of neuroprotective therapies, as well. Given the *in vitro* results of this work, is quite likely that the Bassoon mutation further decreases the solubility of Bassoon, leading to aggregation and functional perturbations in the presynapse. As follows, the Bassoon mutation might be used as a tool to investigate the potential role of Bassoon in presynaptic vesicles (Hoffmann et al., 2021; Tsang et al., 2020) which may lead to novel discoveries concerning both presynaptic processes and the pathological potential of Bassoon.

5. Summary

The relapse-independent progression of MS still imposes a severe therapeutic challenge. Immunosuppressive therapies are impuissant against the progressive accumulation of neurological deficits leaving a high burden to the lives of patients (Scalfari et al., 2014). In a visionary effort to identify therapeutic strategies that tackle neurodegenerative mechanisms in MS more effectively, precisely these mechanisms must be investigated thoroughly.

One pathophysiologically important mechanism of neurodegeneration in the EAE is the neuronal accumulation of the presynaptic protein Bassoon (Schattling et al., 2019). An autosomal-dominant missense mutation of Bassoon has been linked to a hereditary atypical Parkinson syndrome (Yabe et al., 2018) which has led to the central hypothesis of this work: that the mouse Bassoon mutation P3882A increases the toxic potential of Bassoon and might therefore serve as a mouse model to study the Bassoon proteinopathy in EAE and aging.

The primary aim of this work was to explore the potential of the Bassoon mutation P3882A as a mouse model for neurodegeneration in EAE and aging. As a foundation for this aim, the intent was to assess the toxicity of Bassoon MUT and its propensity for aggregation *in vivo* and *in vitro*. The *in vivo* experiments do not reveal increased toxicity of Bassoon MUT, refuting Bassoon P3882A as a tool to study the Bassoon proteinopathy *in vivo*. However, the *in vitro* data strongly indicate increased toxicity in Bassoon MUT cell cultures. The enhanced susceptibility to glutamate stress and the increased frequency of aggregates in Bassoon MUT primary cortical neurons suggest that the increased *in vitro* toxicity of Bassoon P3882A might be mediated by a structural destabilization of Bassoon MUT, leading to a strong aggregation propensity in Bassoon MUT cells.

This work is only a very first step in the endeavor to decipher the nature of Bassoon toxicity using the Bassoon mutation. Ensuing experiments are needed to consolidate the theory of an increased aggregation mediated toxicity of Bassoon MUT and to evaluate specific presynaptic dysfunctions in Bassoon MUT cultures involving proteostasis, ion channel organization and vesicle exocytosis.

5. Zusammenfassung

Die schubunabhängige Progression der MS stellt nach wie vor eine große therapeutische Herausforderung dar. Immunsuppressive Therapien sind gegen die fortschreitende Akkumulation neurologischer Defizite, die eine große Belastung für das Leben der Patient:innen darstellen, unwirksam (Scalfari et al., 2014). Um therapeutische Strategien zu identifizieren, welche die neurodegenerativen Mechanismen der MS wirksam beeinflussen, müssen genau diese Mechanismen gründlich untersucht werden.

Ein pathophysiologischer Mechanismus der Neurodegeneration in der EAE ist die neuronale Akkumulation des präsynaptischen Proteins Bassoon (Schattling et al., 2019). Eine autosomal-dominant vererbte missense Mutation von Bassoon zeigte eine Assoziation mit einem hereditären atypischen Parkinsonsyndrom (Yabe et al., 2018). Folglich ließ sich hypothetisieren, dass die Bassoon Mutation das toxische Potential von Bassoon erhöht und somit als Mausmodell zur experimentellen Charakterisierung der Bassoon Proteinopathie in der EAE und im Alter geeignet ist.

Das primäre Ziel dieser Arbeit war die Validierung dieser Hypothese durch die Charakterisierung der Toxizität und Aggregationsneigung von Bassoon Mut im Vergleich zu Bassoon WT *in vitro* und *in vivo*. *In vivo* zeigte sich in der EAE und in alten Mäusen keine signifikante Toxizität der Bassoon Mutation, sodass eine *in vivo* Modellierung der Bassoon Proteinopathie mit Bassoon P3882A nicht abgeleitet werden kann. Die *in vitro* Daten implizieren jedoch eine erhöhte Toxizität von Bassoon MUT im Vergleich zu Bassoon WT. Die gesteigerte Anfälligkeit gegenüber Glutamat induziertem Zellstress und die erhöhte Aggregatlast in der Bassoon MUT Neuronenkultur legen nahe, dass die Toxizität durch eine verstärkte strukturelle Destabilisierung vermittelt wird, die eine verstärkte Aggregationsneigung zur Folge hat.

Die vorliegende Arbeit ist nur ein erster Schritt in dem Bemühen, die Natur der Bassoon Toxizität anhand der Bassoon Mutation zu entschlüsseln. Weitere Experimente sind erforderlich, um die Theorie einer erhöhten aggregationsvermittelten Toxizität in Bassoon MUT Neuronen zu untermauern und um spezifische präsynaptische Funktionsstörungen in Bassoon MUT Neuronen zu identifizieren, welche beispielsweise die Proteostase, die Organisation von Ionenkanälen oder die Vesikelexozytose betreffen könnten.

6. List of abbreviations

APP	Amyloid precursor protein
ATG	Autophagy related protein
Bsn	Bassoon
CAZ	Cytomatrix active zone
CIS	Clinically isolated syndrome
CSF	Cerebrospinal fluid
DAPI	4',6-diamidino-2-phenylindol
DIV	Days in vitro
DMEM	Dulbeccos' Modified Eagle Medium
DMT	Disease modifying therapy
EAE	Experimental autoimmune encephalomyelitis
EBNA-1	Epstein-Barr-Virus nuclear antigen 1
EBV	Epstein-Barr-Virus
EDTA	Ethylenediaminetetraacetic acid
EGFP	Enhanced green fluorescent protein
ER	Endoplasmatic reticulum
ERAD	Endoplasmatic reticulum associated degradation
FACS	Fluorescence activated cell sorting
FCS	Fetal calf serum
HBSS	Hanks' Balanced Salt Solution
IDR	Intrinsically disordered residue
IF	Immunofluorescence
IL	Interleukine
i.p.	Intraperitoneally
K.O.	Knock out
MFI	Mean fluorescence intensity
MOG	Myelin oligodendrocyte protein

MS	Multiple sclerosis
MUT	Mutant
NAWM	Normal appearing white matter
NDS	Normal donkey serum
NOS	Nitric oxide species
OCB	Oligoclonal bands
PBS	Phosphate buffered saline
PDL	Poly-D-lysine
p-NF	Phosphorylated neurofilament
PNCC	Primary neuronal cell culture
PNGM	Primary neuronal growth medium
PPMS	Primary progressive MS
PTX	Pertussis toxin
RBN	RIM binding proteins
RRMS	Relapsing-remitting MS
ROI	Region of interest
ROS	Reactive oxygen species
SAS	Subarachnoid space
s.c.	Subcutaneously
SPMS	Secondary progressive MS
SV	Synaptic vesicle
UPR	Unfolded protein response
UPS	Ubiquitin proteasome system
VGCC	Voltage gated calcium channel
WT	Wildtype

7. Bibliography

Aharoni, R., Globerman, R., Eilam, R., Brenner, O., & Arnon, R. (2021). Titration of myelin oligodendrocyte glycoprotein (MOG) - Induced experimental autoimmune encephalomyelitis (EAE) model. *Journal of Neuroscience Methods*, *351*, 108999. https://doi.org/10.1016/j.jneumeth.2020.108999

Attfield, K. E., Jensen, L. T., Kaufmann, M., Friese, M. A., & Fugger, L. (2022). The immunology of multiple sclerosis. *Nature Reviews Immunology*, *22*(12), 734–750. https://doi.org/10.1038/s41577-022-00718-z

Azevedo, C. J., Kornak, J., Chu, P., Sampat, M., Okuda, D. T., Cree, B. A., Nelson, S. J., Hauser, S. L., & Pelletier, D. (2014). In vivo evidence of glutamate toxicity in multiple sclerosis. *Annals of Neurology*, *76*(2), 269–278. https://doi.org/10.1002/ana.24202

Barkhof, F., Calabresi, P. A., Miller, D. H., & Reingold, S. C. (2009). Imaging outcomes for neuroprotection and repair in multiple sclerosis trials. *Nature Reviews Neurology*, *5*(5), 256–266. https://doi.org/10.1038/nrneurol.2009.41

Belbasis, L., Bellou, V., Evangelou, E., & Tzoulaki, I. (2020). Environmental factors and risk of multiple sclerosis: Findings from meta-analyses and Mendelian randomization studies. *Multiple Sclerosis Journal*, *26*(4), 397–404. https://doi.org/10.1177/1352458519872664

Bermel, R. A., Rae-Grant, A. D., & Fox, R. J. (2010). Diagnosing multiple sclerosis at a later age: more than just progressive myelopathy. *Multiple Sclerosis Journal*, *16*(11), 1335–1340. https://doi.org/10.1177/1352458510377334

Betegon, M., & Brodsky, J. L. (2020). Unlocking the door for ERAD. *Nature Cell Biology*, *22*(3), 263–265. https://doi.org/10.1038/s41556-020-0476-1

Bittner, S., Afzali, A. M., Wiendl, H., & Meuth, S. G. (2014). Myelin Oligodendrocyte Glycoprotein (MOG₃₅₋₅₅) Induced Experimental Autoimmune Encephalomyelitis (EAE) in C57BL/6 Mice. *Journal of Visualized Experiments*, *86*. https://doi.org/10.3791/51275

Bjornevik, K., Cortese, M., Healy, B. C., Kuhle, J., Mina, M. J., Leng, Y., Elledge, S. J., Niebuhr, D. W., Scher, A. I., Munger, K. L., & Ascherio, A. (2022). Longitudinal analysis reveals high prevalence of Epstein-Barr virus associated with multiple sclerosis. *Science*, *375*(6578), 296–301. https://doi.org/10.1126/science.abj8222

Bø, L., Vedeler, C. A., Nyland, H., Trapp, B. D., & Mørk, S. J. (2003). Intracortical multiple sclerosis lesions are not associated with increased lymphocyte infiltration. *Multiple Sclerosis Journal*, *9*(4), 323–331. https://doi.org/10.1191/1352458503ms917oa

Browne, P., Chandraratna, D., Angood, C., Tremlett, H., Baker, C., Taylor, B. V., & Thompson, A. J. (2014). Atlas of Multiple Sclerosis 2013: A growing global problem with widespread inequity. *Neurology*, *83*(11), 1022–1024. https://doi.org/10.1212/WNL.0000000000000768

Chong, Z. X., Yeap, S. K., & Ho, W. Y. (2021). Transfection types, methods and strategies: a technical review. *PeerJ*, *9*, e11165. https://doi.org/10.7717/peerj.11165

Chung, C. G., Lee, H., & Lee, S. B. (2018). Mechanisms of protein toxicity in neurodegenerative diseases. *Cellular and Molecular Life Sciences*, *75*(17), 3159–3180. https://doi.org/10.1007/s00018-018-2854-4

Cole, J. H., Raffel, J., Friede, T., Eshaghi, A., Brownlee, W. J., Chard, D., De Stefano, N., Enzinger, C., Pirpamer, L., Filippi, M., Gasperini, C., Rocca, M.

A., Rovira, A., Ruggieri, S., Sastre-Garriga, J., Stromillo, M. L., Uitdehaag, B. M. J., Vrenken, H., Barkhof, F., … Ciccarelli, O. (2020). Longitudinal Assessment of Multiple Sclerosis with the Brain-Age Paradigm. *Annals of Neurology*, *88*(1), 93–105. https://doi.org/10.1002/ana.25746

Collorone, S., Prados, F., Kanber, B., Cawley, N. M., Tur, C., Grussu, F., Solanky, B. S., Yiannakas, M., Davagnanam, I., Wheeler-Kingshott, C. A. M. G., Barkhof, F., Ciccarelli, O., & Toosy, A. T. (2021). Brain microstructural and metabolic alterations detected *in vivo* at onset of the first demyelinating event. *Brain*, *144*(5), 1409–1421. https://doi.org/10.1093/brain/awab043

Compston, A., & Coles, A. (2008). Multiple sclerosis. *The Lancet*, *372*(9648), 1502–1517. https://doi.org/10.1016/S0140-6736(08)61620-7

Daumer, M., Neuhaus, A., Morrissey, S., Hintzen, R., & Ebers, G. C. (2009). MRI as an outcome in multiple sclerosis clinical trials. *Neurology*, *72*(8), 705–711. https://doi.org/10.1212/01.wnl.0000336916.38629.43

Davydova, D., Marini, C., King, C., Klueva, J., Bischof, F., Romorini, S., Montenegro-Venegas, C., Heine, M., Schneider, R., Schröder, M. S., Altrock, W. D., Henneberger, C., Rusakov, D. A., Gundelfinger, E. D., & Fejtova, A. (2014). Bassoon Specifically Controls Presynaptic P/Q-type Ca2+ Channels via RIM-Binding Protein. *Neuron*, *82*(1), 181–194. https://doi.org/10.1016/j.neuron.2014.02.012

DeLuca, G. C. (2006). The contribution of demyelination to axonal loss in multiple sclerosis. *Brain*, *129*(6), 1507–1516. https://doi.org/10.1093/brain/awl074

Dendrou, C. A., Fugger, L., & Friese, M. A. (2015). Immunopathology of multiple sclerosis. *Nature Reviews Immunology*, *15*(9), 545–558. https://doi.org/10.1038/nri3871

Dobson, C. M., Knowles, T. P. J., & Vendruscolo, M. (2020). The Amyloid Phenomenon and Its Significance in Biology and Medicine. *Cold Spring Harbor Perspectives in Biology*, *12*(2), a033878. https://doi.org/10.1101/cshperspect.a033878

Eshaghi, A., Marinescu, R. V, Young, A. L., Firth, N. C., Prados, F., Jorge Cardoso, M., Tur, C., De Angelis, F., Cawley, N., Brownlee, W. J., De Stefano, N., Laura Stromillo, M., Battaglini, M., Ruggieri, S., Gasperini, C., Filippi, M., Rocca, M. A., Rovira, A., Sastre-Garriga, J., … Ciccarelli, O. (2018). Progression of regional grey matter atrophy in multiple sclerosis. *Brain*, *141*(6), 1665–1677. https://doi.org/10.1093/brain/awy088

Evangelou, N. (2004). Pathological study of spinal cord atrophy in multiple sclerosis suggests limited role of local lesions. *Brain*, *128*(1), 29–34. https://doi.org/10.1093/brain/awh323

Fischer, M. T., Sharma, R., Lim, J. L., Haider, L., Frischer, J. M., Drexhage, J., Mahad, D., Bradl, M., van Horssen, J., & Lassmann, H. (2012). NADPH oxidase expression in active multiple sclerosis lesions in relation to oxidative tissue damage and mitochondrial injury. *Brain*, *135*(3), 886–899. https://doi.org/10.1093/brain/aws012

Frank, T., Rutherford, M. A., Strenzke, N., Neef, A., Pangršič, T., Khimich, D., Fejtova, A., Gundelfinger, E. D., Liberman, M. C., Harke, B., Bryan, K. E., Lee, A., Egner, A., Riedel, D., & Moser, T. (2010). Bassoon and the Synaptic Ribbon Organize Ca2+ Channels and Vesicles to Add Release Sites and Promote Refilling. *Neuron*, *68*(4), 724–738. https://doi.org/10.1016/j.neuron.2010.10.027

Freria, C. M., Zanon, R. G., Santos, L. M. B., & Oliveira, A. L. R. (2010). Major histocompatability complex class I expression and glial reaction influence spinal

motoneuron synaptic plasticity during the course of experimental autoimmune encephalomyelitis. *The Journal of Comparative Neurology*, *518*(7), 990–1007. https://doi.org/10.1002/cne.22259
Friedman, H. V., Bresler, T., Garner, C. C., & Ziv, N. E. (2000). Assembly of New Individual Excitatory Synapses. *Neuron*, *27*(1), 57–69. https://doi.org/10.1016/S0896-6273(00)00009-X
Friese, M. A., Craner, M. J., Etzensperger, R., Vergo, S., Wemmie, J. A., Welsh, M. J., Vincent, A., & Fugger, L. (2007). Acid-sensing ion channel-1 contributes to axonal degeneration in autoimmune inflammation of the central nervous system. *Nature Medicine*, *13*(12), 1483–1489. https://doi.org/10.1038/nm1668
Friese, M. A., Schattling, B., & Fugger, L. (2014). Mechanisms of neurodegeneration and axonal dysfunction in multiple sclerosis. *Nature Reviews Neurology*, *10*(4), 225–238. https://doi.org/10.1038/nrneurol.2014.37
Frischer, J. M., Bramow, S., Dal-Bianco, A., Lucchinetti, C. F., Rauschka, H., Schmidbauer, M., Laursen, H., Sorensen, P. S., & Lassmann, H. (2009). The relation between inflammation and neurodegeneration in multiple sclerosis brains. *Brain*, *132*(5), 1175–1189. https://doi.org/10.1093/brain/awp070
Gold, R. (2006). Understanding pathogenesis and therapy of multiple sclerosis via animal models: 70 years of merits and culprits in experimental autoimmune encephalomyelitis research. *Brain*, *129*(8), 1953–1971. https://doi.org/10.1093/brain/awl075
Gundelfinger, E. D., Reissner, C., & Garner, C. C. (2016). Role of Bassoon and Piccolo in Assembly and Molecular Organization of the Active Zone. *Frontiers in Synaptic Neuroscience*, *7*. https://doi.org/10.3389/fnsyn.2015.00019
Haider, L., Zrzavy, T., Hametner, S., Höftberger, R., Bagnato, F., Grabner, G., Trattnig, S., Pfeifenbring, S., Brück, W., & Lassmann, H. (2016). The topograpy of demyelination and neurodegeneration in the multiple sclerosis brain. *Brain*, *139*(3), 807–815. https://doi.org/10.1093/brain/awv398
Hallermann, S., Fejtova, A., Schmidt, H., Weyhersmüller, A., Silver, R. A., Gundelfinger, E. D., & Eilers, J. (2010). Bassoon Speeds Vesicle Reloading at a Central Excitatory Synapse. *Neuron*, *68*(4), 710–723. https://doi.org/10.1016/j.neuron.2010.10.026
Hardingham, G. E., & Bading, H. (2010). Synaptic versus extrasynaptic NMDA receptor signalling: implications for neurodegenerative disorders. *Nature Reviews Neuroscience*, *11*(10), 682–696. https://doi.org/10.1038/nrn2911
Hauser, S. L., & Oksenberg, J. R. (2006). The Neurobiology of Multiple Sclerosis: Genes, Inflammation, and Neurodegeneration. *Neuron*, *52*(1), 61–76. https://doi.org/10.1016/j.neuron.2006.09.011
Häußler, V., Ufer, F., Pöttgen, J., Wolschke, C., Friese, M. A., Kröger, N., Heesen, C., & Stellmann, J. (2021). aHSCT is superior to alemtuzumab in maintaining NEDA and improving cognition in multiple sclerosis. *Annals of Clinical and Translational Neurology*, *8*(6), 1269–1278. https://doi.org/10.1002/acn3.51366
Hetz, C., Zhang, K., & Kaufman, R. J. (2020). Mechanisms, regulation and functions of the unfolded protein response. *Nature Reviews Molecular Cell Biology*, *21*(8), 421–438. https://doi.org/10.1038/s41580-020-0250-z
Hipp, M. S., Kasturi, P., & Hartl, F. U. (2019). The proteostasis network and its decline in ageing. *Nature Reviews Molecular Cell Biology*, *20*(7), 421–435. https://doi.org/10.1038/s41580-019-0101-y
Hoffmann, C., Sansevrino, R., Morabito, G., Logan, C., Vabulas, R. M., Ulusoy, A., Ganzella, M., & Milovanovic, D. (2021). Synapsin Condensates Recruit alpha-

Synuclein. *Journal of Molecular Biology*, *433*(12), 166961. https://doi.org/10.1016/j.jmb.2021.166961
Hohlfeld, R., Dornmair, K., Meinl, E., & Wekerle, H. (2016). The search for the target antigens of multiple sclerosis, part 1: autoreactive CD4+ T lymphocytes as pathogenic effectors and therapeutic targets. *The Lancet Neurology*, *15*(2), 198–209. https://doi.org/10.1016/S1474-4422(15)00334-8
Huang, T.-T., Smith, R., Bacos, K., Song, D.-Y., Faull, R. M., Waldvogel, H. J., & Li, J.-Y. (2020). No symphony without bassoon and piccolo: changes in synaptic active zone proteins in Huntington's disease. *Acta Neuropathologica Communications*, *8*(1), 77. https://doi.org/10.1186/s40478-020-00949-y
Jayaraj, G. G., Hipp, M. S., & Hartl, F. U. (2020). Functional Modules of the Proteostasis Network. *Cold Spring Harbor Perspectives in Biology*, *12*(1), a033951. https://doi.org/10.1101/cshperspect.a033951
Ji, Q., Castelli, L., & Goverman, J. M. (2013). MHC class I–restricted myelin epitopes are cross-presented by Tip-DCs that promote determinant spreading to CD8+ T cells. *Nature Immunology*, *14*(3), 254–261. https://doi.org/10.1038/ni.2513
Jing, Z., Rutherford, M. A., Takago, H., Frank, T., Fejtova, A., Khimich, D., Moser, T., & Strenzke, N. (2013). Disruption of the Presynaptic Cytomatrix Protein Bassoon Degrades Ribbon Anchorage, Multiquantal Release, and Sound Encoding at the Hair Cell Afferent Synapse. *The Journal of Neuroscience*, *33*(10), 4456–4467. https://doi.org/10.1523/JNEUROSCI.3491-12.2013
Johnson, C. W. (1999). Issues in Immunohistochemistry. *Toxicologic Pathology*, *27*(2), 246–248. https://doi.org/10.1177/019262339902700214
Jucker, M., & Walker, L. C. (2013). Self-propagation of pathogenic protein aggregates in neurodegenerative diseases. *Nature*, *501*(7465), 45–51. https://doi.org/10.1038/nature12481
Jürgens, T., Jafari, M., Kreutzfeldt, M., Bahn, E., Brück, W., Kerschensteiner, M., & Merkler, D. (2016). Reconstruction of single cortical projection neurons reveals primary spine loss in multiple sclerosis. *Brain*, *139*(1), 39–46. https://doi.org/10.1093/brain/awv353
Kappos, L., Wolinsky, J. S., Giovannoni, G., Arnold, D. L., Wang, Q., Bernasconi, C., Model, F., Koendgen, H., Manfrini, M., Belachew, S., & Hauser, S. L. (2020). Contribution of Relapse-Independent Progression vs Relapse-Associated Worsening to Overall Confirmed Disability Accumulation in Typical Relapsing Multiple Sclerosis in a Pooled Analysis of 2 Randomized Clinical Trials. *JAMA Neurology*, *77*(9), 1132. https://doi.org/10.1001/jamaneurol.2020.1568
Katz Sand, I. (2015). Classification, diagnosis, and differential diagnosis of multiple sclerosis. *Current Opinion in Neurology*, *28*(3), 193–205. https://doi.org/10.1097/WCO.0000000000000206
Kaufmann, M., Evans, H., Schaupp, A.-L., Engler, J. B., Kaur, G., Willing, A., Kursawe, N., Schubert, C., Attfield, K. E., Fugger, L., & Friese, M. A. (2021). Identifying CNS-colonizing T cells as potential therapeutic targets to prevent progression of multiple sclerosis. *Med*, *2*(3), 296-312.e8. https://doi.org/10.1016/j.medj.2021.01.006
Kaufmann, T., van der Meer, D., Doan, N. T., Schwarz, E., Lund, M. J., Agartz, I., Alnæs, D., Barch, D. M., Baur-Streubel, R., Bertolino, A., Bettella, F., Beyer, M. K., Bøen, E., Borgwardt, S., Brandt, C. L., Buitelaar, J., Celius, E. G., Cervenka, S., Conzelmann, A., … Westlye, L. T. (2019). Common brain disorders are associated with heritable patterns of apparent aging of the brain. *Nature*

Neuroscience, *22*(10), 1617–1623. https://doi.org/10.1038/s41593-019-0471-7

Klaips, C. L., Jayaraj, G. G., & Hartl, F. U. (2018). Pathways of cellular proteostasis in aging and disease. *Journal of Cell Biology*, *217*(1), 51–63. https://doi.org/10.1083/jcb.201709072

Kopito, R. R. (2000). Aggresomes, inclusion bodies and protein aggregation. *Trends in Cell Biology*, *10*(12), 524–530. https://doi.org/10.1016/S0962-8924(00)01852-3

Kostic, M., Zivkovic, N., & Stojanovic, I. (2013). Multiple sclerosis and glutamate excitotoxicity. *Reviews in the Neurosciences*, *24*(1). https://doi.org/10.1515/revneuro-2012-0062

Krogsgaard, M., Wucherpfennig, K. W., Canella, B., Hansen, B. E., Svejgaard, A., Pyrdol, J., Ditzel, H., Raine, C., Engberg, J., & Fugger, L. (2000). Visualization of Myelin Basic Protein (Mbp) T Cell Epitopes in Multiple Sclerosis Lesions Using a Monoclonal Antibody Specific for the Human Histocompatibility Leukocyte Antigen (Hla)-Dr2–Mbp 85–99 Complex. *The Journal of Experimental Medicine*, *191*(8), 1395–1412. https://doi.org/10.1084/jem.191.8.1395

Krupp, L. B., Tardieu, M., Amato, M. P., Banwell, B., Chitnis, T., Dale, R. C., Ghezzi, A., Hintzen, R., Kornberg, A., Pohl, D., Rostasy, K., Tenembaum, S., & Wassmer, E. (2013). International Pediatric Multiple Sclerosis Study Group criteria for pediatric multiple sclerosis and immune-mediated central nervous system demyelinating disorders: revisions to the 2007 definitions. *Multiple Sclerosis Journal*, *19*(10), 1261–1267. https://doi.org/10.1177/1352458513484547

KUERTEN, S., KOSTOVABALES, D., FRENZEL, L., TIGNO, J., TARYLEHMANN, M., ANGELOV, D., & LEHMANN, P. (2007). MP4- and MOG:35–55-induced EAE in C57BL/6 mice differentially targets brain, spinal cord and cerebellum☆. *Journal of Neuroimmunology*, *189*(1–2), 31–40. https://doi.org/10.1016/j.jneuroim.2007.06.016

Kuhle, J., Leppert, D., Petzold, A., Regeniter, A., Schindler, C., Mehling, M., Anthony, D. C., Kappos, L., & Lindberg, R. L. P. (2011). Neurofilament heavy chain in CSF correlates with relapses and disability in multiple sclerosis. *Neurology*, *76*(14), 1206–1213. https://doi.org/10.1212/WNL.0b013e31821432ff

Kutzelnigg, A., & Lassmann, H. (2005). Cortical lesions and brain atrophy in MS. *Journal of the Neurological Sciences*, *233*(1–2), 55–59. https://doi.org/10.1016/j.jns.2005.03.027

Kutzelnigg, A., Lucchinetti, C. F., Stadelmann, C., Brück, W., Rauschka, H., Bergmann, M., Schmidbauer, M., Parisi, J. E., & Lassmann, H. (2005). Cortical demyelination and diffuse white matter injury in multiple sclerosis. *Brain*, *128*(11), 2705–2712. https://doi.org/10.1093/brain/awh641

Labbadia, J., & Morimoto, R. I. (2015). The Biology of Proteostasis in Aging and Disease. *Annual Review of Biochemistry*, *84*(1), 435–464. https://doi.org/10.1146/annurev-biochem-060614-033955

Lamark, T., & Johansen, T. (2012). Aggrephagy: Selective Disposal of Protein Aggregates by Macroautophagy. *International Journal of Cell Biology*, *2012*, 1–21. https://doi.org/10.1155/2012/736905

Lanz, T. V., Brewer, R. C., Ho, P. P., Moon, J.-S., Jude, K. M., Fernandez, D., Fernandes, R. A., Gomez, A. M., Nadj, G.-S., Bartley, C. M., Schubert, R. D., Hawes, I. A., Vazquez, S. E., Iyer, M., Zuchero, J. B., Teegen, B., Dunn, J. E., Lock, C. B., Kipp, L. B., … Robinson, W. H. (2022). Clonally expanded B cells

in multiple sclerosis bind EBV EBNA1 and GlialCAM. *Nature*, *603*(7900), 321–327. https://doi.org/10.1038/s41586-022-04432-7

Li, Q., Liu, Y., & Sun, M. (2017). Autophagy and Alzheimer's Disease. *Cellular and Molecular Neurobiology*, *37*(3), 377–388. https://doi.org/10.1007/s10571-016-0386-8

Lim, J., & Yue, Z. (2015). Neuronal Aggregates: Formation, Clearance, and Spreading. *Developmental Cell*, *32*(4), 491–501. https://doi.org/10.1016/j.devcel.2015.02.002

Lovas, G., Szilagyi, N., Majtenyi, K., Palkovits, M., & Komoly, S. (2000). Axonal changes in chronic demyelinated cervical spinal cord plaques. *Brain*, *123*(2), 308–317. https://doi.org/10.1093/brain/123.2.308

Lucchinetti, C. F., Popescu, B. F. G., Bunyan, R. F., Moll, N. M., Roemer, S. F., Lassmann, H., Brück, W., Parisi, J. E., Scheithauer, B. W., Giannini, C., Weigand, S. D., Mandrekar, J., & Ransohoff, R. M. (2011). Inflammatory Cortical Demyelination in Early Multiple Sclerosis. *New England Journal of Medicine*, *365*(23), 2188–2197. https://doi.org/10.1056/NEJMoa1100648

Maggi, P., Macri, S. M. C., Gaitán, M. I., Leibovitch, E., Wholer, J. E., Knight, H. L., Ellis, M., Wu, T., Silva, A. C., Massacesi, L., Jacobson, S., Westmoreland, S., & Reich, D. S. (2014). The formation of inflammatory demyelinated lesions in cerebral white matter. *Annals of Neurology*, *76*(4), 594–608. https://doi.org/10.1002/ana.24242

Magliozzi, R., Howell, O., Vora, A., Serafini, B., Nicholas, R., Puopolo, M., Reynolds, R., & Aloisi, F. (2006). Meningeal B-cell follicles in secondary progressive multiple sclerosis associate with early onset of disease and severe cortical pathology. *Brain*, *130*(4), 1089–1104. https://doi.org/10.1093/brain/awm038

Martinez, P., Patel, H., You, Y., Jury, N., Perkins, A., Lee-Gosselin, A., Taylor, X., You, Y., Viana Di Prisco, G., Huang, X., Dutta, S., Wijeratne, A. B., Redding-Ochoa, J., Shahid, S. S., Codocedo, J. F., Min, S., Landreth, G. E., Mosley, A. L., Wu, Y.-C., … Lasagna-Reeves, C. A. (2022). Bassoon contributes to tau-seed propagation and neurotoxicity. *Nature Neuroscience*, *25*(12), 1597–1607. https://doi.org/10.1038/s41593-022-01191-6

Mathey, E. K., Derfuss, T., Storch, M. K., Williams, K. R., Hales, K., Woolley, D. R., Al-Hayani, A., Davies, S. N., Rasband, M. N., Olsson, T., Moldenhauer, A., Velhin, S., Hohlfeld, R., Meinl, E., & Linington, C. (2007). Neurofascin as a novel target for autoantibody-mediated axonal injury. *The Journal of Experimental Medicine*, *204*(10), 2363–2372. https://doi.org/10.1084/jem.20071053

McCarthy, D. P., Richards, M. H., & Miller, S. D. (2012). *Mouse Models of Multiple Sclerosis: Experimental Autoimmune Encephalomyelitis and Theiler's Virus-Induced Demyelinating Disease* (pp. 381–401). https://doi.org/10.1007/978-1-60761-720-4_19

McGinley, M. P., Goldschmidt, C. H., & Rae-Grant, A. D. (2021). Diagnosis and Treatment of Multiple Sclerosis. *JAMA*, *325*(8), 765. https://doi.org/10.1001/jama.2020.26858

McMahon, E. J., Bailey, S. L., Castenada, C. V., Waldner, H., & Miller, S. D. (2005). Epitope spreading initiates in the CNS in two mouse models of multiple sclerosis. *Nature Medicine*, *11*(3), 335–339. https://doi.org/10.1038/nm1202

Meinl, E., Krumbholz, M., Derfuss, T., Junker, A., & Hohlfeld, R. (2008). Compartmentalization of inflammation in the CNS: A major mechanism driving progressive multiple sclerosis. *Journal of the Neurological Sciences*, *274*(1–2), 42–44. https://doi.org/10.1016/j.jns.2008.06.032

Mendoza Schulz, A., Jing, Z., María Sánchez Caro, J., Wetzel, F., Dresbach, T., Strenzke, N., Wichmann, C., & Moser, T. (2014). Bassoon-disruption slows vesicle replenishment and induces homeostatic plasticity at a CNS synapse. *The EMBO Journal*, n/a-n/a. https://doi.org/10.1002/embj.201385887

Miller, D. H. (2002). Measurement of atrophy in multiple sclerosis: pathological basis, methodological aspects and clinical relevance. *Brain*, *125*(8), 1676–1695. https://doi.org/10.1093/brain/awf177

Miller, D. H., Chard, D. T., & Ciccarelli, O. (2012). Clinically isolated syndromes. *The Lancet Neurology*, *11*(2), 157–169. https://doi.org/10.1016/S1474-4422(11)70274-5

Montenegro-Venegas, C., Fienko, S., Anni, D., Pina-Fernández, E., Frischknecht, R., & Fejtova, A. (2021). Bassoon inhibits proteasome activity via interaction with PSMB4. *Cellular and Molecular Life Sciences*, *78*(4), 1545–1563. https://doi.org/10.1007/s00018-020-03590-z

Needham, P. G., Guerriero, C. J., & Brodsky, J. L. (2019). Chaperoning Endoplasmic Reticulum–Associated Degradation (ERAD) and Protein Conformational Diseases. *Cold Spring Harbor Perspectives in Biology*, *11*(8), a033928. https://doi.org/10.1101/cshperspect.a033928

Oh, J., Vidal-Jordana, A., & Montalban, X. (2018). Multiple sclerosis: clinical aspects. *Current Opinion in Neurology*, *31*(6), 752–759. https://doi.org/10.1097/WCO.0000000000000622

Okerlund, N. D., Schneider, K., Leal-Ortiz, S., Montenegro-Venegas, C., Kim, S. A., Garner, L. C., Waites, C. L., Gundelfinger, E. D., Reimer, R. J., & Garner, C. C. (2017). Bassoon Controls Presynaptic Autophagy through Atg5. *Neuron*, *93*(4), 897-913.e7. https://doi.org/10.1016/j.neuron.2017.01.026

Orton, S.-M., Ramagopalan, S. V, Brocklebank, D., Herrera, B. M., Dyment, D. A., Yee, I. M., Sadovnick, A. D., & Ebers, G. C. (2010). Effect of immigration on multiple sclerosis sex ratio in Canada: the Canadian Collaborative Study. *Journal of Neurology, Neurosurgery & Psychiatry*, *81*(1), 31–36. https://doi.org/10.1136/jnnp.2008.162784

Peng, C., Trojanowski, J. Q., & Lee, V. M.-Y. (2020). Protein transmission in neurodegenerative disease. *Nature Reviews Neurology*, *16*(4), 199–212. https://doi.org/10.1038/s41582-020-0333-7

Piani, D., Frei, K., Do, K. Q., Cuénod, M., & Fontana, A. (1991). Murine brain macrophages induce NMDA receptor mediated neurotoxicity in vitro by secreting glutamate. *Neuroscience Letters*, *133*(2), 159–162. https://doi.org/10.1016/0304-3940(91)90559-C

PORTIANSKY, E., BARBEITO, C., GIMENO, E., ZUCCOLILLI, G., & GOYA, R. (2006). Loss of NeuN immunoreactivity in rat spinal cord neurons during aging. *Experimental Neurology*, *202*(2), 519–521. https://doi.org/10.1016/j.expneurol.2006.07.014

Quinn, T. A., Dutt, M., & Shindler, K. S. (2011). Optic Neuritis and Retinal Ganglion Cell Loss in a Chronic Murine Model of Multiple Sclerosis. *Frontiers in Neurology*, *2*. https://doi.org/10.3389/fneur.2011.00050

Ransohoff, R. M., Kivisäkk, P., & Kidd, G. (2003). Three or more routes for leukocyte migration into the central nervous system. *Nature Reviews Immunology*, *3*(7), 569–581. https://doi.org/10.1038/nri1130

Reich, D. S., Lucchinetti, C. F., & Calabresi, P. A. (2018). Multiple Sclerosis. *New England Journal of Medicine*, *378*(2), 169–180. https://doi.org/10.1056/NEJMra1401483

Ross, C. A., & Poirier, M. A. (2004). Protein aggregation and neurodegenerative disease. *Nature Medicine*, *10*(S7), S10–S17. https://doi.org/10.1038/nm1066

Rothammer, N., Woo, M. S., Bauer, S., Binkle-Ladisch, L., Di Liberto, G., Egervari, K., Wagner, I., Haferkamp, U., Pless, O., Merkler, D., Engler, J. B., & Friese, M. A. (2022). G9a dictates neuronal vulnerability to inflammatory stress via transcriptional control of ferroptosis. *Science Advances*, *8*(31). https://doi.org/10.1126/sciadv.abm5500

Rouillard, A. D., Gundersen, G. W., Fernandez, N. F., Wang, Z., Monteiro, C. D., McDermott, M. G., & Ma'ayan, A. (2016). The harmonizome: a collection of processed datasets gathered to serve and mine knowledge about genes and proteins. *Database*, *2016*, baw100. https://doi.org/10.1093/database/baw100

Saftig, P., & Puertollano, R. (2021). How Lysosomes Sense, Integrate, and Cope with Stress. *Trends in Biochemical Sciences*, *46*(2), 97–112. https://doi.org/10.1016/j.tibs.2020.09.004

Scalfari, A., Neuhaus, A., Daumer, M., Muraro, P. A., & Ebers, G. C. (2014). Onset of secondary progressive phase and long-term evolution of multiple sclerosis. *Journal of Neurology, Neurosurgery & Psychiatry*, *85*(1), 67–75. https://doi.org/10.1136/jnnp-2012-304333

Schattling, B., Engler, J. B., Volkmann, C., Rothammer, N., Woo, M. S., Petersen, M., Winkler, I., Kaufmann, M., Rosenkranz, S. C., Fejtova, A., Thomas, U., Bose, A., Bauer, S., Träger, S., Miller, K. K., Brück, W., Duncan, K. E., Salinas, G., Soba, P., … Friese, M. A. (2019). Bassoon proteinopathy drives neurodegeneration in multiple sclerosis. *Nature Neuroscience*, *22*(6), 887–896. https://doi.org/10.1038/s41593-019-0385-4

Schattling, B., Steinbach, K., Thies, E., Kruse, M., Menigoz, A., Ufer, F., Flockerzi, V., Brück, W., Pongs, O., Vennekens, R., Kneussel, M., Freichel, M., Merkler, D., & Friese, M. A. (2012). TRPM4 cation channel mediates axonal and neuronal degeneration in experimental autoimmune encephalomyelitis and multiple sclerosis. *Nature Medicine*, *18*(12), 1805–1811. https://doi.org/10.1038/nm.3015

Schirmer, L., Srivastava, R., & Hemmer, B. (2014). To look for a needle in a haystack: the search for autoantibodies in multiple sclerosis. *Multiple Sclerosis Journal*, *20*(3), 271–279. https://doi.org/10.1177/1352458514522104

Schuck, S. (2020). Microautophagy – distinct molecular mechanisms handle cargoes of many sizes. *Journal of Cell Science*, *133*(17). https://doi.org/10.1242/jcs.246322

Shapira, M., Zhai, R. G., Dresbach, T., Bresler, T., Torres, V. I., Gundelfinger, E. D., Ziv, N. E., & Garner, C. C. (2003). Unitary Assembly of Presynaptic Active Zones from Piccolo-Bassoon Transport Vesicles. *Neuron*, *38*(2), 237–252. https://doi.org/10.1016/S0896-6273(03)00207-1

Sossin, W. S., & Costa-Mattioli, M. (2019). Translational Control in the Brain in Health and Disease. *Cold Spring Harbor Perspectives in Biology*, *11*(8), a032912. https://doi.org/10.1101/cshperspect.a032912

Soto, C., & Pritzkow, S. (2018). Protein misfolding, aggregation, and conformational strains in neurodegenerative diseases. *Nature Neuroscience*, *21*(10), 1332–1340. https://doi.org/10.1038/s41593-018-0235-9

Stirling, D. P., & Stys, P. K. (2010). Mechanisms of axonal injury: internodal nanocomplexes and calcium deregulation. *Trends in Molecular Medicine*, *16*(4), 160–170. https://doi.org/10.1016/j.molmed.2010.02.002

Thompson, A. J., Baranzini, S. E., Geurts, J., Hemmer, B., & Ciccarelli, O. (2018). Multiple sclerosis. *The Lancet*, *391*(10130), 1622–1636. https://doi.org/10.1016/S0140-6736(18)30481-1

Trapp, B. D., & Stys, P. K. (2009). Virtual hypoxia and chronic necrosis of demyelinated axons in multiple sclerosis. *The Lancet Neurology*, *8*(3), 280–291. https://doi.org/10.1016/S1474-4422(09)70043-2

Travers, K. J., Patil, C. K., Wodicka, L., Lockhart, D. J., Weissman, J. S., & Walter, P. (2000). Functional and Genomic Analyses Reveal an Essential Coordination between the Unfolded Protein Response and ER-Associated Degradation. *Cell*, *101*(3), 249–258. https://doi.org/10.1016/S0092-8674(00)80835-1

Tsang, B., Pritišanac, I., Scherer, S. W., Moses, A. M., & Forman-Kay, J. D. (2020). Phase Separation as a Missing Mechanism for Interpretation of Disease Mutations. *Cell*, *183*(7), 1742–1756. https://doi.org/10.1016/j.cell.2020.11.050

Van Waesberghe, J. H. T. M., Kamphorst, W., De Groot, C. J. A., Van Walderveen, M. A. A., Castelijns, J. A., Ravid, R., Lycklama à Nijeholt, G. J., Van Der Valk, P., Polman, C. H., Thompson, A. J., & Barkhof, F. (1999). Axonal loss in multiple sclerosis lesions: Magnetic resonance imaging insights into substrates of disability. *Annals of Neurology*, *46*(5), 747–754. https://doi.org/10.1002/1531-8249(199911)46:5<747::AID-ANA10>3.3.CO;2-W

Vidal, R. L., & Hetz, C. (2012). Crosstalk between the UPR and autophagy pathway contributes to handling cellular stress in neurodegenerative disease. *Autophagy*, *8*(6), 970–972. https://doi.org/10.4161/auto.20139

Waites, C. L., Leal-Ortiz, S. A., Okerlund, N., Dalke, H., Fejtova, A., Altrock, W. D., Gundelfinger, E. D., & Garner, C. C. (2013). Bassoon and Piccolo maintain synapse integrity by regulating protein ubiquitination and degradation. *The EMBO Journal*, *32*(7), 954–969. https://doi.org/10.1038/emboj.2013.27

Wang, Y., & Qin, Z. (2010). Molecular and cellular mechanisms of excitotoxic neuronal death. *Apoptosis*, *15*(11), 1382–1402. https://doi.org/10.1007/s10495-010-0481-0

Wherry, E. J. (2011). T cell exhaustion. *Nature Immunology*, *12*(6), 492–499. https://doi.org/10.1038/ni.2035

Williams, R., Buchheit, C. L., Berman, N. E. J., & LeVine, S. M. (2012). Pathogenic implications of iron accumulation in multiple sclerosis. *Journal of Neurochemistry*, *120*(1), 7–25. https://doi.org/10.1111/j.1471-4159.2011.07536.x

Winter, C., tom Dieck, S., Boeckers, T. M., Bockmann, J., Kämpf, U., Sanmartí-Vila, L., Langnaese, K., Altrock, W., Stumm, M., Soyke, A., Wieacker, P., Garner, C. C., & Gundelfinger, E. D. (1999). The Presynaptic Cytomatrix Protein Bassoon: Sequence and Chromosomal Localization of the HumanBSNGene. *Genomics*, *57*(3), 389–397. https://doi.org/10.1006/geno.1999.5788

Wojcikiewicz, R. J. H., Pearce, M. M. P., Sliter, D. A., & Wang, Y. (2009). When worlds collide: IP3 receptors and the ERAD pathway. *Cell Calcium*, *46*(3), 147–153. https://doi.org/10.1016/j.ceca.2009.05.002

Yabe, I., Yaguchi, H., Kato, Y., Miki, Y., Takahashi, H., Tanikawa, S., Shirai, S., Takahashi, I., Kimura, M., Hama, Y., Matsushima, M., Fujioka, S., Kano, T., Watanabe, M., Nakagawa, S., Kunieda, Y., Ikeda, Y., Hasegawa, M., Nishihara, H., … Sasaki, H. (2018). Mutations in bassoon in individuals with familial

and sporadic progressive supranuclear palsy-like syndrome. *Scientific Reports*, *8*(1), 819. https://doi.org/10.1038/s41598-018-19198-0

Zhai, R., Olias, G., Chung, W. J., Lester, R. A. J., tom Dieck, S., Langnaese, K., Kreutz, M. R., Kindler, S., Gundelfinger, E. D., & Garner, C. C. (2000). Temporal Appearance of the Presynaptic Cytomatrix Protein Bassoon during Synaptogenesis. *Molecular and Cellular Neuroscience*, *15*(5), 417–428. https://doi.org/10.1006/mcne.2000.0839

8. Acknowledgements

First and foremost, I wish to express my sincere and strong gratitude to Prof. Manuel Friese for the opportunity to work in such a motivating and inspiring environment, for his great knowledge and the scientific mentorship. Additionally, my thanks extend to Dr. Dr. Jan Broder Engler for his support and his excellent scientific supervision. I would like to thank the entire INIMS team, with a special acknowledgement to Dr. Nicola Rothammer for patiently teaching me the *in vitro* experiments and for her experimental mentorship. My gratitude also belongs to the Hertie foundation for their financial support and for the introduction into scientific networks. I want to thank my family and my partner for their encouragement and support.

9. Eidesstattliche Versicherung

Ich versichere ausdrücklich, dass ich die Arbeit selbständig und ohne fremde Hilfe, insbesondere ohne entgeltliche Hilfe von Vermittlungs- und Beratungsdiensten, verfasst, andere als die von mir angegebenen Quellen und Hilfsmittel nicht benutzt und die aus den benutzten Werken wörtlich oder inhaltlich entnommenen Stellen einzeln nach Ausgabe (Auflage und Jahr des Erscheinens), Band und Seite des benutzten Werkes kenntlich gemacht habe. Das gilt insbesondere auch für alle Informationen aus Internetquellen.
Soweit beim Verfassen der Dissertation KI-basierte Tools („Chatbots“) verwendet wurden, versichere ich ausdrücklich, den daraus generierten Anteil deutlich kenntlich gemacht zu haben. Die „Stellungnahme des Präsidiums der Deutschen Forschungsgemeinschaft (DFG) zum Einfluss generativer Modelle für die Text- und Bilderstellung auf die Wissenschaften und das Förderhandeln der DFG“ aus September 2023 wurde dabei beachtet.
Ferner versichere ich, dass ich die Dissertation bisher nicht einem Fachvertreter an einer anderen Hochschule zur Überprüfung vorgelegt oder mich anderweitig um Zulassung zur Promotion beworben habe.
Ich erkläre mich damit einverstanden, dass meine Dissertation vom Dekanat der Medizinischen Fakultät mit einer gängigen Software zur Erkennung von Plagiaten überprüft werden kann.

Datum Unterschrift